

Graphene: An Emerging Electronic Material

Nathan O. Weiss, Hailong Zhou, Lei Liao, Yuan Liu, Shan Jiang, Yu Huang,
and Xiangfeng Duan*

Graphene, a single layer of carbon atoms in a honeycomb lattice, offers a number of fundamentally superior qualities that make it a promising material for a wide range of applications, particularly in electronic devices. Its unique form factor and exceptional physical properties have the potential to enable an entirely new generation of technologies beyond the limits of conventional materials. The extraordinarily high carrier mobility and saturation velocity can enable a fast switching speed for radio-frequency analog circuits. Unadulterated graphene is a semi-metal, incapable of a true off-state, which typically precludes its applications in digital logic electronics without bandgap engineering. The versatility of graphene-based devices goes beyond conventional transistor circuits and includes flexible and transparent electronics, optoelectronics, sensors, electromechanical systems, and energy technologies. Many challenges remain before this relatively new material becomes commercially viable, but laboratory prototypes have already shown the numerous advantages and novel functionality that graphene provides.

1. Introduction

Graphene is an atomically thin, planar membrane of carbon with exceptional properties, particularly electronic. Over the past few years, it has skyrocketed as a hot research topic in nanotechnology, intensively investigated by physicists, chemists, materials scientists and engineers alike.^[1–4] Its vast potential has motivated novel implementation into a wide array of devices. The electronics industry has shown early interest in its numerous possible applications in areas ranging from microprocessors to sensors. Carbon fits right at the top of group IV elements in the periodic table, above semiconducting silicon and germanium. Graphite behaves metallically and diamond is insulating, while graphene has a unique zero bandgap. The charge carrier concentration can be controlled by an applied electric field and consequently the conductivity is gate tunable, as evident in early-fabricated

devices.^[1] Utilizing its unique form factor and unusual physical properties, these devices can exhibit many potential advantages that will likely lead to new and improved technologies one way or another. This review covers a broad overview of graphene science and technology to date with a focus on its potential in electronic devices.

For the past half-century or so, semiconductor technologies have witnessed tremendous growth and revolutionized nearly every aspect of our daily lives, not just with computing, but also for communications, optoelectronics, photovoltaics and sensors. Silicon-based electronics have been the cornerstone for this technological revolution. To date, the exponential growth in computing power and reduction in cost is generally powered by the continued miniaturization of silicon

devices as dictated by Moore's Law,^[5] currently down to 22 nm features. However, with these sizes approaching extreme physical scales, continued increases in device speed and computing power through evolutionary miniaturization are expected to reach the fundamental limits of silicon technology in the near future. Overcoming these obstacles associated with conventional technologies will require profoundly new strategies. To sustain the continued advancement in electronics and fuel the expected demands of our society in the future requires revolutionary breakthroughs and fundamentally new materials, operating schemes and/or manufacturing approaches.

Graphene is a deserving yet controversial candidate to supplant contemporary semiconductor technologies. Its atomic thinness already represents one limit in the nonstop shrinking of device dimensions. Still in its early stages of development, this new material has already shown its unusual physics and distinct capabilities. Though often over-glorified in the media, portrayed as a miracle material, graphene does offer a wide array of advantages over silicon and other semiconductors, as recently reviewed by Schwierz.^[6] Many superior properties, such as the extremely high carrier mobility, make graphene a promising material for high performance electronic devices, but certainly with many obstacles ahead.

As the most fundamental form of the sp^2 -hybridized carbon allotropes, graphene is surprisingly the latest one to be practically isolated in 2004^[1] by Novoselov^[7] and Geim,^[8] more than 10 years after Iijima discovered nanotubes^[9] and nearly two decades after the discovery of C₆₀ by Smalley and co-workers.^[10] Built from the basic graphene honeycomb structure, sheets

Prof. X. Duan, Dr. H. Zhou, Dr. L. Liao, S. Jiang
Department of Chemistry and Biochemistry
UCLA, Los Angeles, CA 90095, USA
E-mail: xduan@chem.ucla.edu

Prof. Y. Huang, N. O. Weiss, Y. Liu
Department of Materials Science and Engineering
UCLA, Los Angeles, CA 90095, USA

Prof. X. Duan, Prof. Y. Huang
California NanoSystems Institute
UCLA, Los Angeles, CA 90095, USA

DOI: 10.1002/adma.201201482



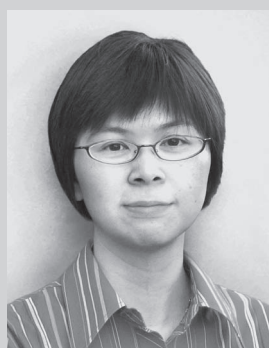
rolled up into cylinders and spheres have already seen a number of applications. Carbon nanostructures have become novel electronic materials for a wide range of electronic devices, as reviewed by Avouris et al.^[11] Carbon nanotubes (CNTs) have many advantages over graphene: these quasi-one-dimensional structures are ideal for wires and interconnects with a minimalist form factor, while two thirds of nanotube varieties have an intrinsic bandgap due to quantum confinement. Current technology, however, is unable to precisely control the type and arrangement of nanotubes in a scalable way, which renders them impractical in commercial integrated circuits. With a two-dimensional structure, graphene is much more conducive to utilize current planar semiconductor processing technologies for scalable fabrication and very large-scale integration (VLSI). This makes graphene more attractive for early implementation of carbon-based electronics, at least until future technologies enable more precise and scalable control of carbon nanotubes. The intense investigation has rapidly propelled graphene to new heights that have usually taken other materials decades to reach. Its status as a relatively new material has been overshadowed by its immense following and continued exploration as a novel material for advanced electronics.

Graphene presents a number of clear advantages over other materials in addition to its size and shape. Its exceptional qualities include atomic thinness, specific surface area, transparency, thermal conductivity, electrical conductivity, charge density, carrier mobility, strength, flexibility, and robustness, which show great promise for a wide spectrum of advanced applications. In particular, the reported carrier mobility in graphene can reach up to $10^6 \text{ cm}^2/\text{Vs}$ ^[12] which is about 2–3 orders of magnitudes higher than typical semiconducting materials such as silicon. This can enable devices with higher operating frequencies, and ultimately superior performance. The electronic structure of graphene is quite unique; it behaves like a semiconductor, but has no bandgap. Analog devices can utilize its high transconductance without need for a gap; however, digital field effect transistors (FETs) need an off-state. In order for a semiconducting channel to be off (insulating state), it must have an energy gap significantly greater than the thermal excitation energy at operating temperatures. Therefore, pristine graphene cannot be used in logic devices in the typical field-effect designs. To this end, many attempts have been reported to induce a bandgap, or at least a transport gap by creating laterally confined graphene nanoribbons (GNRs) or strain engineered lattice distortions. Other strategies such as spintronics^[13] and other novel approaches^[14–17] have been explored to circumvent this constraint by designing unconventional operation schemes. Graphene can ultimately be used as a metal or a semiconductor, depending on how it is implemented or modified and can be patterned into entire integrated circuits with carbon-based interconnects and active channels, to enable all carbon-based circuits.^[18,19] However, it is unlikely that silicon will be completely replaced by carbon in the near future, as graphene is more likely to develop as a complementary technology adjacently integrated into contemporary semiconducting fabrication for more advanced devices.^[20]

Much work remains before the exciting potential of graphene can be practically implemented into commercial devices. Some niche applications have seen earlier adoption, but the



Nathan Weiss is currently pursuing his Ph.D. in Materials Science and Engineering at UCLA. He received his B.S. in Materials Science and Engineering at Columbia University (2009) and his M.S. in Engineering Management at Johns Hopkins University (2010). His current doctoral research is on graphene-based electronic devices and strain engineering of its electronic properties.



Yu Huang is currently an Associate Professor in the Department of Materials Science and Engineering at UCLA. She received her B.S. in Chemistry from USTC, China (1999) and her M.A. degree in Chemistry (2002) and Ph.D. in Physical Chemistry (2003) from Harvard University. Her current research interest focuses on chemical and biological approaches to complex materials structures with atomic precision and the new physical properties arising in these new materials systems.



Xiangfeng Duan is currently an Associate Professor in the Department of Chemistry and Biochemistry at UCLA. He received his B.S. in Chemistry from USTC, China (1997) and his M.A. degree in Chemistry (1999) and Ph.D. in Physical Chemistry (2002) from Harvard University. He was previously a founding scientist at Nanosys Inc. His current research interests include nanoscale materials and devices for future electronics, energy and biomedical sciences.

difficulties preventing graphene from widespread integration into microchip technologies among others are formidable. Two major barriers stand out for graphene-based circuits: synthesis of wafer-scale pristine graphene, and inducing a bandgap into otherwise semi-metallic graphene. Fabrication methods must improve to obtain graphene in highly controlled environments

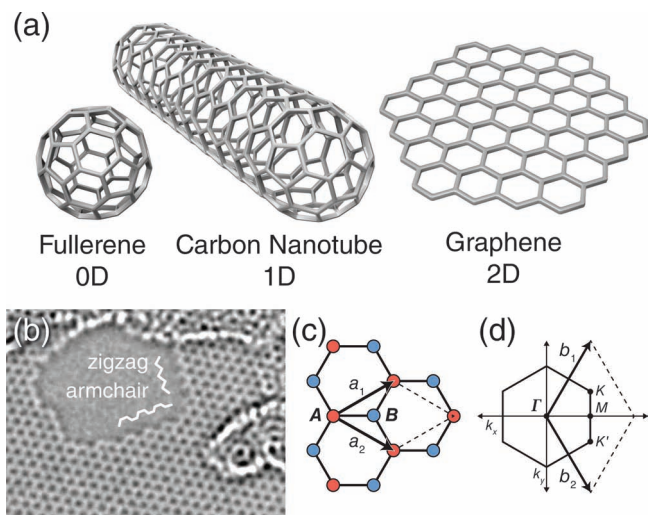


Figure 1. Honeycomb lattice. a) Allotropes of carbon based on two-dimensional graphene (right), quasi-zero-dimensional buckminsterfullerene (left), and quasi-one-dimensional armchair nanotube (middle). b) High-resolution TEM image of suspended graphene, showing a monolayer with a void in the middle and a bilayer region toward the top. Clear zigzag and armchair edges are seen. c) Hexagonal crystal structure of graphene with lattice parameters a_1 and a_2 and inequivalent atomic positions A and B of the diatomic basis shown in red and blue. d) Reciprocal lattice and BZ with reciprocal lattice parameters b_1 and b_2 , showing Dirac points K and K' at the BZ corners, as well as M, the midpoint of the BZ edge and Γ , the center of the BZ. b) Adapted with permission.^[49] Copyright 2009, American Association for the Advancement of Science. c,d) Redrawn.^[46]

to pattern the sheet into the desired device. In addition to integrated circuits, other potential applications include photonic, optoelectronic and sensor devices. Graphene is so thin that it is almost invisible; transparent conducting films have been made from graphene for displays, touch-screens and solar cells. Its incredible strength and flexibility enable bendable devices and is useful in electromechanical systems. Many optoelectronic and sensor applications benefit from the large and planar surface area of a single sheet and take advantage of chemical doping and functionalization of the surface with various species. The vast possibilities of graphene and the rapid advancements in research are propelling this new material towards novel achievements that are already beginning to influence industry.

2. Fundamental Properties

Graphene has a truly two-dimensional lattice, the so-called honeycomb, resembling the hexagons that bees make to store honey (Figure 1). It is the basic structure for various carbon allotropes, including graphite, which consist of stacks of individual graphene layers bonded via van der Waals forces. The high strength of the covalent bonding within the layers and weak interlayer bonding allows them to slide quite easily. This has led to use of graphite in pencils: exfoliating layers with every stroke presumably down to single monolayers, though

difficult to detect. For its atomic thinness, graphene has a surprisingly high absorbance of 2.3%, based on the fine-structure constant.^[21,22]

Graphene is surprisingly stable, withstanding high temperatures, for instance during annealing (up to 250 °C without structural damage) and vapor-based synthesis (~1000 °C), though a clear melting temperature is unknown. Due to its two-dimensionality and out of plane phonons, a negative thermal expansion coefficient is both expected and observed.^[23,24] Graphene exhibits an exceptionally high in-plane thermal conductivity up to approximately 5×10^3 W/mK, which make it an attractive material for efficient heat dissipation and thermal interface composites in computer chips.^[25–28] Additionally, substantial Peltier cooling, a thermoelectric effect, is observed at metal contacts using local temperature measurements.^[29] In graphene devices, this can outweigh Joule heating and current crowding, demonstrating an atypical self-cooling mechanism. Keeping operating temperatures cool is imperative to high performance electronics.

Mechanically, graphene is incredibly strong while remaining very flexible, attributed to the high strength of the carbon-carbon bond.^[30] CNTs have experimental yield strengths up to 53 GPa, while an indentation test of suspended graphene yielded 130 GPa, the record for the strongest known material with a breaking strength of 42 N/m.^[31] Still, the hexagonal structure benefits the relatively high elasticity of graphene and carbon nanotubes, with a Young's modulus of 1 TPa, third order elastic stiffness ≈ 2 TPa,^[31] and a shear modulus ≈ 280 GPa.^[32] It is important to understand that, as with nanotubes, this strength is taken from incredibly small scales, which do not necessarily correlate to or directly compare with macroscopic performance. Graphite is not particularly strong because it shears between layers very easily, important for smooth pencil tips. Composites can better utilize the individual strength, but the performance is not on the order of the intrinsic values of a single sheet or nanotube. Polymers, metals, oxides, etc. combined with graphene can enhance thermal and electrical conductivity in addition to mechanical strength and flexibility.^[33–38]

The π orbitals of conjugated electrons throughout graphene contribute to both the electronic conduction as well as interplanar bonding. Although these van der Waals interactions are fairly weak compared to the intraplanar, covalent bonding, graphene is fairly adhesive, with 0.45 J/m² adhesion strength of a monolayer with SiO₂.^[39] Graphene adhesion to metals such as copper is somewhat stronger, with 0.72 J/m².^[40] Estimates of the interlayer binding energy of graphite range from 0.20–0.38 J/m².^[41] Generally, graphene is hydrophobic: water is repelled from the surface and tends to form droplets.^[42] However, samples bound on certain surfaces show wetting transparency: practically unchanged contact angles of water drops compared to the bare substrates.^[43] Additionally, graphene can act as a corrosion resistant coating for metals, with corrosion rates up to 20 times slower.^[44]

Graphene has a unique electronic structure, which leads to a number of extraordinary properties not seen in conventional materials. Discovering the structure of graphite inspired the theory on the electronic properties of its most basic form, graphene, to be studied as early as 1946,^[45] well before its experimental realization, and thoroughly documented by Castro-Neto et al.^[46] and others.^[47–49] The band structure is a result of the

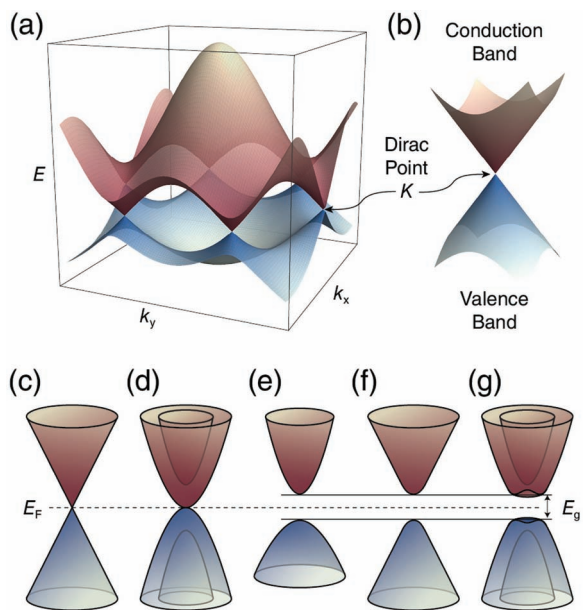


Figure 2. Electronic band structure. a) Band structure of graphene. b) The linear dispersion relation showing the vertically mirrored Dirac cones intersecting at the Fermi energy, E_F . c–e) Comparison of band structures of massless Dirac like particles in monolayer graphene (c); massive Dirac particles in bilayer graphene with parabolic shape (d); and a typical direct bandgap semiconductor with Schrödinger particles, asymmetric electron-hole effective mass (dissimilar curvature), and a substantial bandgap (e). f,g) Opening a bandgap, E_g , in monolayer graphene (f) causes a rounding of the Dirac cone tips, and an inverted tip for bilayer graphene (g). a,b) Redrawn.^[46] c–g) Redrawn.^[3,6]

symmetry in its unit cell, which contains two inequivalent lattice points, with a carbon-carbon bond length of 1.42 Å and lattice parameter of 2.46 Å (Figure 1c). Bloch wavefunction analysis and tight-binding models^[50] lead to mirrored (or depending on the model parameters, at least geometrically similar) valence and conduction bands as shown in Figure 2, which intersect at a single point of zero states, the so-called Dirac point. This intersection, directly at the intrinsic Fermi level, gives rise to its zero-gap semiconducting nature and semi-metallic properties. About the Dirac point, the density of states (DOS) converges to zero and the linear dispersion relation results in an effective mass of zero. Electrons in graphene essentially behave as massless Dirac fermions, which lead to unprecedented carrier mobility, the effective speed at which charge can travel under a unit electrical field and crucial property for high-speed electronics. Room temperature ballistic transport with an electron mean free path over a micrometer has been reported.^[51] The Fermi velocity of electrons in graphene can reach approximately 10^6 m/s, 1/300th the speed of light, which has interesting relativistic consequences. Each individual charge carrier is a conduction channel, and assuming ballistic transport, contributes one quantum of conductance $G_0 = 2e^2/h$ (where e is the elementary charge and h is Planck's constant).^[52] A sufficient chemical potential imbalance (i.e., a source-drain bias) can increase the number of active channels and ultimately the total conductivity in quantized increments. It should be noted that the linear dispersion relation near the Dirac point only holds true for ideal

samples. Perturbations and quasiparticle interactions can alter and distort these cones.^[53] Electron-electron interactions for instance can substantially increase the Fermi velocity.^[54]

The diatomic basis leads to an added degree of freedom for carrier states: an additional type of spin, called pseudospin. This is derived from the Hamiltonian that describes the chiral nature of these quasiparticles that behave like massless Dirac fermions, evident in the Pauli spinor term. The two inequivalent lattice points lead to the K and K' reciprocal points on the Brillouin zone (BZ) edge, two distinct valleys with opposite pseudospin, also referred to as valley-isospin states. If an electron travels in one direction in the K valley, a hole with opposite pseudospin travels in the opposing direction in the K' valley (Figure 3a,b). This phenomenon is further complicated in bilayer graphene, where each layer contributes two pseudospins for a total of four states. This unusual nature of graphene has been observed experimentally.^[55] A number of devices have been proposed that take advantage of this pseudospin state as a controllable degree of freedom for spintronic applications.

Graphene's atomically thin structure confines electron transport within the plane, creating a so-called two-dimensional electron gas (2DEG).^[2] Similar 2DEGs have been artificially fabricated previously through GaAs-AlGaAs heterojunctions and utilized in high electron mobility transistors (HEMTs) by trapping conducting electrons at the interface,^[56] and also observed in topological insulators.^[57,58] By strictly confining electrons to two dimensions, certain unique phenomena are exposed, such as the quantum Hall effect (QHE) and Berry's phase.^[59,60] The conventional Hall effect in a magnetic field forms discreet states:

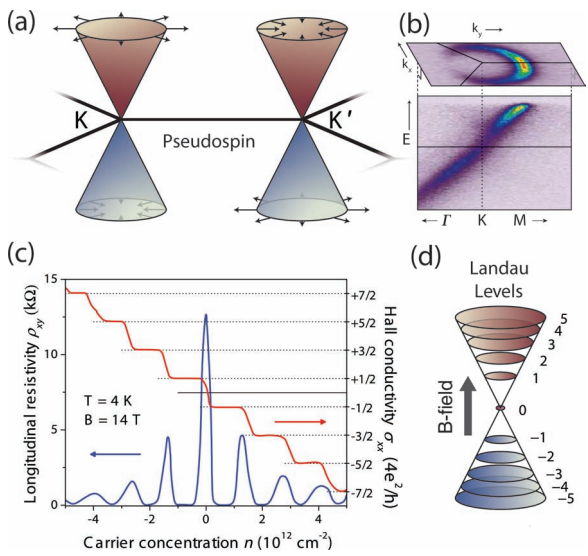


Figure 3. Unique and unusual electronic properties. a) Dirac cones showing pseudospin as it rotates with respect to reciprocal space and the inverted orientation between the two valleys. b) ARPES map of the pseudospin, horizontal cross section (upper) tilted perpendicularly to a vertical cross section (lower) of a Dirac cone observed experimentally using spherically polarized photons. c) Hall resistance measurements, showing quantized peaks and plateaus. d) Landau levels for the anomalous and fractional QHE in graphene, labeled with the quantum number index of Landau levels from -5 to 5. b) Adapted with permission.^[55] Copyright 2010, Institute of Physics. c) Reproduced with permission.^[3] Copyright 2007, Nature Publishing Group.

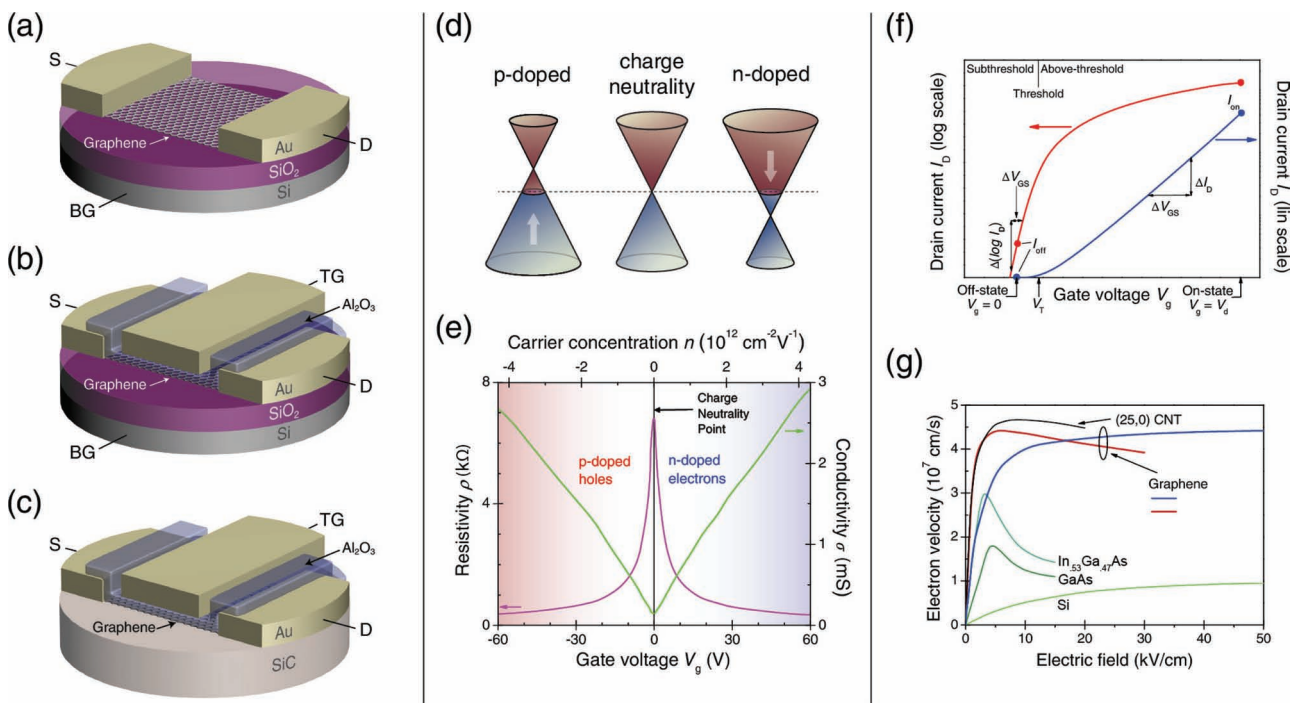


Figure 4. Field-effect transistors. Schematics of: (a) a typical back-gated GFET between two source-drain electrodes, with a potential applied to the conductive, highly-doped silicon bottom of the device acting as a global capacitor that modulates the energy levels of graphene; (b) a dual back- and top-gated device, showing the localized gate capacitor fabricated on top of the channel; (c) a top-gate only device fabricated on EG on an insulating SiC substrate. d) Schematic of band structure shift as gate voltage dopes graphene above and below the Dirac point. e) Typical resistivity as a function of gate voltage for graphene, showing the ambipolar nature as conduction switches between the hole (left) and electron (right) regimes, separated by the charge neutrality (Dirac) point where the resistance reaches its maximum. f) Current saturation and switching threshold voltage in a conventional FET. g) Velocity of charge carriers in graphene as a function of electric field, compared with other semiconductors. a–c) Redrawn.^[6] e) Redrawn.^[3] f,g) Reproduced with permission.^[6] Copyright 2010 Nature Publishing Group.

quantized orbital energies called Landau levels (Figure 3c,d). Due to additional complexities of graphene's electronic structure (e.g., accounting for pseudospin), this phenomenon has been expanded into further classifications: the anomalous QHE with a Landau level residing at 0, as well as half-integer, fractional, spin, and valley QHEs that account for otherwise degenerate physical complexities of graphene. Experiments have verified this magnetically tunable conductivity, matching models of the proper Landau levels.^[59,61–64] Magnetotransport measurements have also uncovered a giant nonlocality about the Dirac point due to spin and valley degrees of freedom.^[65] There are numerous physical phenomena that are exhibited in graphene, for instance the Shubnikov–de Haas effect, which creates measurable oscillations useful for determining carrier mobility.^[1] So far, most fail to offer practical benefit from an engineering standpoint, but are still quite interesting and necessary for a thorough science of graphene.

Another key feature of graphene, which is a product of its electron transport's chiral nature, is Klein tunneling, as explained by Katsnelson et al.^[66] Electrons have a 100% transmission rate through a potential barrier of any size; this paradoxical proposition has been experimentally observed.^[67,68] The quantum mechanical basis for this phenomenon is that in order for electrons traveling in one direction in a particular valley to be reflected back by the barrier, it must switch orientation,

which is inhibited by conservation of chirality. This can make working with graphene difficult, as square potential barriers used to form the device channel yield ineffective.

The field effect of graphene sheets was observed shortly after its isolation on thermally oxidized surfaces of highly doped silicon wafer^[1] that conveniently acts as a global back-gate in a graphene FET (GFET) and later with top gates (Figure 4a–c). Electron and hole densities are tuned using a gate voltage, which raises and lowers the Fermi energy. At the charge neutrality point, K and K' , the resistivity reaches a maximum, and above or below this energy the conductivity increases. This zero bandgap material has an insufficient maximum resistance (i.e., no distinctive off-state). GFETs are ambipolar: switching from n- to p-type behavior above and below the charge neutrality point, shown schematically in Figure 4d. Ideally this forms a symmetric "V" shape in source-drain current/conductivity vs. gate voltage plots (Figure 4e). The mobility of graphene is dependent on the density of charge carriers, with its maximum at the charge neutrality point. This ambipolar behavior is also seen in CNTs, nanowires, and organic transistors. Local side and top gates can be used to form p- and n-type regions and junctions, or selective chemical modification can be used to locally dope graphene. Both p-n^[69–72] and p-n-p^[73–75] devices can be fabricated with interesting and tunable electronic response. Additionally, electric field potential barriers can be used to

Table 1. Mobility of charge carriers with various synthesis and substrate conditions.

Synthesis	Substrate	T	μ^a	Mobility (cm^2/Vs)	Ref.
ME	Suspended	$\approx 4 \text{ K}$	μ_{DIFE}	1.0×10^6	[12]
		240 K	μ_{DIFE}	1.2×10^5	[81]
		RT	μ_{DIFE}	1.0×10^4	[82]
	hBN	4 K	$\mu_{\text{FE}^-}: \mu_{\text{FE}^+}$	$1.4 \times 10^5: 2.5 \times 10^4$	[83]
			μ_H	2.5×10^4	
		OTS on SiO_2	μ_{DIFE}	6.0×10^4	[84]
			μ_{DIFE}	4.0×10^4	[85]
	SiO_2	RT	μ_{DIFE}	2.4×10^4	[86]
		RT	μ_{DIFE}	$7.0 \times 10^4: 2.1 \times 10^4$	[87]
CVD	hBN	1.6 K	$\mu_{\text{FE}^-}: \mu_{\text{FE}^+}$	6.5×10^4	[87]
			μ_H	2.5×10^4	
	SiO_2	1.6 K	$\mu_{\text{FE}^-}: \mu_{\text{FE}^+}$	$2.7 \times 10^4: 2.4 \times 10^4$	[87]
EG	SiC	4 K	μ_H	2.7×10^5	[88]
		27 K	μ_H	2.0×10^3	[89]
		RT	μ_H	1.8×10^3	[90]
rGO	SiO_2	RT	μ_{FE}	$3.6 \times 10^2-5.0 \times 10^3$	[91]
GNRs	SiC	RT	μ_H	$<3 \times 10^3$ (see Figure 12c)	[93]

^aMobility can be calculated from either field effect (μ_{FE}) transconductance measurements or Hall effect (μ_H), the former of which tends to yield a lower μ at higher carrier density (μ_{FE}^+) and higher μ in lower carrier density (μ_{FE}^-), showing a range in stated values. FET transport models can be used to extract contact resistance and give a density independent mobility (μ_{DIFE}) from the transport data.^[92] Values reported here are for the most part the highest reported results, and typical values are generally within one to two orders of magnitude lower.

control the direction of electron movement like a lens to collimate or focus a beam and guide electrons as quantum wave packets using similar principles to internal reflection, refraction and diffraction of light.^[76-78] Furthermore, doping graphene to the *M* point in the BZ is believed to yield a *d*-wave chiral superconducting state caused by electron-electron interactions.^[79,80]

3. Extrinsic Performance

Real graphene samples, no matter how structurally pristine, are subject to their environment, such as adjacent substrates and gate dielectrics. The properties of graphene, and ultimately electronic performance, are highly dependent on factors such as synthesis and processing techniques, in addition to surrounding materials, exemplified by the large range in carrier mobility shown in **Table 1**.^[12,81-93] Epitaxially grown graphene that is coherently bound to the substrate crystal can have a substrate-induced band gap.^[94] In real devices, the charge neutrality point can be shifted away from zero gate bias, and retardation of the electron transconductance leads to a lower mobility in the n-type regime due to doping.^[95] Remnant charged impurities cause hysteresis in the transport response,^[96] which is detrimental to device performance, but can be mitigated via vacuum and/or annealing. Alternatively, adsorbed species can be engineered to controllably dope graphene.^[97] The use of resist layers for photolithography or electron-beam lithography (EBL) to pattern device structures will leave undesirable residue

that tends to dope graphene.^[98] It is difficult to completely avoid using them in conventional fabrication techniques. However, one approach uses a shadow mask during electrode deposition, though it has a limited feature resolution that is on the order of micrometers.^[99,100]

Annealing graphene after device fabrication is useful to remove adsorbate impurities,^[101] but will not completely remove residue.^[98] Additionally, at high enough temperatures, edges will restructure themselves into lower energy, presumably more ordered configurations.^[102] Suspending graphene facilitates desorption of species underneath the layer during annealing.^[82] Heating the substrate in gas or vacuum helps remove impurities off of the surface, but samples can regain contaminants from the environment. Current annealing can be more efficient, however it risks electrical breakdown and destruction of the graphene channel.^[103] Another albeit tedious strategy to remove residue and improve performance is through contact mode atomic force microscopy (AFM) to mechanically clean the surface.^[104]

SiO_2 is a popular substrate for micromechanically exfoliated graphene, desirable due to the high thickness contrast under optical microscopy.^[105] Although the weak van der Waals interactions keep the π orbitals mostly intact and retain graphene's linear dispersion, the relatively rough oxide surfaces^[106] have a significant influence on its electronic performance of graphene.^[85,107] Puddles of high electron and hole concentration disrupt transport, as conduction behaves like tunneling through an array of quantum dots or along the valleys through

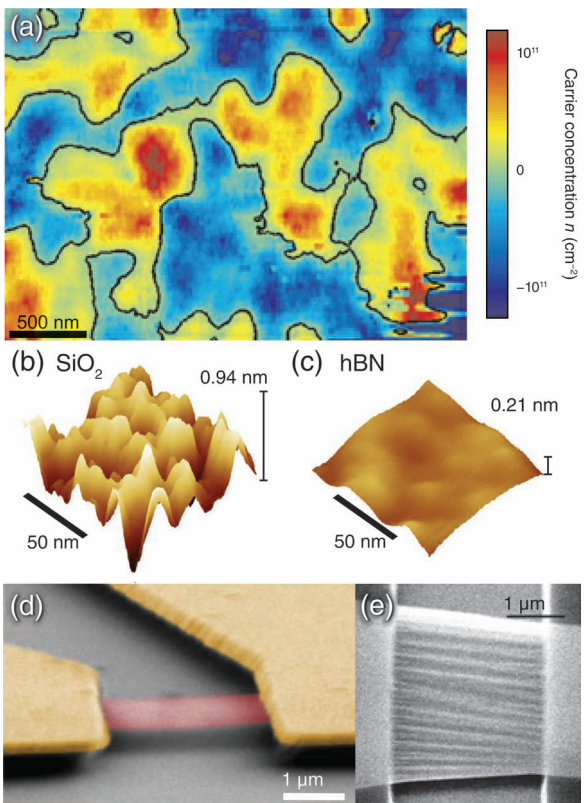


Figure 5. Supported and suspended graphene. a) Electron-hole puddles within graphene samples on a substrate measured through STS. Surface roughness via STM topography images for graphene on SiO₂ (b) and hBN (c) showing the ultraflat hBN surface. d) False-color SEM image of suspended graphene sample (red) between two electrodes (yellow) used to reduce substrate effects such as scattering and improve mobility. e) Ripples in an annealed, suspended sample. a) Reproduced with permission.^[109] Copyright 2008, Nature Publishing Group. b,c) Reproduced with permission.^[119] Copyright 2011, Nature Publishing Group. d) Reproduced with permission.^[64] Copyright 2009, Nature Publishing Group. e) Reproduced with permission.^[132] Copyright 2009, Nature Publishing Group.

the path of least resistance (**Figure 5a**).^[108,109] These puddles can also reduce Anderson localization effects that would otherwise result in a metal-insulator transition at low temperatures in disordered conductors.^[110] Other thin film substrates such as Al₂O₃,^[111] and the ferroelectric oxide PZT^[112–114] (piezoelectric lead zirconate titanate) benefit from higher dielectric constants for enhanced gate response, which is also achieved with top-gate dielectrics of HfO₂,^[115] ZrO₂,^[116] Y₂O₃,^[117] and Si₃N₄.^[118] Attempts to mitigate surface bonding and roughness effects, by using sheets of hexagonal boron-nitride (hBN, “white graphene,” a honeycomb structured insulating compound) as a substrate and gate dielectric reduces scattering and increases mobility (**Figure 5b,c**).^[65,83,87,110,119–126] Alternatively, utilizing a self-assembled monolayer of organic molecules such as octadecyltrichlorosilane (OTS) on an oxide surface has a comparable effect, improving mobility to as high as 6 × 10⁴ cm²/Vs.^[84] Graphene submerged in nonpolar, high dielectric constant solvents help to screen impurities, reduce scattering and improve mobility.^[127] The superior thermal conductivity of diamond substrates is used to increase the current carrying capacity.^[128]

In free suspension (**Figure 5d,e**) graphene behaves like an unstable membrane^[129] and tends to ripple.^[130–133] True two-dimensional crystals were thought to be unstable but do in fact exist:^[3] when unconfined to extra-planar displacements, graphene crystals can have an extra degree of freedom that is sensitive to entropy, and out of plane displacements are required to stabilize the structure. Graphene membranes can roll up^[131,134] and fold,^[135,136] which can strongly impact its electronic properties. Suspending monolayer graphene mitigates substrate effects that enable the highest reported electron mobilities.^[12,82,137] However, a lack of physical support can introduce additional complications in experimental devices (e.g., the electrostatic forces from high gate fields can bend the sheet and lead to rupture of the membrane). Suspended graphene is relatively robust, but the single layer of atoms is prone to ripping,^[138] for example from liquid surface tension during wet processes of transfer, etching, and fabrication of suspended devices. Additionally, this atomically thin membrane is practically impermeable to everything, save hydrogen, as observed in microcapsules sealed with suspended graphene monolayers.^[139] However, stacked layers of oxidized graphene behave as a highly selective water filter: virtually invisible to water, yet air tight to even helium.^[140]

Another important consideration for both fundamental property measurements and practical device design is contact resistance (R_C) and the choice of contact material. This effect was measured and characterized by contact area variation,^[141] transfer length methods (varying gate lengths in a series of devices on a single graphene sample),^[142] and scanning photocurrent microscopy (SPCM).^[143,144] The size of the contacts is also significant at lengths below 200 nm, where contact resistance increases and transconductance is reduced.^[145] Additionally, the presence of the metal itself influences the graphene sample, as it can dope graphene regions directly under the electrode,^[146] which could also be used to tune the electron-hole asymmetry by varying contact length.^[147] Gold is the de facto choice for electrode metals, for its noble properties, high conductivity, and chemical stability. It is consequently relatively unadhesive to graphene or the substrate, and makes poor contact; therefore a thin adhesion layer (e.g., chromium or titanium) is usually required. It is also imperative to choose an appropriate metal with proper work function alignment (i.e., whether it makes an Ohmic or Schottky junction). Some metals (e.g., palladium) make good electrical contact, but have poor adhesion.^[148] These metals can be deposited in a second step, such as in self-aligned fabrication processes.^[149] One study improved the metal-graphene contact by pretreating the contacted area of graphene with a low-power oxygen plasma, seeing over 3 orders of magnitude improvement, and no significant dependence on contact metal work function.^[150] Additionally, to minimize contact resistance effects during measurements, standard four-point probe geometries are used to separate the driven current from the measured voltage, as well as the six-point Hall bar configuration for measuring Hall resistance in magnetic fields. Contact resistance suppresses the on current, which is detrimental to high-frequency transistor performance;^[151] however, in optoelectronics this effect enhances photocurrent efficiency.^[152] Furthermore, ferromagnetic contacts can be used for injecting and detecting spin polarized currents,^[153]

while superconducting electrodes were used to induce a supercurrent through a graphene channel as well as detect Andreev reflections in a Josephson junction.^[154,155]

The electronic transport properties of graphene are of course temperature dependent. Low temperatures are often used to measure the fundamental properties of materials; as there is less noise, even small bandgaps become substantial, but are less practical in real world applications. In suspended samples at low temperatures, the mean free path increases to the order of micrometers, suggesting near-ballistic transport in short channel devices.^[81] Temperature dependence is metal-like at high carrier concentrations, with conductivity decreasing with increasing temperature due primarily to electron-phonon scattering. Near the Dirac point, the conductivity decreases at low temperature in suspended graphene, showing a reduced charge inhomogeneity compared to SiO₂ supported samples. In current-annealed, suspended samples at low carrier densities, the mobility can reach 10⁵ cm²/Vs^[82] at room temperature and 10⁶ cm²/Vs^[12] at liquid helium temperatures.

Distortions lead to an alteration in the electronic properties. Strain produces artificial gauge fields, which physically involves a strange pseudomagnetic effect on the band structure at zero applied magnetic field.^[156,157] Structural deviations break the intrinsic band structure and can locally alter charge transport through distortions, defects, substrates, functionalization, or bends and folds out of the plane. For example, a real but slight paramagnetism is found in graphene with sufficiently separated point defects, such as vacancies via high-energy proton bombardment or fluorine adatoms, but ferromagnetic ordering has yet to be observed.^[158] Evidence for the magnetism of defects in graphene is seen in the vacancy tunable Kondo effect.^[159] Theoretically, precise control of larger vacancies, could lead to piezoelectric behavior due to flexoelectric effects,^[160] or even with selective Li adatom doping.^[161]

Functionalizing graphene with other species can have a significant impact on its properties and is often referred to as chemically modified graphene (CMG).^[162,163] The carbon atoms in pristine graphene adopt an sp²-hybridized scheme, with three σ bonds in plane and a conjugated π orbital out of plane. Upon covalently binding elements or molecules to the surface, the three bonds can be converted to a tetrahedral sp³ configuration and form so-called chair/herringbone and boat configurations. Bonding on the basal plane is typically reversible, for example oxidation is used to facilitate chemical exfoliation before reduction back to graphene, though carboxyl groups on the edges are difficult to remove. Edge passivation is believed to have a significant impact on the electronic properties of graphene, particularly for graphene nanostructures. While theoretical studies have revealed interesting predictions, experiments to date are much less conclusive. Hydrogenation causes a metal-semiconductor-insulating transition, yielding so-called graphane.^[164–166] Other theoretical derivatives include graphone (semihydrogenated graphene) which leads to ferromagnetism,^[167] and graphanol (OH decorated graphene hydrate).^[168] Similarly, fully fluorinated graphene (also called fluorographene or grafane) is a two-dimensional analog to Teflon, which could have a significant impact in similar low-friction applications as well as in devices.^[169–171] Patterned functionalization can be used to create inhomogeneous regions and superlattices.^[172–174] More complex organic molecules can be attached for both chemical and

biomolecular interfacing, useful in photonics, catalysis^[175,176] and sensing^[177] applications. The effects of nanoparticles such as gold or nanodiamond decorating the surface of graphene have also been studied.^[178] Functionalization opens new avenues with exponential possibilities to alter and build off from the basic structure of graphene.

Similarly, substitutional doping, typically with boron or nitrogen will remove or add an electron respectively, and disrupt the structural symmetry and electronic bands in graphene, predicted to create a metal-insulator transition.^[179–183] The trivalent nitrogen atoms can form pyridinic, graphitic, and pyrrolic structures, which are difficult to realize using other growth methods. An n-type transport behavior was observed in nitrogen-doped GFET devices, demonstrating the tunable electronic properties of substitutional doping.^[184,185] Hybrid hexagonal films of boron, nitrogen, and carbon domains could be useful for bandgap engineering and FETs.^[186,187] Carbon isotopes (i.e., ¹³C) can also be introduced during growth for observational purposes,^[188] or for an enhanced thermal conductivity.^[189]

4. Synthesis

Creating high-quality graphene in scalable, economical processes is the first step towards practical application of graphene. Work on isolating graphene has progressed over many decades of research.^[190] The structure of graphite, and essentially graphene as well, was known since the invention of x-ray diffraction crystallography. However, it was unknown whether or not a truly two-dimensional crystal could exist, as extraplanar phonons would be entropically overwhelming over long ranges.^[191] Solution-based exfoliation of graphite (i.e., via oxidation or graphite intercalation compounds (GICs)) gave an early look at realizing atomic planes of carbon.^[192] In the 1960s, Boehm speculated that reducing exfoliated graphite oxide would yield monolayers in solution,^[193] though the term 'graphene' was not coined until 1986^[194] and formally accepted in 1994.^[195] A number of early studies found monolayers of carbon in graphitic structures, formed on various carbide^[196–198] and transition metal^[199–203] surfaces, as early as van Bommel in 1975 with SiC.^[204] These surface science and chemistry studies did not explore any electronic properties, as the strongly bound metallic surfaces disrupt the perpendicular π orbitals, with the exception of SiC. The first electronic measurements of ultrathin graphitic carbon around 2004 required samples sufficiently isolated from its substrate, (e.g., on SiO₂) and ignited an explosion of interest in the field.^[1,205,206] Synthesis techniques can be categorized into micromechanical exfoliation, solution-based and chemically assisted exfoliation, chemical synthesis, epitaxial growth through sublimated SiC surfaces, and the pyrolysis of hydrocarbons on metal surfaces. Each has its own advantages, challenges, shortcomings, and unique features in terms of processability, quality, scalability and cost.

4.1. Exfoliation

4.1.1. Mechanical Cleavage

The exfoliation of graphite is a process in which bulk graphite can be separated into single atomic planes. Attempts prior to

development of the so-called “Scotch tape method” were unable to observe isolated single layers.^[206–208] Ever since the first graphene discovered using micromechanical cleavage of bulk graphite, this method has been widely used to prepare high-quality graphene samples, which is less formally called peeled graphene. The technique is quite simple; utilizing everyday adhesive tape to repeatedly peel layers off of highly oriented pyrolytic graphite and pressing it onto an appropriate substrate, typically but not limited to oxidized silicon.^[105] An initial wet transfer technique was

supplanted by a simpler dry transfer from the tape directly onto the oxide. Sizes of individual crystals can reach millimeter range as seen in Figure 6a, but production suffers from low throughput. Far from scalable, these highly crystalline samples are best suited for the study of fundamental properties such as ballistic transport,^[82] carrier mobility,^[12,209] thermal conductivity^[25] and so on.^[31,210] Although the mechanical exfoliation approach can produce the best quality graphene to probe intrinsic performance limits, it is hardly applicable for any practical applications.

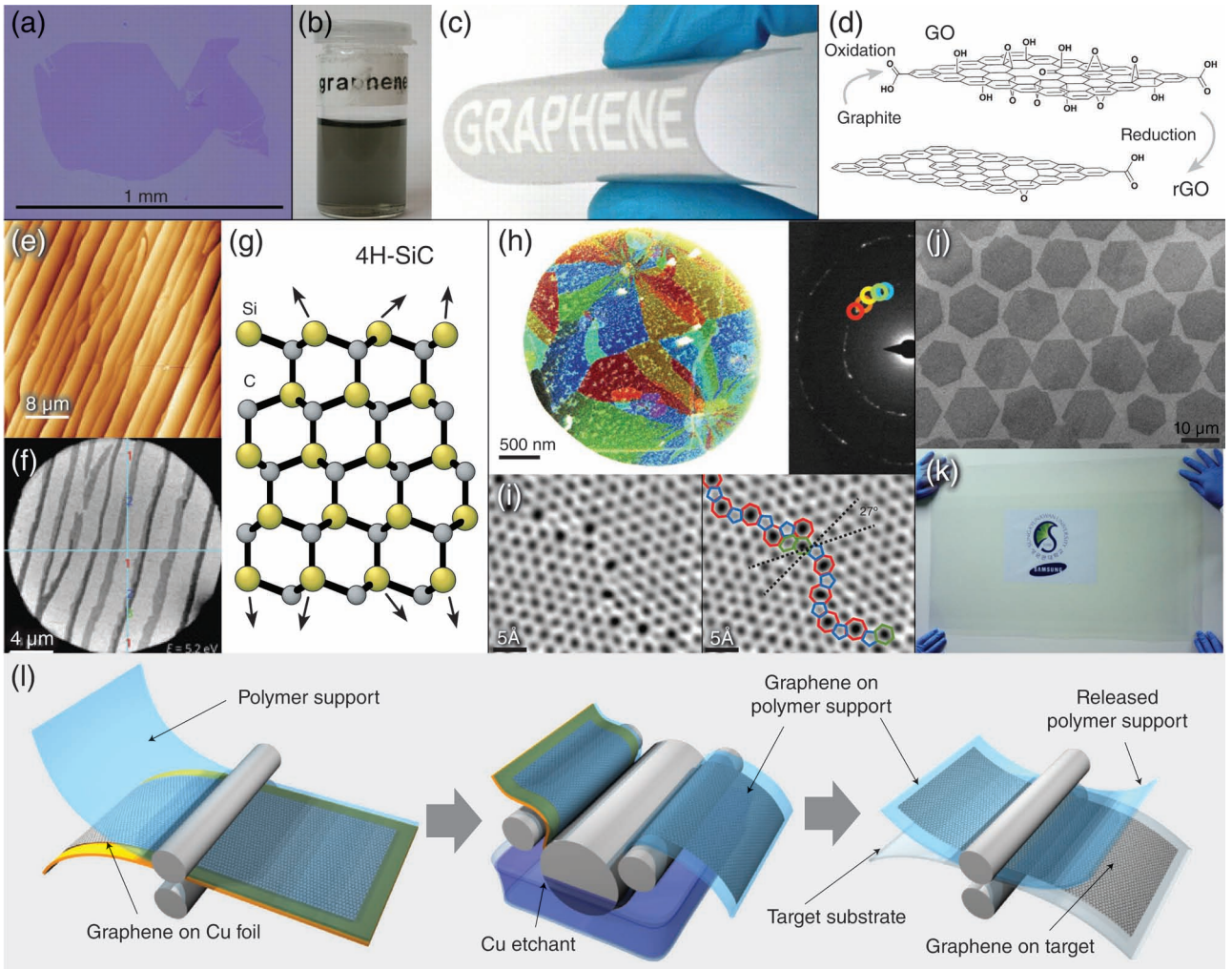


Figure 6. Synthesis techniques. a) Optical microscopy image of a very large micromechanically exfoliated (tape method) monolayer of graphene. Note the considerable contrast for the single atomic layer. b) Photograph of dispersed graphene by ultrasonic exfoliation of graphite in chloroform and (c) that deposited on a bendable film. d) Graphene oxide and reduced graphene oxide showing the remaining oxygen-rich functional groups after reduction. e,f) OM and SEM images of graphene grown epitaxially on SiC. The number of layers is shown in (f), with multiple layers forming at step edges. g) Crystal structure of 4H-SiC with Si (top) and C (bottom) faces. h) False-colored dark-field TEM reconstruction of CVD graphene domain patchwork. Each color is a domain with a certain lattice orientation (left), imaged separately using the corresponding diffracted beams for crystal-orientation-dependent contrast (right). i) High-resolution ADF-STEM of a domain boundary in CVD graphene showing a rotational mismatch of 27° and a series of pentagon-heptagon pairs (Stone-Wales defects) along the boundary. j) SEM of an array of seeded growth hexagonal domains of CVD graphene on copper. k) Large-area graphene transferred using roll-to-roll production spanning 30 inches diagonally. l) Schematic of the roll-to-roll process showing adhesion to a thermal release tape polymer support, run through an etching medium to remove the copper foil, before being released via heat treatment from the polymer support onto the final substrate. a–c) Reproduced with permission.^[4] Copyright 2009, American Association for the Advancement of Science. d) Adapted.^[219] e,f) Reproduced with permission.^[89] Copyright 2009, Nature Publishing Group. g) Redrawn.^[336] h,i) Reproduced with permission.^[274] Copyright 2011, Nature Publishing Group. j) Reproduced with permission.^[275] Copyright 2011, Nature Publishing Group. k,l) Reproduced with permission.^[364] Copyright 2010, Nature Publishing Group.

4.1.2. Solution and Chemical Exfoliation

Chemical exfoliation of graphite in solution represents one potential approach to high volume production of graphene. As opposed to direct physical cleavage, chemicals are used to intercalate bulk graphite by inserting reactants between layers that weaken the cohesive van der Waals force.^[211] Dai's group was the first to report success in producing high-quality, single-layer graphene sheets, stably suspended in organic solvents by steps of chemical intercalation, reintercalation, and sonication.^[212] They first heated expandable graphite in sulfuric acid and nitric acid, where most of the exfoliated particles found in the reacted solution are still multiple layers thick. An oleum treatment following with tetra-butyl alcohol reintercalation is the key step for high-quality single layer graphene. About 90% of graphene sheets are in single layer form after sonication in a surfactant solution based on AFM measurements. A liquid exfoliation approach has also been reported to produce graphene by sonicating graphite powder in N-methylpyrrolidone.^[213] A homogeneous colloidal suspension of graphene sheets or ribbons can be made simply by stirring in surfactant solution.^[214] The library of available exfoliating solvents has expanded: some belong to a peculiar class of perfluorinated aromatic molecules and an assortment of other suitable dispersing media.^[215] Low-power sonication for weeks at a time to avoid the damage of the graphene sheets yields a high concentration (up to 1.2 mg/mL up to 4 wt%) of monolayer graphene.^[216] Sonication-free, mild dissolution of graphite by synthesizing well-documented GICs achieved large graphene flakes and ribbons.^[217]

4.1.3. Oxidation and Reduction

A more efficient way to obtain large volumes of graphene is by firstly synthesis of graphite oxide, then exfoliation into monolayers, and finally reduction to remove the oxygen groups (Figure 6d).^[218,219] Each oxidized flake possesses a large number of negative charges and repels one another. The Brodie, Staudenmeier and Hummers methods are the three most common ways to oxidize graphite. Among these, a slightly modified Hummers method has become the most popular in producing graphite oxide, for its relatively shorter reaction time and absence of toxic side products.^[219] After oxidation, the interlayer spacing increases from 0.34 nm in graphite to above 0.6 nm, with weakened van der Waals forces between the layers. Exfoliation is typically augmented with sonication,^[220] yielding single layers of graphene oxide (GO),^[221] which are soluble in water without the assistance of surfactants to form a stable colloidal system.

Many methods of removing the oxygen from the GO structure through chemical,^[222] thermal,^[223] electrochemical^[224] or electromagnetic flash^[225] and laser-scribe^[226] techniques have been successful, but generally resulted in inferior samples which are hence more precisely named reduced graphene oxide (rGO). GO films reduced via chemical methods typically use highly toxic hydrazine,^[220,222,227–230] while less effective but more environmentally friendly alternatives exist such as Vitamin C^[231] or *Escherichia coli* (*E. coli*) bacteria.^[232] Homogeneous colloidal suspensions of electrically conducting graphene are stable in many organic solutions in the presence of either a polymer or a surfactant.^[222] Solutions without these extraneous surfactant

agents are also possible by changing to an alkaline condition, with single sheets up to 40 μm in diameter.^[230] Chemical reduction usually cannot completely remove all the oxygen in GO, leading to relatively poor electrical quality when compared to pristine graphene.^[233] Electrochemical reduction is an eco-friendly and economical option, producing high-quality rGO in large scales.^[224,234,235] The reduction of GO films on graphite electrodes can be effectively tuned by varying the applied potential.^[224] Thermal treatment is another way to reduce GO^[223] by heating in alkaline conditions^[236] or with microwave irradiation.^[237] Thermal reduction can be combined with chemical treatments to achieve more complete removal of oxygen.^[238–240] A room temperature, chemical-free flash reduction process uses an instantaneous photographic camera flash to trigger photothermal reduction.^[225,241] Commercial optical-drive-based laser-scribes were used to pattern and tune reduction along a disc coated with GO.^[226] Photochemical methods were found to effectively reduce GO by UV-irradiation of a mixture with TiO₂ particles suspended in ethanol.^[242]

4.2. Epitaxy on Silicon Carbide

Epitaxial graphene (EG) growth on silicon carbide (SiC) surfaces is an effective bottom-up approach to create carbon-based electronics, which has been demonstrated on wafer scale.^[243,244] The pioneering work on EG was conducted by heating 6H-SiC in ultrahigh vacuum (UHV) in the temperature range of 1200–1600 °C.^[205,245–248] The silicon atoms on the surface sublimate at high enough temperature and the exposed carbon atoms reconstruct to form graphitic layers (Figure 6e–g). EG can grow on both the C-terminated (0001) and Si-terminated (0001) surfaces, though films grow much faster on the carbon face.^[249,250] The primary difference between graphene formed on the C-terminated and the Si-terminated surfaces is the weak and strong coupling of both the substrate and successive graphene layers.^[250] Selective synthesis of EG on a templated substrate was demonstrated by using patterned AlN caps.^[251,252] Surfaces of cubic 3C-SiC (β -SiC) are also capable of epitaxial growth, with low interface interaction, and cheaper, commercialized β -SiC/Si wafers.^[253] Most EG growth is accomplished in UHV; however, larger, several-micrometer domains have been obtained in an argon atmosphere.^[89] Direct growth of graphene nanoribbons has been achieved on prefabricated SiC (110n) nanofacets, utilizing crystal plane selective growth rates from a lowered surface free energy. SiC offers a suitable insulating structure in which devices can be fabricated with a sufficient buffer layer that isolates the graphene π orbitals, keeping the linear dispersion intact. Transferring EG to arbitrary substrates using thermal release tape has been accomplished, without a significant drop in carrier mobility.^[254] Industrial scale growth on SiC is primarily limited by the high cost of single-crystal SiC wafers.

4.3. Chemical Vapor Deposition

Chemical vapor deposition (CVD) method has emerged to be one of the most promising techniques for the large-scale

production of single and multiple layer graphene films. Uniform, wafer size graphene films have been grown on both single crystal and polycrystalline transition metal surfaces at high temperatures by pyrolysis of hydrocarbon precursors such as methane.^[255–259] Figure 6k shows the largest continuous area of CVD graphene reported to date: 30-inch diagonal length, grown on copper foil in an 8-inch diameter quartz tube at low pressure.

The number of graphene layers depends highly on the carbon solubility of the substrate. For metals with relatively high carbon solubility, such as nickel,^[96,260,261] the carbon atoms can dissolve at high temperature, then precipitate onto the metal surface and form single or multilayer graphitic films upon cooling. These non-uniform films with a wide thickness range from 1 to around 10 layers with monolayer domain sizes up to several tens of micrometers in diameter were produced on nickel substrates.^[262] The thickness and crystal ordering can be controlled by the cooling rate and hydrocarbon gas concentration. On the other hand, low carbon solubility in certain transition metals, for instance copper^[263] and platinum^[264] enables complete monolayer coverage.^[265] Under typical atmospheric pressure (APCVD) conditions, the graphene growth is mainly limited by mass transport through the boundary layer, while the surface reaction is the rate-limiting step at low pressure (LPCVD).^[188,265,266] The predominately uniform monolayer graphene grown by the LPCVD method is proposed by the self-limiting nature of the growth process.^[265] Lattice mismatch between the metal surface and graphene typically forms a pseudodomorphic interface and generally displays a moiré pattern as well as lattice strain. Graphene epitaxially grown on single crystal metal substrates can avoid surface defects on the metal grain boundaries and help to mitigate orientation mismatch, however still has significant misaligned domains and grain boundaries.^[256,267–269] Polycrystalline films offer a more economical alternative that is still capable of large domains without noticeable performance difference within individual domains.

Yan and coworkers broke the self-limiting effect of the LPCVD process to enable second layer growth on prepared monolayer graphene using a fresh copper foil placed in the high-temperature upstream regime. Bernal AB-stacked bilayer graphene is possible with coverage area as high as 67%, which shows typical gate response.^[270] Furthermore, Chen and coworkers report the synthesis of controllable mono- and multi-layer graphene films on Cu_{0.69}Ni_{0.31} alloy foils by LPCVD. By using the alloy of low- and high-solubility catalysts, both thickness and quality of the films can be controlled by the growth temperature and cooling rate.^[271]

A better understanding of the mechanisms of graphene growth is demanded for controlling domain size and number of layers. Different combinations of temperature and pressure benefit lower nucleation rates as opposed to faster growth and fuller coverage. A two step CVD synthesis was therefore developed with different parameters for the nucleation and growth phases, yielding domains hundreds of square micrometers large^[272] and later millimeter sizes.^[273] The shape of domains during growth dictates the final morphology, and varies under different conditions between stochastic structures,^[274] hexagonal shapes that follow lattice symmetry,^[275] and more erratic flower-like structures.^[272]

From a practical point of view, it is desirable to reduce growth temperatures. To this end, it has recently been demonstrated that graphene can be grown at a temperature as low as 300 °C using a liquid benzene hydrocarbon source.^[276] Plasma enhanced CVD (PECVD) can achieve growth at moderate temperatures ≈700 °C.^[277–279] A laser-induced CVD process writes line patterns of graphene directly by irradiation with a focused laser beam (5 W, 532 nm wavelength, 20 μm spot size) on a thin foil in a low-pressure system at room temperature.^[280] Localized heating decomposes the gas, with a growth rate thousands of times faster than typical thermal CVD.

Instead of using the hydrocarbon gases as the carbon precursors, solid state carbon sources such as poly(methyl methacrylate) (PMMA) or even table sugar, virtually any carbon-based material, is shown to produce graphene on select metal substrates at high enough temperature.^[281] By controlling the Ar/H₂ gas flow ratio, monolayer, bilayer, or few-layered graphene can be grown using a copper thin film catalyst on SiO₂/Si substrates with a 100 nm thick spin-coated PMMA film at temperatures as low as 800 °C.^[282]

Graphene grown on metal foils is not particularly useful for electronic applications without transferring it to an insulating substrate. The transfer process adds additional complications to the quality and consistency of samples such as cracking and polymer residue.^[283] It would be very desirable for a CVD process that eliminates this transfer step (i.e., deposition directly onto arbitrary substrates, particularly insulating oxides or hBN).^[284–286] Techniques to avoid the extra processing step use thin metal films on insulating substrates that are removed during^[287] or post growth,^[288–290] or with remote catalyzation by copper atoms in the atmosphere.^[291] Other attempts are completely metal-free, which loses the self-limiting catalyzed reaction.^[285,292] A promising approach to isolating CVD graphene from its metallic growth substrate and regain its intrinsic electronic properties is through intercalation with a buffer layer such as Si.^[293] Typically, the convenience and practicality of transfer-free growth is at the expense of quality and performance.

Another useful feature of CVD is the ability to dope graphene with substitutional impurities by introducing other gases during growth, such as ammonia (NH₃) or borane (BH₃). This simple approach uses nitrogen and boron to displace normal carbon atoms within the lattice. Alternatively, annealing under ammonia atmosphere or ion bombardment offer post growth routes towards nitrogen-doping.^[294]

4.4. Chemical Synthesis

Another alternative route for the controllable production of graphene is bottom-up organic synthesis. Graphene can be composed of interconnected polycyclic aromatic hydrocarbons (PAHs), which are very small two-dimensional graphene segments. This approach is attractive due to its high versatility and compatibility with various organic synthesis techniques.^[295] Müllen and coworkers are pioneers in this field, reporting synthesis of nanoribbon like PAHs with lengths over 30 nm.^[296,297] Recently, the largest stable colloidal graphene quantum dots were synthesized using a benzene-based chemical route, which compose 132, 168, 170 conjugated carbon atoms.^[298,299]

However, the size of the as-grown graphene dots is limited due to decreasing solubility as sizes increase as well as an increasing number of possible side reactions, which is still a major challenge for organic synthesis of graphene molecules with controllable shapes, sizes and edge structures.

5. Characterization

Its atomic thinness and often-microscopic size make graphene difficult to spot. The ability to identify and characterize graphene is a key component in its discovery and continued success. For practical application and quality control, it is important to identify the number of layers, structure, and electronic quality. Fortunately, many approaches from subjective observation to accurate spectroscopic analysis offer their own advantages. Multiple complementary approaches are often used together to achieve robust and verifiable characterization.

5.1. Optical Microscopy

Early on, in conjunction with the micromechanical peeling technique, simple optical microscopy was the de facto method for classifying layers on thin film oxide (280–300 nm) on silicon substrates. So-called Fabry–Pérot interference in the dielectric surface layer governs the diffracted intensity that produces contrast between graphene and the underlying substrate, based on thickness.^[300,301] A slight contrast difference between mono-, bi- and few-layer graphene is enough to distinguish samples under conventional optical microscopes with a trained eye. Furthermore, the wavelength and the incident angle of the illuminated light were found to be another factor to modulate the optical contrast.^[105,184] A novel technique to optically characterize arbitrarily large domains within CVD graphene on any substrate utilizing the birefringence of polarized liquid crystals coated on the surface.^[302] The near ubiquity of optical microscopy and adhesive tape in laboratories lowered the barriers to entry and contributed to the fast growth of the field. The low throughput of manually finding individual samples and the imprecise thickness distinguishability limit its practical use industrially.

5.2. Electron Microscopy

Electron microscopes are vital tools in nanoscience and have many advantages over conventional optical microscopy, yielding alternative methods to identify and characterize graphene. However, exposure to electron beams with enough energy is destructive, and will unavoidably alter the pristine structure of graphene, causing defects that alter its properties.^[303] Scanning electron microscopy (SEM) can provide rapid examination of graphene grown on both metals and dielectrics. The contrast of SEM images is mainly induced by the different conductivity between the CVD graphene and exposed metal surface,^[304] while graphene on dielectric surfaces are generally less distinguishable. The dark area is the graphene film while the light area is the exposed metal oxide surface, which is oxidized by air after unloading the sample from the CVD reactor.^[305]

Transmission electron microscopy (TEM) is a powerful tool, which can show the atomic features of single layered graphene (Figure 1b). A direct, high-resolution imaging of the graphene lattice clearly reveals each individual carbon atom arranged in the honeycomb structure.^[306] The atomic lattice, defects and surface contamination can also be depicted in high-angle annular dark-field (HAADF) images using scanning transmission electron microscopy (ADF-STEM) and further characterized with electron energy loss spectroscopy (EELS).^[274,306–308] Additionally, graphene has helped advance TEM technologies: suspended over a grid, it can be used as ultrathin support material for various samples.^[309,310] Two layers can even encapsulate water droplets for a unique exploration of transmission through liquids and species in solution, which is otherwise prevented by high-vacuum conditions.^[311]

5.3. Scanning Probe Microscopy

Scanning probe microscopy, including AFM and scanning tunneling microscopy (STM) are the most powerful tools for determining layer thickness and structure as well as scanning tunneling spectroscopy (STS) to probe the electronic properties.^[312,313] The detection limit is about 0.1 nm in AFM, which is suitable for imaging of a step height ≈ 0.34 nm per layer. However, due to the varying interactions between the AFM tip and graphene or the supporting substrate, it is difficult to obtain the precise theoretical thickness. Moreover, it can be even worse if the graphene surface adsorbs a thin layer of water or other contaminants. Such complications introduce a variety of reported data for single layers using AFM, with thicknesses ranging from 0.4 to 1.0 nm. In general, AFM can only give topographic contrast, which cannot distinguish graphene from its oxide using typical operation modes. Phase imaging of AFM is found to distinguish between a freestanding graphene and a functionalized layer. This is due to the variation of the interaction forces between the AFM tip and the attached functional groups.^[314] STM has been used to observe the electronic topography of graphite for a long time.^[315] Since the synthesis of polycrystalline graphene through epitaxy or CVD, STM has been widely used to reveal graphene domains and grain boundaries.^[275] The electron densities of the six carbons are completely equivalent on the STM images of graphene, which shows the high crystal quality of the samples.^[316] In STM, in addition to high-resolution TEM, moiré patterns are observed in graphene on various substrates with slight lattice parameter mismatch or rotated crystals in multilayer graphene on SiC, showing the non-epitaxial relation of the layers.^[119,317,318]

5.4. Raman Spectroscopy

Raman spectroscopy has emerged as a convenient way to efficiently distinguish the crystal quality, layer thickness, mechanical strain, and even edge structures of graphene (Figure 7). The fingerprints of graphene under Raman spectroscopy are D, G, and 2D (G') peaks at about 1350 cm^{-1} , 1580 cm^{-1} , and 2700 cm^{-1} , respectively, with a smaller D' peak near 1620 cm^{-1} .^[319] The G peak is introduced by in-plane optical

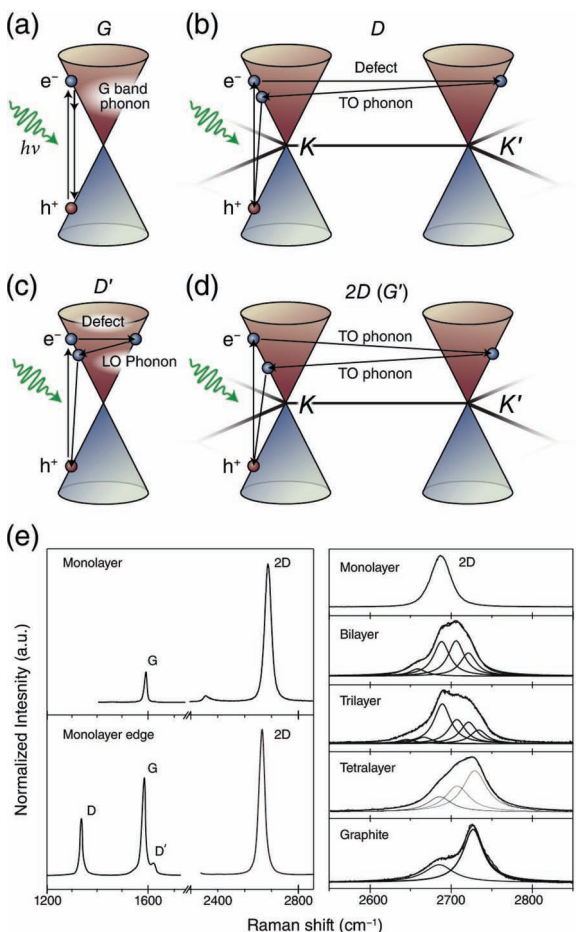


Figure 7. Raman spectroscopic characterization. Schematic band diagrams of Raman resonance pathways for (a) G, (b) D, (c) D', and (d) double resonance 2D (G') peaks of monolayer graphene. e) Raman spectroscopy of pristine (upper left) and at an edge (lower left) of a monolayer, showing D, G, D' and 2D (G') peak heights and 2D peaks of 1 through 4 layers and bulk graphite (right), showing the broadened FWHM and multipoint fits for multilayers. a-d) Redrawn.^[319] e) Reproduced with permission.^[319] Copyright 2009, Elsevier.

vibrations of the sp^2 -bonded carbon atoms (degenerate zone center E_{2g} mode), whereas the 2D peak arises from second-order zone boundary phonons. The D peak is attributed to first-order zone boundary phonons, which is absent from defect-free graphene, and is therefore a useful measure of quality. It has also been shown that the quality and layer number of the peeled graphene can be determined by the shape, width, and position of the 2D peak.^[320] Figure 7e shows how the number of graphene layers changes the number of subpeaks present, increasing the full-width at half maximum (FWHM) of the 2D peak and upshifting in wavenumber, while the peak height is roughly unchanged. In a single layer, the D⁺ and D⁻ subpeaks degenerate into a single 2D peak, while in a bilayer it splits into 4 subpeaks. The G peak of single layer graphene is found upshifted 3–5 cm⁻¹ from bulk graphite and is much less intense. The position and the height ratio of peaks between G and 2D bands vary with the number of layers: the relative G peak intensity is about 10% to 50% of the 2D height for

monolayers, roughly equivalent in bilayers, and higher than the 2D peak in few-layer (>2) graphenes and bulk graphite.

The splitting and shifting of Raman peaks can also indicate strain relaxation between the graphene and supporting substrate. For instance the blueshift of the G and 2D peaks of graphene grown on SiC is mostly induced by the compressive strain from substrates when the sample is quenched after growth,^[321] while compressive strain of peeled graphene yields a redshift.^[322] Tensile strain can also redshift both peaks as well as split the G peak into otherwise degenerate G⁺ and G⁻.^[323] The frequency and intensity ratio of the G and 2D peaks is also found to be modulated by charge carriers: the G peak stiffens and sharpens for both n- and p-type samples, and the ratio of the intensities between the G and 2D peaks shows a strong dependence on doping.^[324] At graphene edges, the intensity of the D peak is strong at armchair but weak at zigzag type edges.^[325]

5.5. Photoelectron Spectroscopy

A powerful, yet complex tool for analyzing the electronic structure of graphene is through photoemission spectroscopy. A widespread surface analysis technique, this process illuminates the sample with high-energy photons that excite electrons into vacuum for detection, measuring the kinetic energy of the photoelectrons, in coordination with the incident photon energy. X-ray photoelectron spectroscopy (XPS) reaches core level electrons, and yields the composition and some bonding information from the binding energy, averaged over a large area. This is useful for instance with doping or functionalizing graphene, or in determining the degree of reduction of GO.^[184,326–329] EG on different SiC faces has also been studied chemically with XPS,^[218] and structurally using x-ray absorption to analyze disorder.^[330]

On the other hand, using lower energy ultraviolet light, valence electrons are emitted and probed to investigate the band structure. By measuring the angle and direction of the photoelectrons in conjunction with the particles' momenta, one can effectively map out the valence band of the sample's electronic structure: so-called angle-resolved photoemission spectroscopy (ARPES). This powerful tool plots the Dirac cone structures of graphene on substrates^[331] and suspended samples,^[332] as well as more complex distortions of these cones due to quasiparticle interactions (e.g., electrons with other electrons, phonons and plasmons) and environmental influences such as dopants.^[53,55,333] The pseudospin and Berry's phase of monolayer and bilayer samples is observed by a crescent ring around the Dirac points in k -space by utilizing circularly polarized light.^[55,334,335] Additionally, induced bandgaps have been observed using ARPES in epitaxial graphene adhered to a SiC substrate^[94,336] and patterned adsorption of hydrogen.^[173] Photoemission experiments are quite costly, as they require UHV and ARPES typically utilizes synchrotron light sources.

6. Metallic and Passive Components

Graphene is intrinsically metallic and can be found in a number of promising applications utilizing it as a passive conducting component.^[337] Use of graphene as a conductor

takes advantage of the exceptionally high conductivity considering its incredibly small form factor. The sheet resistance of an undoped pristine graphene monolayer is around $6\text{ k}\Omega/\square$ at the charge neutrality point.^[3] The conductivity can be increased by using electrostatic doping, or more practically via chemical doping, to increase carrier concentration. Additional advantages include its exceptional transparency, surface area, mechanical strength and flexibility.

6.1. Transparent Conductors

Transparent conductors (TCs) are an essential part of a number of technologies, in particular display panels and other photonic devices. The basic requirement is that one side of the device must allow light to pass in or out while simultaneously acting as an electrode, and they are typically used in a planar geometries. Different technologies have specific needs, but ultimately all of them rely heavily on the conductivity and transparency of the material. Traditional TCs typically consist of highly doped semiconducting oxides such as indium tin oxide (ITO), and are limited by several factors, including mechanical brittleness that makes them unsuitable for flexible displays; the short supply of indium that dramatically inflates prices; and diffusion of indium atoms that contaminate the neighboring films and degrade device performance (particularly in more sensitive and degradable organic solar cells or light emitting diodes). To sustain the continued increasing demand in TCs, new technologies must be developed to supplement or even replace ITO; carbon-based films among other nanomaterials could prove much more economical and versatile.^[338,339] Here, the current status of graphene-based TCs and flexible electronics is recounted.

Single layers of graphene can exhibit uniform, high optical transparency $\sim 97.7\%$ throughout the visible light regime (Figure 8a) with decent sheet resistance ($\sim 0.1\text{--}6\text{ k}\Omega/\square$) depending on quality and doping. It can therefore be explored as a new TC. To use graphene for TCs, it must be supported by a solid transparent substrate such as glass or plastics. There are two main strategies for the fabrication of graphene TCs: solution deposition of interconnected graphene flakes, and transfer of continuous (typically CVD) graphene onto transparent substrates. Although films derived from CVD and peeled graphene offer superior performance, solution derived films are far more cost effective and easily scaled. GICs introduced into mechanically exfoliated few-layer graphene such as vapor exposure to FeCl_3 help to enhance conductivity with greater transparency compared to ITO films of similar sheet resistance.^[340]

Solution-processed graphene films are formed on substrates as a contiguous network using vacuum filtration,^[341] Langmuir–Blodgett assembly^[342] and transfer,^[343,344] printing,^[345,346] drop-casting,^[91] dipping,^[347] spraying,^[233] or spin-coating^[239] approaches. Other flexible, though usually opaque, macroscopic structures can be created such as GO and rGO paper,^[229,237,348–350] typically through vacuum filtering, as well as three-dimensional graphene foams and aerogels formed through freeze-drying,^[351,352] and supercritical drying^[353] of aqueous solutions, or directly grown using CVD.^[354,355] Typically, graphite oxide is used for processing, but is itself insulating, and must be reduced either before or after film deposition to be useful as

a TC. Annealing at both low and high temperatures has been used to facilitate reduction and solidify the percolation network of solution deposited graphene flakes, which can greatly reduce the resistance down to $800\text{ }\Omega/\square$ at 82% transmittance for rGO films.^[280,347] Some applications, such as with polymer substrates may not benefit from annealing as the high temperatures may destroy other parts of the device. Hybrid structures and composites, with a silica matrix,^[356] metallic grid,^[357] or carbon nanotubes^[358,359] mixed with graphene have been used to form TC films. The graphene-silica network films obtained this way typically have a transparency as high as 94% with a sheet conductivity of 0.45 S/cm , while carbon nanotube hybrids with sheet resistances as low as $240\text{ }\Omega/\square$ have transparency of 84%.

Alternatively, a continuous film of graphene can be used as a TC. Large area graphene can now be readily grown on metallic foil through the CVD approach with the sizes only limited by the size of metallic foil and the reaction furnace. However, the CVD grown graphene is generally bound to an opaque material rendering it useless for TCs. Unless technologies capable of controllable growth of quality CVD graphene directly on a transparent insulator improve, it must be transferred from the growth metal substrate to the transparent substrate.^[360–363] A number of methods to transfer graphene sheets have been developed, for example applying a transfer material such as PMMA to secure the graphene while the underlying substrate can be etched away. In particular, a scalable roll-to-roll process was recently developed to transfer 30-inch graphene onto a flexible polyethylene terephthalate (PET) substrate (Figure 6l).^[364] Here the CVD graphene on copper foil is first rolled onto a thermal release tape and run through FeCl_3 to etch the copper before transfer to the final PET film. Multiple transfers can also be applied to obtain multiple layer graphene to further improve the conductivity. With four layers of graphene, a sheet resistance as low as $30\text{ }\Omega/\square$ along with 90% transmittance is achieved.

In general, TCs have a transparency proportional to sheet resistance and inversely proportional to thickness (Figure 8b). Optimization of these two parameters is needed to meet the different requirements of specific applications. These analyses show that graphene has a transmittance and sheet resistance combination comparable to conventional ITO films, and can be a viable alternative technology. Many devices that utilize TCs can benefit from using graphene electrodes such as transparent transistors,^[365–367] displays, touch-pans, and optoelectronics.

6.2. Flexible Electronics

With excellent mechanical strength and elasticity in addition to its electronic properties, graphene on a flexible substrate can offer exciting opportunities for bendable, rollable, foldable, and stretchable electronics.^[368] A CVD graphene TC-based organic solar cell was capable of 138° of bending without degradation, while an ITO control film failed after 60° .^[369] Graphene can also allow for flexible and transparent integrated circuits, demonstrating gigahertz operation with solution-processed films.^[370] A major characteristic necessary for flexible electronics is the robustness in both the structure and the electrical properties upon flexing over numerous cycles. A flexible, semitransparent

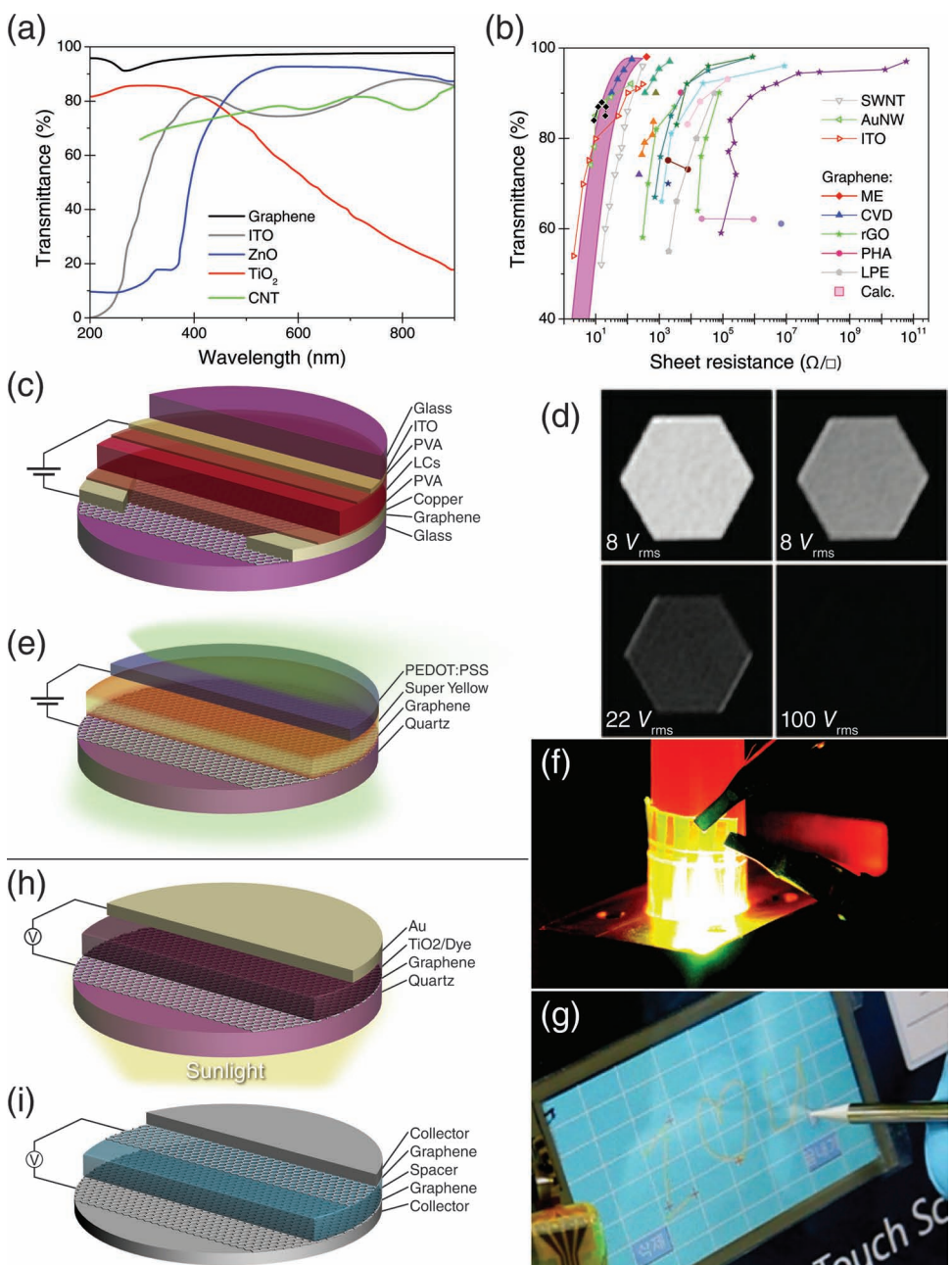


Figure 8. Metallic components. a) Transmittance vs. wavelength compared to other TCs. b) Transmittance vs. sheet resistance of graphene (solid shapes) and other materials (hollow triangles). The lowest sheet resistance graphene samples are CVD graphene [364] and FeCl₃ intercalated, ME few-layer graphene [340]. c,d) Device schematic and performance of a graphene-based LCD. e) A light-emitting electrochemical cell, using graphene and poly(3,4-ethylenedioxythiophene) (PEDOT) as transparent electrodes and n-/p-doped Super Yellow (SY) polymer as the active emitter. f) Photograph of the transparent cell bent around a secondary red light. g) Photograph of a CVD graphene-based resistive touch screen. h) A dye-sensitized solar cell with graphene TC. i) An ultracapacitor unit cell using two stacked CMG electrodes with a porous spacer impregnated by electrolyte, sandwiched by metal-foil current collectors. a) Reproduced with permission.^[376] Copyright 2010, Nature Publishing Group. b) Redrawn.^[340,376] c) Redrawn.^[375] d) Reproduced with permission.^[375] Copyright 2008, American Chemical Society. e) Redrawn.^[383a] f) Reproduced with permission.^[383b] Copyright 2011, American Chemical Society. g) Reproduced with permission.^[364] Copyright 2010, Nature Publishing Group. h) Redrawn.^[238] i) Redrawn.^[421]

memory device concept with limited functionality but good mechanical stability was recently demonstrated with multilayer graphene electrodes, which are able to withstand over 10⁴ cycles flexing without much device variation.^[371] A memristor type device based on spin-coated graphene oxide shows promise for

cheap, flexible, non-volatile memory, at a sacrifice of storage density compared to rigid metal oxide memristors.^[372] Many types of electronics could find their way into bendable devices, such as displays, data storage, sensors,^[373] solar cells, wearable nanogenerators, and energy storage. Printable devices utilizing

graphene-based conductive inks offer a relatively inexpensive and scalable approach to fabricating flexible electronics.^[374]

6.3. Displays and Light-Emitters

Liquid crystal display (LCD) devices using peeled graphene on glass slides as the TC cathode have been demonstrated (Figure 8c,d).^[375] To fabricate the device, a copper layer is deposited with a window less than 10 μm wide around the graphene. An alignment layer of polyvinyl alcohol separates the electrode from the liquid crystals and dopes the graphene, which increases the electron carrier concentration to 10^{12} cm^{-2} and reduces the sheet resistance down to $400 \Omega/\square$. This low resistance is impressive for a monolayer of graphene that transmits roughly 98%, comparing favorably over the 95% transmission of ITO films of similar resistance. Similarly, polydispersed liquid displays^[376] or electrochromic devices^[377] could utilize graphene TCs in smart windows that can turn opaque and transparent or even different colors electronically without physical blinds.

Light emitting diodes (LEDs) and other photonic devices are able to utilize graphene as a transparent and flexible electrode. An array of GaN-based LEDs with patterned, multilayer CVD graphene TC electrodes demonstrate scalable fabrication.^[378] Organic LEDs (OLEDs) are a newly commercialized technology for displays that contain electroluminescent polymer-based active regions, and have been shown to enable ultrathin, flexible screens. Many light-emitting device concepts have utilized carbon-based TC films with nanotubes^[373,379] and graphene as the anode^[380–382] as well as the cathode.^[383a,b,384] A completely carbon-based light-emitting electrochemical cell was made using a graphene cathode, and an anode made of conducting polymer (Figure 8e,f).^[383a,b] Matching electrode work functions for efficient injection of electrons and holes into the active layer's lowest occupied molecular orbital (LUMO) and highest occupied molecular orbital (HOMO) respectively is critical. Graphene has a comparable work function to ITO, at around 4.5 eV, which can be slightly tuned by doping.^[91,385,386] Another study created a hybrid GO sheet functionalized with aryl diazonium salts, which fluoresce blue light, blueshifted from the intrinsic cyan color of the individual monomers.^[387] Graphene itself can also be photoluminescent after oxygen plasma treatment,^[388] or by moderate reduction of GO.^[389]

6.4. Touch Panels

Two main touch screen varieties exist, based on either resistance or capacitance changes of spatially resolved touching of the display panel. Resistive-based devices use physical means to alter the resistance when the screen is pushed in with a stylus or finger, but can be somewhat less accurate with poor responsivity. The roll-to-roll production of large area graphene conductive films have been implemented into a typical four-wire resistive touch screen (Figure 8g).^[364] The device works by having two conductive films, separated by spacers. When the front panel is pushed in, it makes contact with the underlying layer between the spacers, creating a change in resistance dependent on the specific spot at which the films touch. A

biaxial array of spacers makes a two-dimensional map of where the screen is being touched.

Capacitive touch screens have seen major growth as the dominant touch screen technology for many applications in consumer electronics. Utilizing a transparent conductor on one side connected to a capacitance sensing circuit, a conductive bare finger can be used to complete the capacitor to determine touch location. Graphene has not yet been implemented in such a device, but it could certainly benefit from the same useful qualities it provides.

6.5. Energy Harvesting and Storage

Graphene is a promising material for a number of energy related applications.^[390] Solar cells and similar light harvesting devices depend heavily on TC films. Solution-processed^[391] and CVD^[392] grown graphene TCs have been implemented for inorganic,^[97,393] organic,^[91,394–398] hybrid,^[399] and dye sensitized^[238,400] solar cells (Figure 8h). In particular for dye sensitized solar cells, graphene can be incorporated into the TiO₂ electron transport material and anode to reduce the recombination rate for improved efficiency. It has also been reported that a conducting polymer/GO composite can be used as a cheaper alternative to the platinum counter electrode for cells with lower costs, yet comparable efficiencies.^[400] Other methods that go beyond use of graphene as a TC and charge collector such as is in graphene/semiconductor-based Schottky diode solar cells.^[97,401,402] A contrasting mechanism of light harvesting using graphene is through absorbed photons that heat electrons faster than their nuclei: these hot carriers result in a substantial photocurrent produced from this photo-thermoelectric effect.^[403] Other thermoelectric applications could utilize graphene's thermoelectric power generation in addition to its high electrical and thermal conductivity.^[404–408] Mechanically based energy harvesting devices have utilized the flexible nature of graphene electrodes in rollable nanogenerators based on piezoelectric ZnO nanowires.^[409,410] Another type of power generating function of graphene is by flowing an electrolytic solution over its surface, originally attributed to charged Cl⁻ ions with a net drift velocity coupled with electrons within graphene.^[411] This produced a modest voltage up to roughly 175 mV, however the mechanisms is shown to be dependent on the metal electrodes, as isolating the metal from the flowing electrolyte produced no voltage.^[412]

Energy storage devices such as batteries,^[413–418] supercapacitors,^[419–435] and fuel cells^[183,185,436–438] benefit from the integration of graphene materials. Graphite has been extensively used as electrodes in such applications for a long time. Graphene and its derivatives and composites enhance the surface area over graphite-based electrodes and increase conductivity, among other advantages. For example, CMG-based electrochemical double layer capacitors (ultracapacitors) have been demonstrated (Figure 8i).^[421,423] Platinum nanoparticle decorated graphene nanoflakes^[436] and rGO^[437] have found interesting applications in fuel cells. Pt-ITO-graphene triple junctions have been used to enhance catalysis.^[438] Non-platinum-based catalysts for oxygen reduction typically have much lower catalytic performance, but would be much cheaper alternatives.

Doping graphene with sulfur^[439] or combining Fe and nitrogen with rGO enhances stability with comparable activity over similar carbon-black-based, non-platinum catalysts.^[440] Graphene-Si nanoparticle composites with nanoscale holes can be utilized for enhanced ion transport in flexible Li-ion batteries with both high capacity and high power density.^[418] Similarly, a Li-air battery utilizing a porous graphene morphology as the air electrode demonstrated a record breaking capacity of 1.5×10^4 mA h/g,^[414] while doping the graphene cathode with nitrogen enhanced discharge capacity by 40%.^[441] The network of tunnels enhances oxygen flow as well as the efficiency of the reaction, which also benefits from functionalized defects. Graphene foams (three-dimensional conductive networks with high surface area) have shown promise for supercapacitors^[431] and as porous anodes for Li-ion batteries,^[351] as have rGO papers.^[442] Graphene-based materials can also be an efficient storage medium for lithium in batteries,^[415–417] or potentially for fuels such as hydrogen in fuel cells.^[443,444]

7. High-Frequency Devices

High-frequency analog devices and circuits are of crucial importance to many technologies, especially in communications technologies such as wireless transmission and signal processing. With exceptionally high carrier mobility and saturation velocity (5.5×10^7 cm/s),^[445] as well as large critical current densities ($\approx 10^8$ A/cm²)^[1] and low 1/f noise and phase noise levels,^[446–448] graphene is well suited for analog devices with unprecedented switching speeds. Intrinsic graphene transistors have a significant off current and cannot be fully switched off, which prevents its application for digital electronics, but does not rule out use in analog radio-frequency (RF) devices.^[449,450] In addition to exceptionally high cutoff frequencies, the ambipolar transport characteristics add another dimension for possible device configurations.

The intrinsic carrier mobility of graphene can be as large as 10^6 cm²/Vs in low temperature, suspended devices^[12] and $\approx 4 \times 10^4$ cm²/Vs in room temperature SiO₂ supported devices,^[85] which promises the fast operating speed of graphene transistors. Another important measure of material characteristics for high-speed devices, particularly at short gate lengths, is the carrier saturation velocity.^[451] As the channel length shortens, the electric field between the source-drain electrodes increases. At such high fields, the steady-state carrier velocity starts to saturate. Theoretical investigation predicts a peak intrinsic average carrier velocity up to 4.6×10^7 cm/s in graphene,^[452] twice that of GaAs and 4 times that of Si. As devices shrink to the nanometer scale, saturated carrier velocity becomes a more significant measure of the transport properties.^[6] Figure 4g shows the electron velocity vs. electric field for conventional semiconductors and graphene.

The high-frequency performance of transistors can be investigated by measuring scattering (S) parameters. The short-circuit current gain, the ratio of small-signal drain and gate currents in an alternating current (AC) circuit, can be derived from the S parameter measurements and typically exhibits a 1/f dependence for an ideal device. When the current gain becomes unity, the signal propagation has reached its ultimate

switching limit, known as the cutoff frequency, f_T . In addition to the current gain, another important figure of merit for microwave performance is the maximum oscillation frequency f_{MAX} , which corresponds to the highest frequency with non-vanishing power gain. Both f_T and f_{MAX} are important measures of device performance: while f_T shows the intrinsic limits of the device channel, f_{MAX} is more dependent on specific device configuration and can be enhanced through device layout optimization.

Graphene transistors made using conventional fabrication techniques of lithography, metal electrode deposition, and dielectric integration processing have yielded devices with gigahertz cutoff frequencies. These conventional processes, however, can often introduce defects and contaminants into the graphene devices, degrading its performance. UCLA researchers developed an approach to avoid these limitations, utilizing a self-aligned nanowire as a mask for defining the channel between source-drain electrodes, enabling devices with f_T as high as 300 GHz,^[149] and further projected that terahertz operation can be achieved at shorter channel lengths.^[453] Although the intrinsic cutoff frequency of pristine graphene has reached rather high levels, these devices usually exhibit a relatively low extrinsic cutoff frequency around 10 GHz or less. This discrepancy is attributed mainly to the large ratio between parasitic pad capacitance and gate capacitance. A recent study employing a glass substrate that can substantially reduce the parasitic pad capacitance resulted in a highest extrinsic cutoff frequency up to 55 GHz.^[454] Additionally, short channel CVD GFETs down to 90 nm showed a length dependent shift of the Dirac point.^[455] Shifting of the Dirac point can actually be tuned by changing the metal of the gate electrode with a different work function.^[456] Although the high values for f_T are exciting, the f_{MAX} is typically only a few tens of gigahertz and a small fraction of the extrapolated f_T . Contact resistances, gate charging, and parasitic capacitive effects, as well as weak drain current saturation and large output conductance, can greatly reduce the power gain performance, achievable switching speeds, and ultimately the utility of the device. Design elements such as improved dielectrics, self-alignment, and T-gate structures^[457,458] can help to mitigate these effects.

7.1. Top-Gated Transistors

For most fundamental research, graphene transistors are typically fabricated on SiO₂/Si wafers with the highly doped silicon underneath the oxide layer as the bottom-gate. However, for practical applications, most designs typically adopt a top-gated structure to improve the device reliability and reduce substrate parasitics. In 2009, the IBM group presented the first comprehensive experimental studies on high-frequency top-gated devices with different gate voltages and gate lengths. The fabrication of top-gated graphene transistors first requires the deposition of an oxide dielectric layer on graphene, which is a significant challenge due to the intrinsic incompatibility of graphene with most oxide deposition approaches. They combated this problem by first treating the graphene with NO₂ prior to atomic layer deposition (ALD) of the Al₂O₃ gate oxide. This improves the quality of subsequent ALD of Al₂O₃ and allows uniform films thinner than 10 nm to be grown on graphene

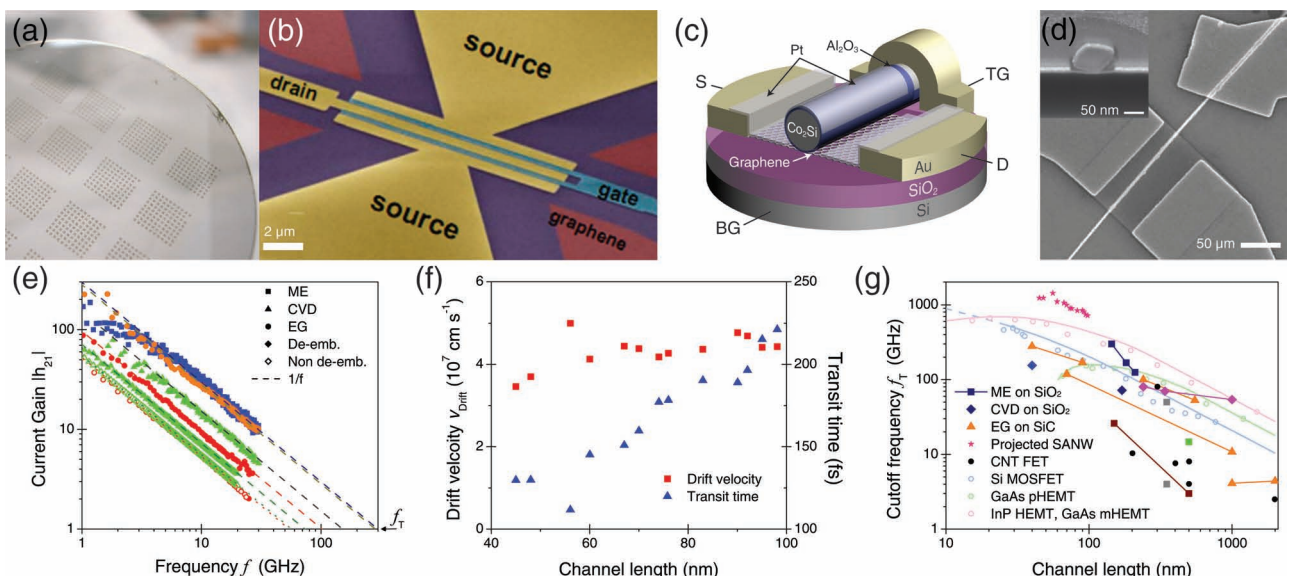


Figure 9. Radio-frequency top-gated devices. a,b) Photograph and SEM false-color image of two EG on SiC FETs patterned on the surface. c,d) Schematic and SEM image with cross section (inset) of a self-aligned nanowire-gated (SANW) device. e) Current gain vs. frequency for EG as well as SANW gated devices of peeled and CVD graphene. The cutoff frequency is the extrapolated intersection of the $1/f$ trend line with a current gain $|h_{21}|$ of one. f) Gate length dependence of transit time and drift velocity, v_{Drift} , of short channel self-aligned devices. g) Comparison of cutoff frequency and channel length of high-mobility materials. The hollow circles are for bulk semiconductors: silicon-based metal oxide semiconductor FET (MOSFET) (light blue) and GaAs and InP HEMTs (light green and light red), and the black circles are for carbon-nanotube-based devices, all adapted from.^[6] Micromechanically exfoliated/peeled (ME) graphene (squares),^[459,460,475] CVD graphene (diamonds)^[470,471] and epitaxial graphene on SiC (orange triangles)^[218,463–466] Self-aligned nanowire-gated device with ME (navy blue squares)^[149] and CVD (navy blue diamond)^[454] as well as projected cutoff frequencies (pink stars)^[453] are shown. a,b) Reproduced with permission.^[463] Copyright 2009 American Association for the Advancement of Science. c) Redrawn.^[149] d) Reproduced with permission.^[149] Copyright 2010, Nature Publishing Group. e) Redrawn.^[149,453,454,463,464,466,470] f) Redrawn.^[453] g) Redrawn.^[6,149,453,454,463,464,466,460]

without pinholes. On the other hand, this treatment can cause severe damage to the graphene lattice with substantial mobility degradation (down to $400 \text{ cm}^2/\text{Vs}$).^[459] Nonetheless, this process allows the fabrication of functional graphene transistors with the intrinsic current gain exhibiting the typical $1/f$ dependence. The cutoff frequency, deduced from measurement of the S parameter, exhibits a strong dependence on the gate voltage and is proportional to the transconductance (g_m). The peak frequency is found to be inversely proportional to the gate length squared. A cutoff frequency as high as 26 GHz is obtained with a channel length of 150 nm.^[460]

An alternative approach to fabricating uniform top-gates is using an oxidized metal thin film^[460] or organic-polymer-based films^[461] as a buffer layer. In the former technique, a thin layer of metal is deposited on the graphene and subsequently oxidized to form a thin dielectric layer, which acts as a nucleation layer for further oxide deposition by ALD. Within this approach, Lin et al. investigated dual-gated GFETs to determine how access resistance impacts high-frequency device performance. A back-gate modulates the access resistance of the device by up to 50% with a subsequent increase of transconductance by 400% in a 350 nm long gate to result in a maximum f_T of 50 GHz.^[460] Other gate oxides such as Si₃N₄, HfO₂, and Y₂O₃, with thicknesses down to a few nanometers, have been used for higher performance top-gated GFETs. At such small oxide thicknesses, quantum

capacitance starts to play an important role in determining the gate capacitance.^[462]

In early 2010, the IBM group further demonstrated GFETs with a gate length of 240 nm and f_T as high as 100 GHz using EG on 2-inch SiC wafers (Figure 9a,b).^[463,464] More recent studies have reached 170 GHz^[465] and 280 GHz^[466] in 90 nm and 40 nm length EG channels respectively. EG nanoribbon-based RF devices have an f_T up to 60 GHz, even at a low mobility of $500 \text{ cm}^2/\text{Vs}$.^[467] In the 2010 study, large-area graphene is prepared on the Si-face at 1450°C , with carrier density of $3 \times 10^{12} \text{ cm}^{-2}$ and Hall mobility up to $1500 \text{ cm}^2/\text{Vs}$. The top-gate dielectric is fabricated by spin-coating a polyhydroxystyrene buffer layer before the deposition of 10 nm HfO₂ by ALD. The devices typically exhibit Dirac points below -3.5 V gate, corresponding to n-type electron conduction and a high carrier density above $4 \times 10^{12} \text{ cm}^{-2}$ at zero gate bias. This results in a nearly constant transconductance over a wide range of gate voltages in the on-state due to low series resistance of the graphene channel. The transconductance increases with drain voltage with no clear current saturation observed before breakdown of the device.

CVD graphene has also been explored for the fabrication of high-speed transistors due to its potential for large-scale fabrication desirable for practical application. A few recent studies have explored use of this scalable material.^[454,468,469] In particular, the IBM group fabricated CVD graphene-based RF transistors with gate lengths down to 40 nm and a cutoff frequency as

high as 155 GHz.^[470] To bypass the challenges associated with directly growing dielectric films on graphene, an alternative approach uses localized back gates that are embedded within the substrate prior to transfer of CVD graphene.^[458,471]

7.2. Self-Aligned Electrodes

Despite significant advancements, the graphene transistors fabricated using conventional lithography are still limited by a number of undesirable factors.^[149] In particular, the conventional dielectric deposition and device fabrication processes can severely degrade the transport properties by introducing defects into the graphene lattice. To address this problem and mitigate the adverse effects of deposition, a physical integration approach was developed to physically transfer preformed high-quality dielectric materials onto graphene.^[86,115,116,451] With this approach, top-gated graphene transistors with mobilities exceeding 2×10^4 cm²/Vs have been achieved.^[86]

In general, the switching speed of a transistor is determined by the time required for the charge carriers to travel from the source to the drain electrode. The high carrier mobility ensures the high electrical carrier speed. To push the speed limit of graphene transistors, it is important to scale down the channel length to further reduce the required time for charge carriers to travel from source to drain. However, for most reported graphene transistors, there is a gapped region between source and gate, and gate and drain, which cannot be modulated by the gate and therefore functions as a series resistance to the graphene transistor, and is referred to as the access resistance. This originates from imprecisely aligned source, drain and gate electrodes and is particularly detrimental to transistor performance in short channels due to the increasing contribution of the series resistance to the overall device resistance. Therefore, to achieve short channel transistors with higher f_T , precise electrode alignment becomes increasingly important. A self-aligned processing technique is usually employed in state-of-the-art CMOS technologies to ensure precise positioning of source, gate and drain electrodes with no overlapping or gaps.^[464] Unfortunately, these conventional processes cannot be readily applied to graphene devices due to potential damage to the monolayer.

To address this challenge, a new self-aligned strategy was developed at UCLA to fabricate graphene transistors using a nanowire as both the top-gate and shadow mask to define the source and drain electrodes in the close proximity of the gate (Figure 9c,d).^[149] In this approach a metal/dielectric core/shell nanowire is physically transferred on top of the mechanically peeled graphene. Ti/Au source and drain electrodes are fabricated followed by the deposition of a thin layer of platinum all the way from source to drain atop the nanowire mask to complete the self-aligning process. The nanowire separates the platinum thin film into two isolated source-drain metallic contact regions that are precisely aligned with the gate and the channel, defined by the mask geometry. The nanowire diameter determines the channel length; the thin oxide shell acts as gate dielectric; and the metallic core acts as the top-gate electrode.

In this study, Co₂Si/Al₂O₃ core/shell nanowires with a diamond cross section are used as the self-aligned gate. The cross-sectional SEM image of a typical self-aligned device confirms that

the source and drain electrodes are precisely positioned next to the nanowire gate. This self-aligned approach enables dramatic reduction of the access resistance, and increases the device current up to 3.32 mA/μm at a source-drain bias of -1 V. Importantly, the self-aligned electrode deposition can increase the peak transconductance by a factor of 60 to a highest obtained transconductance (up to 1.27 mS/μm) of comparable devices, and thus promise unprecedented RF transistors. Indeed, a cutoff frequency of 300 GHz was achieved for a transistor with 144 nm channel length, a record marking an important milestone for high-speed graphene transistors.

The Co₂Si/Al₂O₃ core/shell nanowire gate used in the initial study have a diamond cross section with an air gap existing between the nanowire gate and graphene at both the source and drain side of the device, resulting in a non-ideal gate coupling that negatively impacts the device performance. To address this problem, GaN nanowires with triangular cross sections were used to achieve optimum gate coupling between the nanowire gate and graphene channel. Importantly, using different sized GaN nanowires as the self-aligned gate, channel length scaling studies project that terahertz operation is achievable in sub-70 nm transistors.^[453] It should be noted that the frequency response of the graphene devices described in this study is projected based on the direct current (DC) performance, since the actual AC performance in such devices is not limited by the graphene channel but by the nanowire resistance in the gate. Nonetheless, these experimental results demonstrate the performance limits of the graphene channel, which match well with theoretical predictions by self-consistent quantum simulations,^[472] highlighting that the self-aligned approach can be used to fabricate graphene transistors of nearly ideal performance.

More recently, this self-aligned approach was applied to scalable fabrication of graphene transistor arrays using large area CVD graphene and dielectrophoretically assembled nanowire gates.^[454] The intrinsic performance of such a device is generally worse than those obtained from mechanically exfoliated graphene (e.g., f_T of 72 GHz for 170 nm CVD graphene device compared to 168 GHz for 182 nm peeled graphene device). On the other hand, with CVD graphene, the device can be readily fabricated on essentially any substrate, including glass or plastics. With these insulating substrates, the parasitic pad capacitance can be greatly reduced to allow for the demonstration of unprecedented extrinsic cutoff frequencies over 50 GHz. The extrinsic f_T represents the practically achievable switching frequency obtained without sophisticated de-embedding processes. Such high extrinsic f_T can allow for the configuration of functional circuits operating in the gigahertz regime.^[454] It should be noted that a current saturation is also observed in these self-aligned devices, which is unusual at such small scales and is more noticeable with increasing channel length.^[473–475] The observed saturation is attributed to large gate-drain capacitance coupling that shifts the Dirac point at higher drain bias. This achievement of current saturation reduces the drain source conductance and can be beneficial for power gain performance.

7.3. Functional Circuits

Building more complicated circuits beyond just a single transistor is the next step in utilizing graphene in practical RF

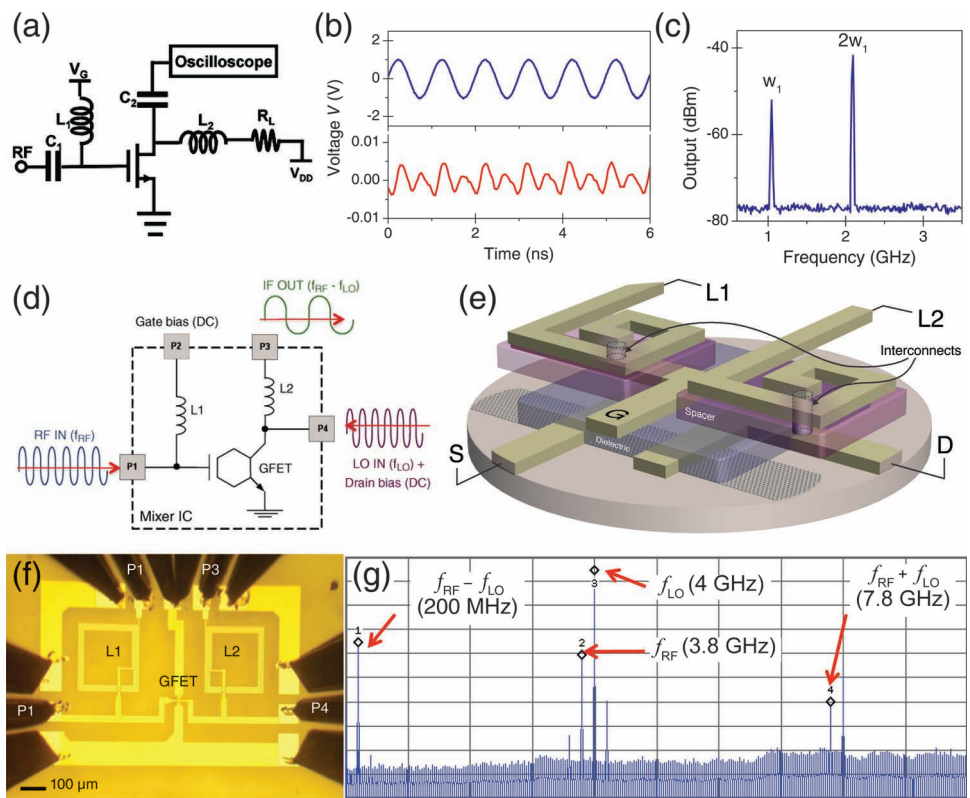


Figure 10. Integrated Circuits. Circuit designs for a GFET-based frequency doubler (a) and mixer (d). b) Oscilloscope readout of input (top) and output (bottom). c) Frequency spectrum of the frequency doubler. e) Schematic of a frequency mixer device and components. f) Optical micrograph of the fabricated device on a SiC substrate. g) Output frequency spectrum of the mixer. a–c) Reproduced with permission.^[454] Copyright 2012 American Chemical Society. d,f,g) Reproduced with permission.^[479] Copyright 2011, American Association for the Advancement of Science. e) Redrawn.^[479]

applications. AC voltage amplifiers and audio amplification are both simple uses for RF transistors.^[476,477] Frequency multipliers are a bit more complex, but also an important component in many communications applications. They are used to output harmonic frequencies of an input frequency, which is useful in generating signals using nonlinear circuit design. Frequency multipliers based on Schottky diodes and conventional FETs have been popular, with operation as high as 1 THz for the former. Both have limitations in signal amplification and efficiency respectively. Additionally, these devices suffer from degraded output signals that need to be further processed and filtered to obtain the desired frequency.^[478]

The ambipolar nature of graphene makes for unique FETs that can enable novel applications. The “V” shape of the I_d-V_g curve behaves like a full-wave rectifier by itself. With an alternating gate voltage centered at the charge neutrality point, the output current at the drain of the device will result in full-wave rectification, alternating between electron and hole conduction. In this way, much simpler frequency doublers can be realized. This ability is not new, but GFETs offer a far less complicated design and potentially superior performance for rectifier devices.^[450]

Efforts have been made to integrate these graphene-based devices into higher functioning circuits.^[479–481] Frequency mixers are useful circuits designed for signal processing,

turning two frequencies into the sum or difference of the inputs. An RF signal, f_{RF} and a local oscillator signal, f_{LO} are applied to the gate and the drain, modulating the GFET, resulting in an output of the mixed, summed, and differenced (intermediate) frequencies. An inductor placed between the input and gate contacts removes the parasitic capacitances through resonance, while another works as a low-pass filter between the drain and the output. With the achievement of high extrinsic f_T in the self-aligned graphene transistors, GFET-based RF circuits operating in the gigahertz regime can be readily configured (e.g., a frequency doubler as shown in Figure 10a–c). Importantly, RF characterization of the circuit shows a clear doubling signal at 2.1 GHz with the input signal frequency at 1.05 GHz. Spectrum analysis shows that the frequency-doubler device exhibits a high spectral purity in the output RF signal, with 90% of the output RF energy at the doubling frequency of 2.1 GHz. This study clearly demonstrates that a single graphene transistor-based frequency doubler can operate in the gigahertz regime with high-output spectral purity. Similarly, a single graphene transistor-based RF mixer has also been demonstrated. The two-tone signals with adjacent frequencies are applied to the gate through a power combiner to manipulate the transistor channel resistance. With an RF input $f_{RF} = 6.72$ GHz and local oscillator $f_{LO} = 2.98$ GHz, the output spectrum shows clear RF mixing function at intermediate frequency (IF) $f_{IF} = f_{RF} - f_{LO} = 3.74$ GHz and $f_{IF} = f_{RF} + f_{LO} = 9.70$ GHz.

The above RF circuits were obtained by interconnecting different elements together. For eventual application, it is highly desired to incorporate all functional components directly on the chip to achieve a fully integrated RF circuits. To this end, IBM scientists have fabricated such devices using EG on SiC with inductors integrated on chip (Figure 10d–g).^[479] The frequency spectrum of the mixer output with inputs of 3.8 GHz and 4 GHz shows the 200 MHz and 7.8 GHz outputs. The drain inductor weakens the higher frequency tone, and lowers its amplitude. Power signals of f_{IF} are proportional to the signal with expected high linearity and conversion loss of about –27 dBm.

8. Bandgap Engineering

Although bulk graphene can exhibit exceptional switching speeds for analog devices, the lack of an inherent bandgap is a significant disadvantage for applications in logic circuits, that is, digital transistors that read a 0 or 1: an off- or on-state. The necessity to induce a bandgap in graphene devices is evident in order to mitigate the problem associated with low on/off ratios and the inability to fully inhibit conduction in the graphene channel. For commercial logic circuits, an on/off ratio of at least three to four orders of magnitude is required, which corresponds to a bandgap of roughly 360 meV.^[20] At the charge neutrality point, carriers in this semi-metal are quite easily thermally excited into a conducting state, resulting in a sizable minimum conductance at the Dirac point. Ultimately, the application of graphene as a digital transistor at room temperature requires a gap large enough to suppress the conductance at charge neutrality. The ability to controllably tune a bandgap would prove valuable for many electronic applications. To this end, various strategies have been explored with limited success to date, usually at the expense of performance. Fundamentally, forming a bandgap will unavoidably break the linear dispersion relation at the Dirac point, degrading the high mobility characteristics.

A popular method initially explored is to pattern graphene into nanostructures such as GNRs that create lateral confinement and transport gaps, which is at least able to increase the on/off ratio. Application of a perpendicular electric field across bilayer graphene has also been proven to induce a tunable bandgap. Strain engineering is predicted to induce a gap in graphene, which has been observed experimentally, but is difficult to implement into practical device structures. Nonetheless, bandgap engineering offers potential solutions to a significant obstacle in the path towards practical and scalable, high-performance graphene-based logic devices.

8.1. Graphene Nanostructures

Many attempts to synthesize and fabricate laterally constrained graphene nanostructures to induce a bandgap have met with moderate success.^[261,482] By further confining the width down to small enough scales, the band structure can be significantly altered with the opening of a transport gap. Nanoconstrictions, shown in Figure 11a, are samples that have been fabricated into a nanostructured channel between two larger regions. This

small bridge acts as a bottleneck, and becomes the dominant region in which the semiconducting performance is observed. Even without an energy gap, the resistance is increased due to the smaller dimension; the rest of the graphene can generally be neglected as simply part of the contact electrodes.

Quasi-one-dimensional nanoscale graphene behaves as a quantum dot. Single electron transistors (SETs) have been designed from a graphene quantum dot connected by quantum point contacts (Figure 11b), which behave as the Coulomb blockades necessary to trap charge within the dot. The first graphene SET was patterned with EBL and described as a chaotic Dirac billiard, similar to that of neutrinos as billiards.^[483,484] SETs are made up of a conductive island (a quantum dot) that can hold charge and is separated from the source drain electrodes by a tunneling barrier (quantum point contacts). Electrons tunnel into and are trapped on the island, which then becomes negatively charged. Because of the small size of the charged quantum dot, it creates a Coulomb gap, an additional energy barrier to adding another electron: one electron must leave through the drain before the next can be added from the source, meaning single electrons travel through the channel one at a time. SETs have been fabricated from conventional semiconductor nanostructures with nanoparticle islands, nanowires and CNTs.

Theoretically, ideal GNRs work much like CNTs do: quantum confinement in the lateral direction leads to a modified DOS, of which certain configurations lead to bandgap formation. It should be noted that the zigzag and armchair names are reversed for nanoribbons and nanotubes, as the defined direction runs along the length of the structure for the former and is the wrapping vector around the circumference of the latter. Armchair graphene nanoribbons (AGNRs) can be semiconducting,^[485] similar to the zigzag nanotube counterparts. While zigzag graphene nanoribbons (ZGNRs) were predicted to be half-metallic,^[486] further examination showed that electron-electron interactions require a self-energy correction, yielding larger bandgaps in both varieties.^[487] Furthermore, zigzag edges create a unique spin-polarization at opposite sides of the ribbon, which has implications for spintronics. Bandgaps that form due to confinement are inversely proportional to the ribbon width, much like nanotubes. The theoretical analyses of ideal GNRs usually do not directly apply to experimentally fabricated GNRs (Figure 11c–l), which are influenced by a number of internal and external factors. Figure 12a–c shows theoretical and experimental ribbon bandgaps and mobilities as a function of width, compared with other semiconductors. An effective transport gap exhibits similar semiconducting behavior as a real bandgap, but undermines the performance expected of graphene.

8.1.1. Fabrication

A number of fabrication techniques, both top-down and bottom-up with plenty in between, have been explored to obtain GNRs with varying degrees of control over size, edge roughness, edge passivation, functionalization, substrate effects, and scalability. EBL and photolithography are naturally suited to pattern this two-dimensional film. Many attempts at simply using resist to mask graphene have been implemented to study GNRs of

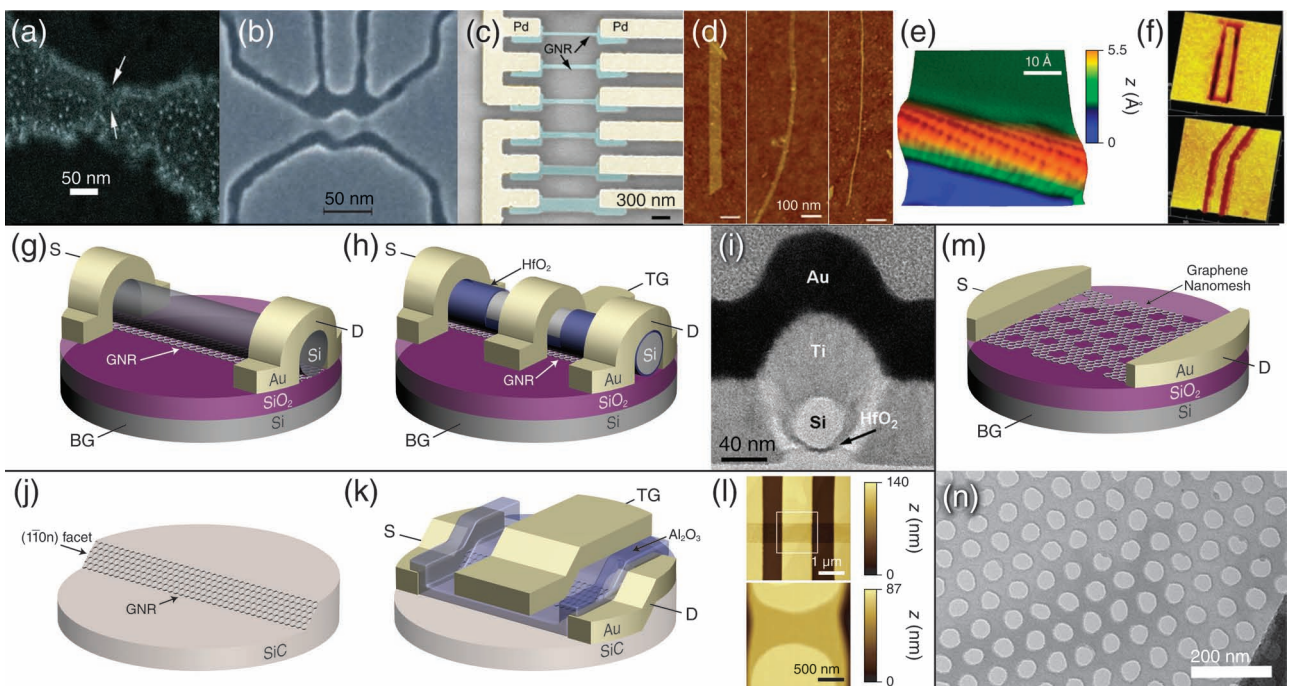


Figure 11. Nanostructures. a–c) Nanoconstriction (a), quantum dot/point contact SET (b) and GNRs of varying width (c), patterned using EBL and imaged using SEM. d) AFM topography of sonicated GNRs with widths of ≈50 nm, ≈20 nm, and ≈10 nm from left to right; the narrowest GNR is two layers thick. e) STM topography of the curled edge of a carbon nanotube (CNT)-derived ribbon deposited on metal. f) STM topography of GNRs with atomically smooth edges: 10 nm × 120 nm straight (top) and 8-nm-wide with a 30° kink (bottom). g–i) Schematics of GNRs fabricated with a nanowire mask (g) and nanowire top-gate (h), with an SEM cross section of the latter (i). j,k) EG nanoribbons grown on a prepatterned, nanofaceted SiC (1̄10n) crystal surface (j), and the device schematic (k). l) AFM topography of trenches on a SiC substrate (top) and post-growth semicircular plateaus with a sub-40 nm GNR along the nanofacet. m,n) Schematic and TEM image of a graphene nanomesh patterned using block-copolymer-based lithography. a) Reproduced with permission.^[515] b) Reproduced with permission.^[483] Copyright 2008, American Association for the Advancement of Science. c) Reproduced with permission.^[490] Copyright 2007, Elsevier. d) Reproduced with permission.^[503] Copyright 2008, American Association for the Advancement of Science. e) Reproduced with permission.^[501] Copyright 2011, Nature Publishing Group. f) Reproduced with permission.^[506] g) Redrawn.^[533] h) Redrawn.^[115] i) Reproduced with permission.^[115] Copyright 2010, American Chemical Society. j,k) Redrawn.^[93] l) Reproduced with permission.^[93] Copyright 2010, Nature Publishing Group. m) Redrawn.^[512] n) Reproduced with permission.^[512] Copyright 2010, Nature Publishing Group.

varying widths and channel lengths with a limited degree of edge control. Photolithography is much more scalable but has lower resolution than EBL (down to 10 nm features at best), yet both yield relatively rough edges. Kim and co-workers fabricated the first nanoribbons devices,^[485] while further improvements have been made by using top gate^[488,489] and side gate^[392] structures. EBL has been used to create GNRs down to 20 nm widths (Figure 11c).^[490] Single charge transport characteristics have been observed in GNRs in various studies.^[483,491–494]

Etching is typically accomplished with oxygen plasma. Edge roughness and disorder is inherent from not only the mask itself, but also by damage done by intense bombardment of oxygen ions during etching, the imprecise mask edge, and undercut, which severely limit the performance of these devices. It is also unclear how the edges of the ribbons are passivated. Other less abrasive etching techniques might better maintain the structural quality and could even enable precise control over edge passivation and functionalization.

The edge morphology can have a significant impact on GNR performance.^[495] Though in practice, nanoribbons are too disordered for orientation of the lattice to have a significant influence. Nonetheless, both width and edge morphology do have an impact on the properties. A unique approach to etching

graphene is to use nanoparticles as an etching catalyst that move along the zigzag crystallographic directions, creating precise cuts within the graphene sheet.^[102,496–498] Simple annealing as well as Joule heating via e-beam or with current annealing have been used to reconstruct edges into predominantly zigzag or armchair configurations.^[498]

Less conventional, yet useful ways to pattern graphene have also been developed, such as etching directly with an electron beam or a focused ion beam of He⁺.^[499] These are not scalable options and offer little advantages over EBL, other than a lack of a resist layer. Tour and coworkers, using a solution-based technique,^[500,501] alongside the Dai group who used a plasma etch,^[502] simultaneously developed a novel bottom up approach of obtaining atomically smooth edges by chemically “unzipping” carbon nanotubes into flat ribbons (Figure 11e). In another study, Dai and coworkers also found highly smooth edged GNRs after intense sonication of exfoliated graphite.^[503] Various unconventional nanolithography techniques have also been used for GNR fabrication. Scanning probes can be used in a number of different schemes to produce nanostructures. AFM tips can carve out shapes like a scalpel, carving out ribbons or other shapes.^[504] AFM can also be used in local anodic oxidation of graphene or by local reduction of GO through

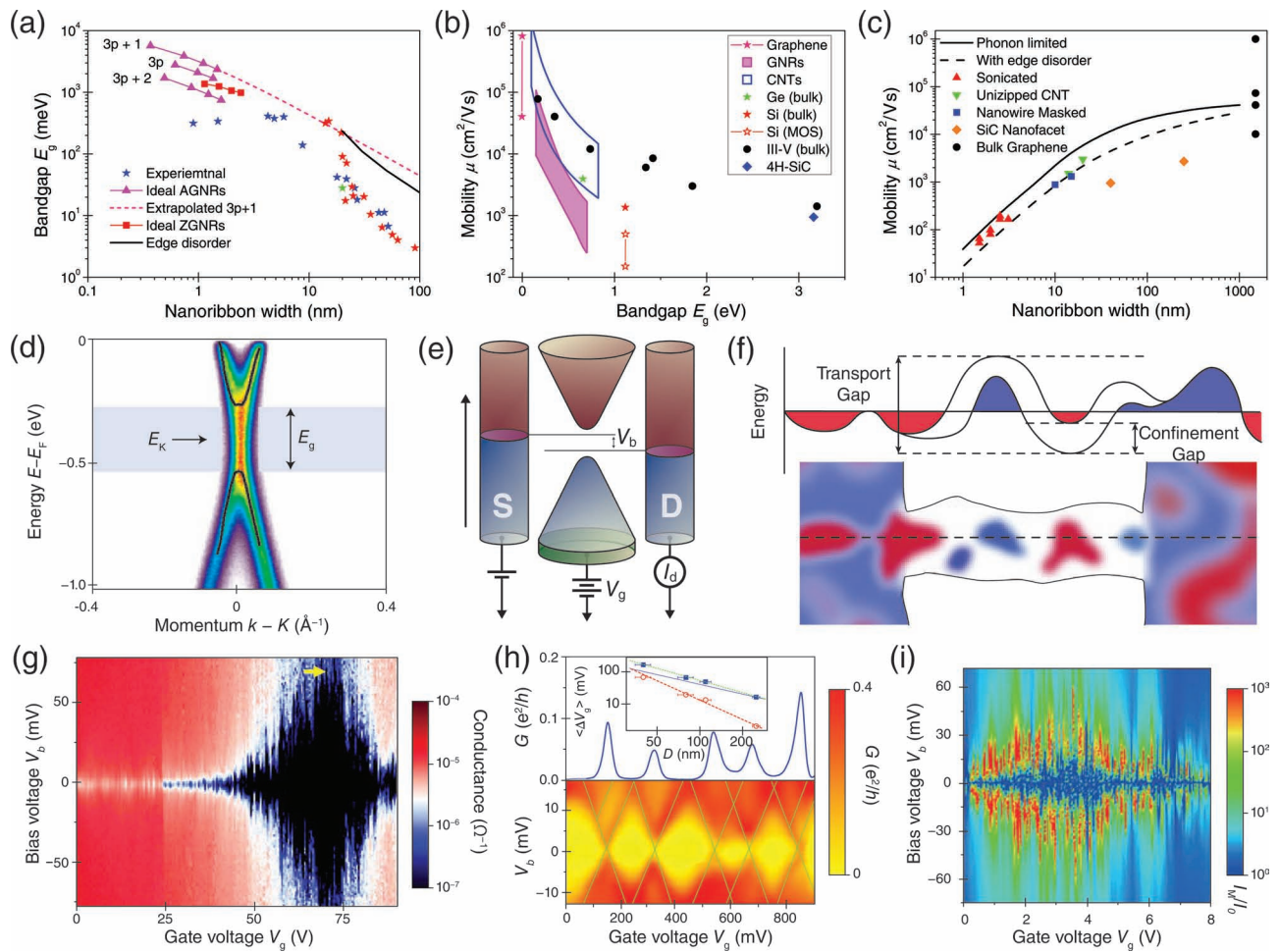


Figure 12. Bandgap engineering. a) Energy-gap vs. width. b) Mobility vs. ribbon width. c) Bandgap vs. ribbon width. d) Substrate induced bandgap in EG on SiC, measured by ARPES. e) FET band schematic: as the source-drain bias overcomes the bandgap, a current will begin to flow. Applying a gate voltage will shift the cones and gap up and down, aligning the source-drain Fermi levels with the valence and conduction bands respectively where the current will then flow. f) GNR band structure schematic and potential puddles, demonstrating an enhanced transport gap. g) Two-dimensional electron transport plot of conductance vs. gate and bias voltages showing Coulomb diamond of a GNR. The height of the diamond represents the effective bandgap. h) SET Coulomb diamonds: the height of the diamonds represents the transport gap. Inset: Dependence of the diamond widths on the diameter of the quantum-dot islands. i) Current ratio of GNR magnetoresistance $I(8 \text{ T})/I(0 \text{ T})$ as a function of gate and bias voltages, showing the large increase in current with application of magnetic fields. a–c) Redrawn.^[6,93,115,524,533] d) Reproduced with permission.^[194] Copyright 2007, Nature Publishing Group. e) Redrawn.^[485] f) Reproduced with permission.^[519] Copyright 2010, American Physical Society. g) Reproduced with permission.^[485] Copyright 2007, American Physical Society. h) Reproduced with permission.^[483] Copyright 2008, American Association for the Advancement of Science. i) Reproduced with permission.^[533] Copyright 2010, Nature Publishing Group.

thermochemical nanolithography.^[505] Scanning tunneling microscopy can form precise edges of graphene nanostructures on a metallic surface with great precision (Figure 11f).^[506] GNRs with widths down to 2.5 nm have been obtained with atomically smooth edges and a bandgap up to 0.5 eV. However these GNRs are attached to a conducting substrate, making them unsuitable for incorporation into a functional device. These nanolithographic methods can be powerful, but are far from practical. Nanoprinting lithography is more scalable, which is used to create graphene nanostructures with sizes not readily achievable with conventional lithography.^[507]

Bai et al. developed a nanowire masking approach for the top down fabrication of nanoribbons with widths below those

obtained from photolithography or EBL.^[508] Nanowires with well defined morphologies and nanoscale diameters can be controllably grown using well-known CVD techniques. Silicon nanowires make adequate masks for oxygen plasma etching of the graphene that is not covered by the wire to form a ribbon under it (Figure 11g). Nanoribbon widths can be tuned directly by the nanowire diameter, as well as with over-etching and undercut to further decrease the width to <5 nm. With this approach, a conductive/insulating core/shell wire can simultaneously function as a nanowire mask and local top gate.^[115] Here the conductive core functions as a local gate, and the thin dielectric layer between the core and graphene, acts as the gate dielectric (Figure 11h,i). The etching processes leaves an

uncontrollably rough edge, which tends to decrease in amplitude as the nanoribbon width decreases.^[509]

Walt de Heer and co-workers developed a unique way to form graphene nanostructures by growing them on a prepatterned SiC substrate.^[93] It was observed that graphene preferentially forms on certain crystallographic planes. In this way, GNRs are formed on predefined faceted nanostructures (i.e., on strips of (110n) face of the SiC substrate surface as shown in Figure 11j–l, as narrow as 40 nm at temperatures ≈1450 °C. The patterned surface is prepared using scalable photolithography and fluorine-based reactive ion etching (RIE), which realized direct nanoribbon growth and avoided further damages than with traditional post-growth etching processes. Pretreated SiC surfaces with ion implantation can also selectively grow EG nanoribbons.^[510] Similar attempts form nanostructures on pre-patterned catalysts using CVD.^[262,511]

A perceived advantage of graphene over carbon nanotubes is that its two-dimensional nature could lead to large-scale integration without sophisticated assembly steps. Experimentally handling and precisely assembling one-dimensional nanostructures into integrated arrays have significant challenges. The formation of one-dimensional nanoribbons defeats this intrinsic advantage of graphene and it may be desirable to keep the inherent two-dimensional structure while still introducing lateral confinement. An innovative form of graphene called nanomesh is produced by patterning the graphene with an ordered array of nanoscale voids (Figure 11m,n). Structurally mimicking a network of nanoribbons, the nanomesh opens up an energy gap while maintaining a large form factor, enabling a continuous, semiconducting thin film that can be used for scalable fabrication of graphene devices and circuits using conventional planar processing steps. Approaches to fabricating nanomeshes include block-copolymer,^[512] polystyrene-sphere,^[513] and nanoimprint^[514] lithography-based techniques.

8.1.2. Performance

Though spectroscopic techniques exist for observing a bandgap (Figure 12d), a more crucial measure is the transport properties of the device itself. If a gap exists, sweeping transistor source-drain and gate voltages will yield non-linear I_d - V_d plots with a region of conductance suppression (Figure 12e,g). Within this conductance-suppressed, diamond-shaped region, the device is turned off, where the gate voltage tunes the Fermi level within the gap and the source-drain bias does not overcome it. At the peak of the diamond, a critical source-drain bias needed to turn on the device is known as the transport gap, which in an ideal case corresponds directly to the bandgap. An SET exhibits a series of similar diamond structures in the two-dimensional differential conductance plot (Figure 12h). The transport gap corresponds to the Coulomb gap, $e^2/2Ch$, where C is the capacitance of the quantum dot island and is a function of size. As the gate is tuned up and down, more electrons can fit on the island, which shifts the gap up, and forms the row of diamonds.

Experimentally, a number of factors contribute to the suppression of conductivity and non-linear transport measurements of nanoribbons^[485] and nanoconstrictions^[489] that end up degrading device performance. Typically, at lower temperatures, the diamond becomes more prominent, as thermal excitation

and noise effects are less pronounced. Small bandgaps can be difficult to detect at room temperature, and often the nonlinearity of the I_d - V_d curve is irresolvable, so cryogenic transport measurements are typically used to probe the nature and magnitude of the transport or bandgap of graphene nanostructures.

The on/off ratio of GNRs of varying dimensions typically increases with decreasing width. Lithographically defined GNRs are limited by resolution, but still show a ratio of up to 10 for 10–15 nm wide nanoribbons,^[490] while EBL fabricated nanoconstrictions have seen on/off ratios as high as 10^3 .^[515] An on/off ratio over 10^4 at room temperature was also reported in relatively wide suspended and current-annealed nanoribbons (widths > 15 nm) fabricated from unzipped nanotubes.^[516] Sub-10 nm ribbons using nanowire masks or sonochemical exfoliation are able to increase the on/off ratio, with a value as high as 10^7 achieved at room temperature in the latter case.^[503,508,517] Graphene nanomesh with neck widths ≈7 nm wide necks exhibits an on/off ratio exceeding 100,^[512] which is comparable to GNRs of similar critical width. Importantly, with the nanomesh structure, the overall current or conductance of the device can be readily tuned by varying the device dimension, to reach a value up to 100 times that of comparable GNRs, which is significant for practical device and circuit design.

The observed transport gap in graphene nanostructures is generally only partially due to a confinement induced bandgap. Edge roughness, substrate effects, and impurities can play an important role in the overall observed transport gap. In contrast to ideal nanoribbons, orientation and edge morphology have little impact on experimental transport properties.^[485] Increased scattering and Anderson localization due to line edge roughness can reduce the overall conductivity.^[518] A proposed mechanism for transport gap formation is a Coulomb blockade effect similar to SETs.^[519,520] With the line edge roughness^[521,522] that forms nanoconstrictions along the nanoribbon and local potential fluctuations that form electron-hole puddles,^[519] GNRs behave like a series of quantum dots with tunneling barriers in between. Figure 12f shows a schematic of the band structure along a ribbon, showing the contributions of both lateral confinement and potential fluctuations to the ultimate transport gap. Annealing is often used to improve the device performance, which usually ends up lowering the transport gap via a reduction of charge puddle depths.

With the development of a transport or bandgap, the high carrier mobility nature of graphene is often compromised. Fundamentally, the formation of a bandgap inevitably breaks the linear dispersion relationship. The effective mass of the charge carriers is no longer zero, which leads to a reduced mobility. For experimental GNR devices, mobilities are typically suppressed by a combination of the altered band structure as well as disorder effects. The transport characteristics of GNRs are less sensitive to line edge roughness and have mobilities close to bulk systems when the width is above 50 nm; below this, edge disorder starts to play an important role and dramatically affects carrier mobility. The typical values reported for GNRs with sufficient confinement is around $1500 \text{ cm}^2/\text{Vs}$ or less,^[523] but has exceeded $3000 \text{ cm}^2/\text{Vs}$ in a suspended, unzipped nanotube sample approximately 20 nm wide.^[524]

Theoretical studies have also suggested interesting magnetoelectronic properties in GNRs, originating from the magnetic

edge states or the Hall-edge states under a perpendicular magnetic field, with very large magnetoresistance (MR) predicted.^[486,525–532] The existence of magnetic edge states is yet to be confirmed. Nonetheless, recent experimental studies have demonstrated a very large negative MR of nearly 100% at low temperature, with more than 50% remaining at room temperature.^[533–535] Interestingly, the observed MR can be easily tuned from a few times to $>10^4$ times by simply varying the gate or source-drain bias (Figure 12i). On the other hand, the charge transport in the GNRs is not significantly modified by an in-plane magnetic field. The observed large MR is attributed to the reduction of quantum confinement by the formation of cyclotron orbits. These findings demonstrate the significant magnetotransport properties in GNRs, which have the potential to open up exciting opportunities for a new class of magnetoelectronic devices.

8.2. Bilayers and Trilayers

With a precise Bernal stacking (AB) of an additional layer, bilayer graphene has a number of unique features that make it of particular interest (Figure 13). Inversion symmetry electronically couples the two single layers of graphene to allow for an additional dimension to adjust the electronic structure while retaining the zero bandgap. The coupling creates massive Dirac fermions with 4 distinct valleys and two pseudospins per layer.^[46,536] Without any stacking order (e.g., with rotated layers which is common in multilayer EG), it is no longer considered bilayer graphene and retains the electronic properties of single sheets.^[537]

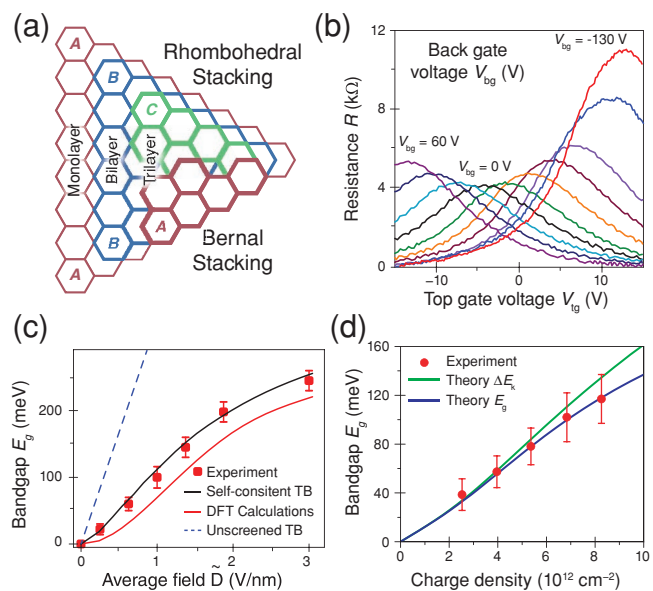


Figure 13. Stacked Graphene. a) Stacking order of rhombohedral (ABCA) and Bernal (ABAB) varieties. b) Dirac point tunability and increased on/off ratio of dual-gated bilayer graphene. c,d) Bandgap dependence on the applied vertical field, shown as a function of the average displacement field in bilayer graphene (c) and as a function of charge density in trilayer graphene (d), with comparisons to theoretical models. b,c) Reproduced with permission.^[540] Copyright 2009, Nature Publishing Group. d) Reproduced with permission.^[547] Copyright 2011, Nature Publishing Group.

It was predicted and observed that an electric field perpendicular to the bilayer plane would induce a bandgap by breaking inversion and time reversal symmetries.^[538–540] Wang and co-workers fabricated a top and back dual-gated device capable of such a tunable bandgap. Infrared photoabsorption microspectroscopy is used to determine a gap as high as 250 meV. Figure 13c shows the dependence of the induced bandgap on the applied field strength. The IBM group later implemented this into a functional FET device with significant on/off ratios up to 2000.^[541] A limitation of using physical vertical fields is the requirement of two gate electrodes with high voltage applied to both. An alternative approach to this problem is by using various chemical dopants on the top and bottom layer of the bilayer graphene.^[542–544] An imbalance of charge above and below the bilayer causes a similar symmetry breaking effect without the use of an additional gate. It is also found that a new and unique quasiparticle formed by spontaneous, interaction-induced symmetry breaking in bilayer graphene at the charge neutrality point results in an insulating state with a magnetic field dependent gap.^[545,546] This observed insulating transition is expected to have a larger gap in trilayer and tetralayer graphene.

Additional layers introduce their own complexities. There are two possible stacking orders for trilayer graphene: typical Bernal ABA or less common rhombohedral ABC configurations, each have different electrical properties. Bernal stacking produces bands of a superimposed Dirac cone onto a parabolic structure similar to bilayers (Figure 13d), and loses the induced bandgap effect of bilayer graphene, while ABC stacking is more similar to a normal bilayer and does in fact produce a significant gap.^[547,548] Semi-metallic trilayers have a gate-tunable overlap of valence and conduction bands that enables a decrease in resistivity with increasing electric field.^[549] Additionally, an unexpected insulating state is found in ABC stacked trilayers while in charge neutrality.^[550] This result is attributed to quasiparticle interactions and has unique implications for observed QHE peaks and plateaus.

8.3. Strain Engineering

With a single atomic thickness and exceptional mechanical strength, graphene can readily deform,^[129] which opens yet another degree of freedom to tailor its properties. To this end, strain engineering has been proposed to alter the electronic properties and potentially open a band or transport gap (Figure 14).^[551] By precise stretching of the graphene lattice, gauge fields are formed which alter the local electronic structure. This results in electrons behaving as if they are traveling through a fictitious magnetic field, with distinct Landau levels normally seen in QHE measurements, and in certain cases the formation of a bandgap. This phenomenon has been observed in STS measurements of highly strained nanobubbles of CVD graphene on a cooled platinum substrate with pseudomagnetic fields as high as 300 T (Figure 14e–h).^[157] Current studies on strain engineering are largely limited to theoretical investigations, and sometimes with conflicting views whether strain will induce a bandgap in graphene, depending on the particular strain modes and theoretical analysis techniques used.

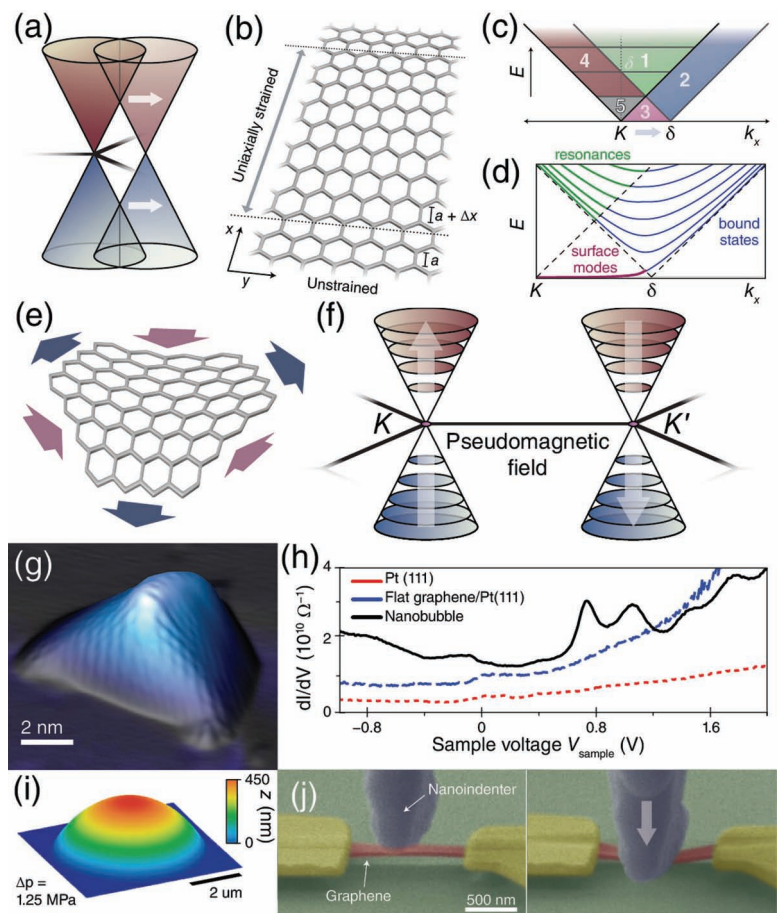


Figure 14. Strain Engineering. a) Schematic diagram of strain induced shifting of the Dirac cones. b) A region of uniaxial strained graphene separates two unstrained regions, creating a transport gap between the two misaligned Dirac cones. c) Overlapping cones showing regions of possible states through a barrier of uniaxially strained graphene: 1) scattering states, 2) band states within the strained region, 3) localized states at boundary, 4) filtered states, and 5) filtered, evanescent waves. d) The resonant bands between the unstrained and strained region, and surface modes that appear at the junction, similar to the edge states of a nanoribbon. e) Triangularly symmetric strain profile that produces gauge fields and in turn pseudomagnetic effects in graphene. f) Band structure showing the opposite direction of the pseudomagnetic field on each sublattice point, with quantized Landau levels, and no net field. g) STM topography of a highly strained graphene nanobubble. h) STS of the Landau levels of the observed pseudomagnetic field in experimentally produced nanobubbles. i) Microcapsule sealed by suspended graphene that forms a bubble due to pressure differentials. j) False-color SEM images of a graphene device suspended over a trench that is then strained into the trench using an in situ nanoindenter with electromechanically coupled measurements. b–d) Redrawn.^[49] e) Redrawn.^[156] g,h) Reproduced with permission.^[157] Copyright 2010, American Association for the Advancement of Science. i) Reproduced with permission.^[39] Copyright 2011, Nature Publishing Group. j) Reproduced with permission.^[552] Copyright 2011, American Chemical Society.

Experimentally implementing controllably strained graphene into a working device is challenging, and attempts have found limited success. The key is to induce a bandgap that is substantial enough to be measured, and the gapped region must comprise the entire channel in which electrons can pass, (i.e., no source-drain leakage through regions of graphene with no gap). For example, a uniaxial strain can be applied to a suspended graphene ribbon (Figure 14j) using an in situ nanoindenter

inside an SEM.^[552] However, this approach was only capable of about 1% strain, not enough to observe a substantial alteration of the transport properties. It is theorized that by introducing a scalar potential field, the strain necessary for inducing a bandgap can be significantly reduced.^[553] Substrates that have a thermal coefficient mismatch with graphene and are cooled enough can cause the membrane to buckle if pinned to the substrate.^[157] Graphene on a material that can be bent or stretched uniaxially or biaxially, and analyzed using Raman spectroscopy, shows a clear redshift of G and 2D peaks, as well as a splitting of the G peak due to disruption of the lattice symmetry.^[322,323,554–556] Current dependence of strained graphene is measured on an already fabricated device transferred onto a polydimethylsiloxane (PDMS) substrate prestrained up to 30%.^[557] Relaxing the substrate causes the graphene and electrodes to buckle into a wavelike corrugated structure, with a limited amount of strain. No bandgap was observed, but a tunable resistance was seen, which can be utilized as a strain gauge.

Other techniques to control strain within a graphene device have been proposed, such as utilizing pressure differentials across the impermeable membrane,^[139,558] or using micromechanical and piezoelectric systems to apply strain. Heterogeneous regions of the surface materials can be used to locally alter the substrate/graphene bonding interactions. Topographical features can introduce controlled strain;^[559] engineering surface structure and adhesion of the substrate can manipulate the atomic membrane. Depending on bonding and feature dimensions of the surface it can ‘snap’ between suspension and close adhesion.^[560,561] Controlled defects are another form of lattice distortion; line defects could be used to form metallic wires within graphene itself.^[562] Folding these membranes, into so-called “graffles,” has been observed both by chance and with precise engineering.^[135,563,564] Devices have yet to apply enough strain to induce a sufficient bandgap. Nonetheless, complex structures can be contrived for interesting and unforeseeable applications with the advantage of keeping the membrane intact: modeled after origami rather than paper cutting.

9. Spintronics

A novel approach to logic-based devices utilizes particle spin as an extra degree of freedom for signal processing and propagation, called spintronics. First emerging with the discovery of the giant magnetoresistance effect, the concept of spintronics is not unique to graphene.^[565] The long spin-relaxation time and low spin-orbit coupling in graphene makes it an attractive material for use in spin valves^[566,567] (filters that only let one spin variant through the barrier) and other components necessary for practical

spintronic circuits. Edges can have a significant impact on magnetotransport properties,^[568,569] and nanoribbons have been proposed for spintronic applications, with unique spin states in zigzag^[486] (Figure 15a) or armchair^[570] edges with tunable edge passivation.^[571] Transverse electric fields can polarize spin in ZGNRs without the need for magnetic contacts for spin filters or spin FETs.^[570,572] Simulations of spin caloritronic devices show a thermally induced spin current of opposite sign in opposite directions: a spin Seebeck effect in magnetized ZGNRs.^[573] Nanoconstriction GFETs are capable of sensing single molecular magnets on the surface of its graphene channel.^[574] For bulk graphene, Figure 15b–d shows a four-point device and nonlocal magnetoresistance measurements to separate the voltage and current probes with ferromagnetic electrodes of varying dimensions; the magnetic polarity of each can be switched sequentially.^[153] Antiparallel states will have a higher resistance as precession of spin polarized electrons needs to be inverted. Spin injection (flow of spin polarized current into graphene, usually from a magnetized electrode) through both transparent (in direct contact with the electrode)^[575] and tunneling (through a thin dielectric barrier to improve polarization)^[576] is effective, with an asymmetry observed between electron and hole conduction.^[577] The robust spin polarization in graphene is ideal for spin current channels.^[578]

Analogous to normal spintronics, which uses the standard quantum mechanical spin of electrons, pseudospintrronics has been theorized as a way to instill logic operations through unconventional means. Similarly, proposed valleytronics utilizes the charge carriers distinct position in the K or K'

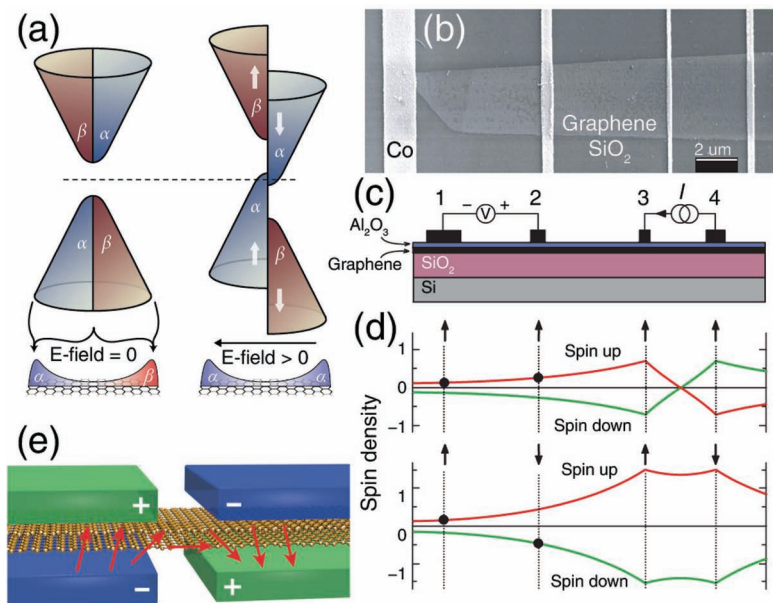


Figure 15. Spintronics. a) Half-metallicity of ZGNRs. DOS schematics show a polarized spin at the edges (left). With an in-plane electric field applied, the DOS shifts to remove the bandgap (right). b,c) SEM image and schematic of four-terminal spin-injection measurements. d) Schematic of the diffusion and precession of spin-polarized currents in the four-terminal device when electrode magnetization is aligned parallel or antiparallel. e) Schematic of a proposed valley valve using perpendicular electric fields applied to bilayer graphene to polarize pseudospin. a) Redrawn.^[486] b-d) Reproduced with permission.^[153] Copyright 2007, Nature Publishing Group. e) Reproduced with permission.^[582] Copyright 2009, American Physical Society.

valleys.^[579] The valley isospin is a more robust form of information, as it takes a larger (on the order of inverse lattice spacing) momentum to scatter compared to pseudospin.^[322] Creating a pseudospin or isospin valve can be as simple as distorting graphene in a controllable way. A narrow constriction neck^[579] or asymmetric bilayer interfaces^[580] that break symmetry are potential valley filter designs. Other proposed structures for pseudospin filters and valves utilize line defects^[581] in monolayers or by alternating perpendicular electric fields in bilayers.^[582] Switching the applied field reverses the pseudospin direction creating a tunable filter (Figure 15e). A digital logic bilayer pseudospin FET has been theorized to use ultralow power.^[583] Strain engineering and subsequent pseudomagnetic fields have a clear link with this pseudospin polarization, and could be used as a mechanism for valley filtration.^[584–590] These proposed devices have yet to be realized, but potentially add a whole new dimension to logic devices.

10. Photonics

10.1. Photodetectors

Photodetectors convert light signals or optical power into electrical current and are a key component for optoelectronic devices: absorbed light creates excitons that separate to form a photocurrent. Conventional photodetectors are mostly based on conventional semiconductor materials; their performance is limited by two factors arising from intrinsic material properties. The first limitation is cutoff wavelength, which depends on the bandgap. Photons with energy below the gap will not be absorbed, resulting in a maximal detectable wavelength (1100 nm for silicon and 2600 nm for InGaAs). Long wavelength transparency limits the far-infrared application for semiconductor photodetectors. The second limitation is operation speed, which is mainly ruled by charge carrier mobility and lifetime. In contrast with traditional semiconductors, graphene has no bandgap, leading to broader wavelength absorption (up to 6 μm) for broadband detection (Figure 16a). Additionally, the exceptionally high carrier mobility makes graphene ideally suited for ultrafast photodetectors. Absorbing only 2.3% of light per layer may limit the photocurrent responsivity, but means photodetectors could be built into transparent electronics.

The photoelectric effect of graphene has been widely studied using SPCM, with observed photocurrents near the graphene-metal junction.^[143] The photocurrent is antisymmetrical over the source-drain electrodes and becomes nearly zero in the middle of the channel (Figure 16b). This observation can be attributed to the nearly symmetric band structure at both metal contacts. Figure 16c shows the schematic potential profile of the device, with the solid line representing the Dirac point and

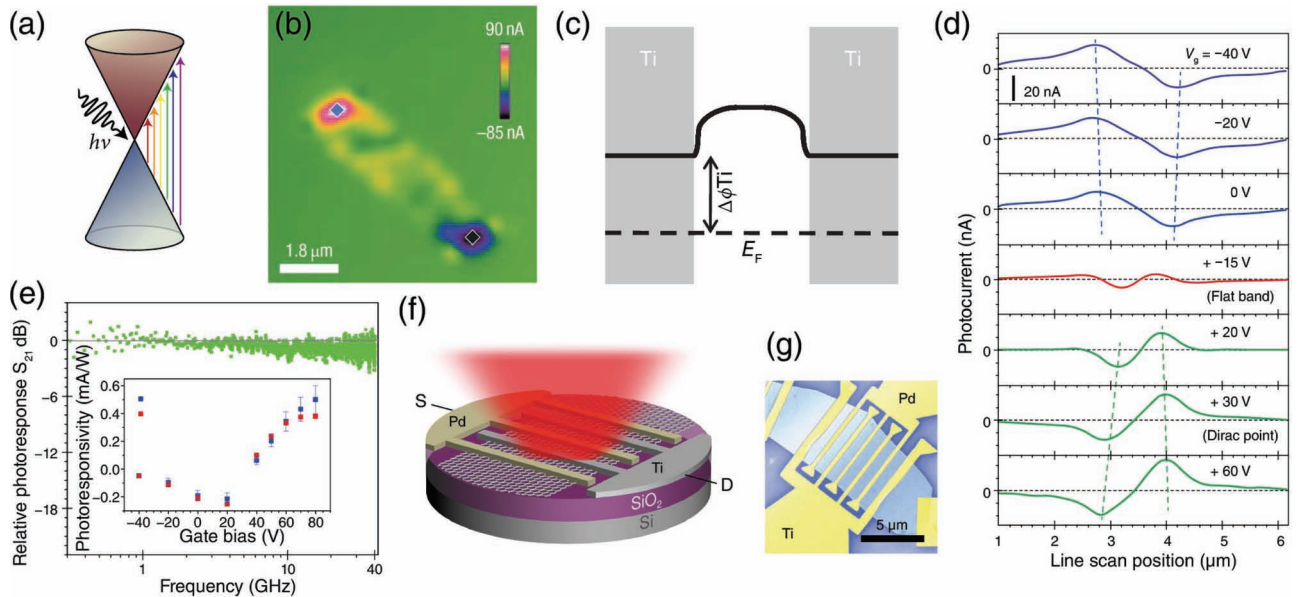


Figure 16. Photodetectors. a) Energy band schematic of the broadband absorption of light by graphene. b) Photocurrent measurements of a graphene photodetector over the whole channel by SPCM. The results clearly show the antisymmetric photocurrent at source electrode and drain electrode, while nearly zero photocurrent is observed at the middle of the device channel. c) Band profile of the graphene photodetector. $\Delta\phi_{Ti}$ represents the difference between the Dirac point energy and Fermi level in Ti-doped graphene. The titanium electrode contact slightly dopes the graphene with electrons to shift its Fermi level up towards the Dirac point, and creates a potential barrier between the graphene under the electrodes and within the channel. d) The photocurrent measure at different gate voltages (from -40 V to 60 V). The results indicate that both increasing or decreasing the gate voltage from 15 V will enlarge the peak amplitude and shift the peak position toward the electrode. e) High-frequency measurements, which show the device performs well up to 40 GHz. The inset pictures the photoresponsivity at different gate voltage both for DC measurements or high-frequency AC measurements. f) The schematics of the antisymmetric design to break the band mirror. The multifinger design enlarges the photoresponsivity. g) False-color SEM image of a real multifinger photodetector. b) Reproduced with permission.^[143] Copyright 2008, Nature Publishing Group. c) Reproduced with permission.^[594] Copyright 2011, Nature Publishing Group. d) Reproduced with permission.^[596] Copyright 2009, Nature Publishing Group. e) Reproduced with permission.^[152] Copyright 2009, American Chemical Society. f) Redrawn.^[598] g) Reproduced with permission.^[598] Copyright 2010, Nature Publishing Group.

the dashed line denoting the Fermi level. Due to the contact metals' smaller work function than graphene, the area under the contact electrode is slightly electron-doped compared to the area within the channel, leading to a built-in potential barrier across the graphene in the channel and under the metal contact. This is analogous to traditional p-n junction photodiodes, where the photon-generated electron-hole pairs can be separated by the built-in potential, contributing to the total measurable photocurrent. The built-in potential is strongest at this junction, resulting in maximum detected photocurrent when these areas are selectively illuminated. Additionally, the same contact of both electrodes can create an opposite symmetric potential profile resulting in antisymmetrical photocurrent characteristic. With further investigation, Xia et al. found that the photocurrent peak amplitude and position can be tuned by a back gate voltage.^[152] As shown in Figure 16d, there is a minimum photocurrent and peaks farthest from the electrode at an applied gate potential of 15 V. Apart from that, either increasing or decreasing the gate voltage will increase the photocurrent and shift the peak position closer to the electrode. This was explained by separating the graphene-metal junction into three parts. One part is the graphene under the electrode (contact-controlled), where the electrical properties are dominated by the metal above. The second is the bulk graphene channel, far from the electrode where the Fermi level is controlled by the back gate. Between these two is the transition region.

With a gate voltage of 15 V, the potential difference between the contact-controlled and bulk graphene is near zero, leading to a flat band and minimal photocurrent. Either increasing or decreasing the gate voltage will enlarge the potential barrier and increase the photocurrent. A peak occurs in the transition region, where the potential barrier is sharpest. Similar to the depletion region in conventional semiconductor junctions, the width of the transition region decreases as potential bending increases, resulting in a shift of the photocurrent peak.

Due to the intrinsically low optical absorption of monolayer graphene, these photodetectors usually have a rather low photocurrent responsivity of 1 mA/W or lower, more than two orders lower than traditional photodetectors, which strongly limits its application.^[591,592] To address this problem, Echtermeyer et al. and Liu et al. respectively coupled gold plasmonic structures with graphene.^[593,594] The nanostructure decorated graphene photodetectors demonstrate very large photocurrents up to 6 mA/W, which is more than one order of magnitude higher than the control devices without plasmonic nanostructures. Such a high enhancement effect is rarely observed in traditional planar semiconductor photodetector because the local enhancement of plasmonic resonance can only affect the material in close proximity to the nanostructures, and the active depth of the traditional semiconductor device is usually much larger. The entire atomic thickness of graphene is within the enhanced field of the nanostructures, and therefore can fully

exploit the local plasmonic enhancement effect to achieve such a large improvement.

Besides the built-in potential theory, the photothermoelectric (PTE) effect was also reported to play a significant role in the photocurrent generation around the monolayer-bilayer and bottom-dual gated interfaces.^[403,595] In theory, the total PTE voltage can be represented as $(S_2 - S_1)\Delta T$, where S_1 and S_2 are the Seebeck coefficients of different sides of the junction and ΔT is the temperature difference.^[403] This theory successfully explains the nonlinear and six fold region photocurrent measurement and may dominate in the graphene-graphene interface, but the photocurrent generation mechanism in the graphene-metal junction is still not fully understood.

High-frequency measurements shown in Figure 16e demonstrate that there is no performance degradation in graphene-based photodetectors up to 40 GHz, which is the limitation of the measurement system itself. Further analysis suggests that the intrinsic bandwidth of graphene can go up to 500 GHz, which is comparable to the fastest III-V based photodetectors.^[596] Recent pump-probe measurements demonstrate that

graphene photodetectors can exhibit intrinsically high response speeds up to the terahertz regime.^[597] With the same metal on both electrodes in the metal-graphene-metal device, the potential profile is symmetric within the channel with opposite photocurrent at each end, leading to a zero total current if the entire device is illuminated. To break the mirror band structure, asymmetric metal electrode design to allow observation of an overall photocurrent with titanium and palladium contacts. This multifinger design (Figure 16e,f) can greatly enhance the active area that exists in one focused laser spot and thus increasing the responsivity. These designs can reach a photocurrent as high as 6.1 mA/W and were successfully implemented in a 10 Gbit/s data link.^[598]

10.2. Mode-Locked Lasers

Mode-locking is a technique widely used in lasers to produce a periodic train of ultrashort pulses, usually on the order of picoseconds to femtoseconds. Saturable absorbers are the most commonly used passive material for mode-locking techniques, which behave as a nonlinear, intensity-dependent filter. An ideal saturable absorber should absorb light at low intensity and become transparent when the light is intense enough. The key features are speed, optical bandwidth and saturation intensity. Conventional semiconductors are widely used in mode-locked lasers; however, they are limited by small optical bandwidths of only tens of nanometers. Saturable absorption can be achieved in graphene due to Pauli blocking. At high incident laser intensity, the concentration of electron-hole pairs increases too much and fills all the states near the conduction or valence bands, obstructing further absorption. The ultrahigh Fermi velocity and large optical bandwidth make graphene an ideal material to be integrated into mode-locked laser devices. Bao et al.^[599] and Sun et al.^[600] demonstrated graphene-based lasers, easily integrated into fiber systems (Figure 17a). Using atomic layer graphene or graphene-poly(vinyl alcohol) composites as a saturable absorber integrated in a fiber layer, they can generate ultrafast soliton pulses (Figure 17b). These have advantages including low saturation intensity, high speed, tunable modulation depth, large optical bandwidth and low inherent costs.

10.3. Optical Modulators

Optical modulators are used to modulate a beam of light. They are commonly used in on-chip optical interconnects and have become increasingly important as electrical

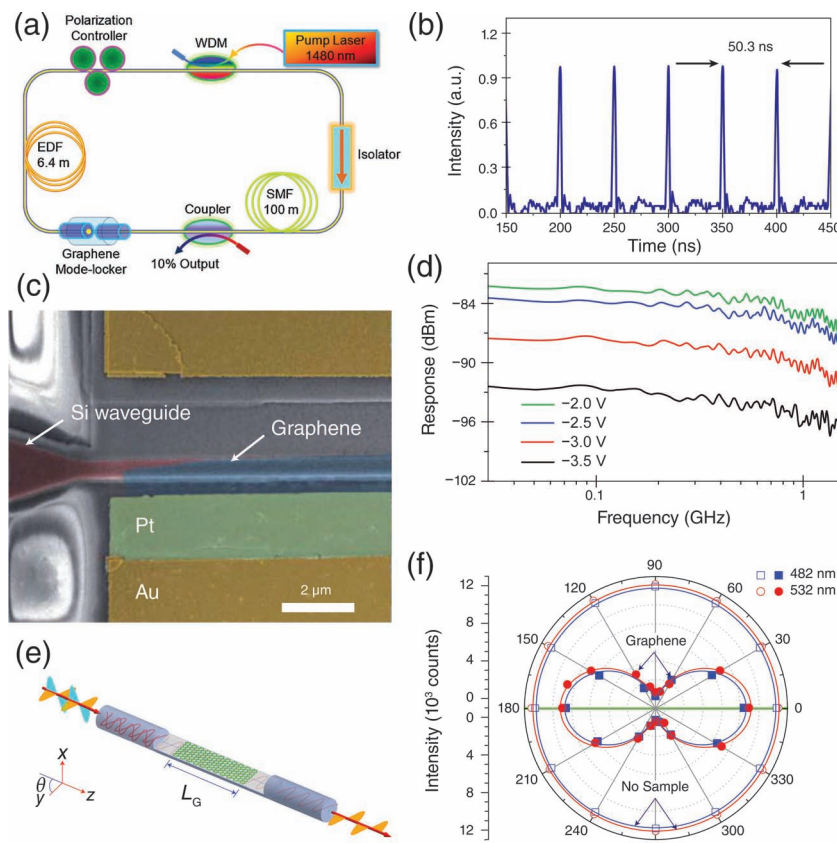


Figure 17. Manipulating light waves. a) Schematic showing the components in a graphene-based mode-locked laser system. b) The oscilloscope data show the graphene-based mode-locked laser can perform at ultrafast speeds. c) SEM image of a graphene optical modulator structure. d) High-frequency measurement of device response as a function of frequency. The 3 dB bandwidth results are around 1 GHz with different gate voltage at -2 V , -2.5 V , -3 V , -4 V . e) Schematic of a graphene-based polarizer with graphene embedded in a side-polished optical fiber. f) Optical intensity at different polarized angles. a) Reproduced with permission.^[599] b) Reproduced with permission.^[600] Copyright 2010, American Chemical Society. c,d) Reproduced with permission.^[601] Copyright 2011, Nature Publishing Group. e,f) Reproduced with permission.^[602] Copyright 2011, Nature Publishing Group.

interconnects face limitations such as high loss, crosstalk, and limited speed. Key features such as high speed, large optical bandwidth, and small footprint are desirable for optical modulators and their on-chip integration. However, the field-effect-based optical modulation (e.g., Franz-Keldysh, Kerr and Pockels effects) in silicon-based devices is usually rather weak, resulting in a millimeter scale footprint. This increases the insertion loss and hinders high-speed performance. An alternative solution to reduce this footprint is via integration with resonant structures. Unfortunately, devices with this kind of structure tend to work over very narrow bandwidths (less than 1 nm), thus greatly reducing the fabrication and environmental tolerance.

Compared with contemporary semiconducting materials, graphene shows many advantages in addition to its high carrier mobility and large optical bandwidth, such as its compatibility with current CMOS processing, low cost, and strong modulation ability, which are all essential features for high-performance optical modulators. Importantly, a graphene-based optical modulator was recently demonstrated with an operation frequency up to 1 GHz (Figure 17c).^[601] The footprint is only 25 μm^2 and the optical bandwidth range demonstrated is from 1.35 μm to 1.6 μm , far from exceeding the ability of current modulators. In this device, silicon waveguides are used to couple in and couple out light, with thin dielectric layers (7 nm) of Al₂O₃. CVD graphene is physically transferred on top of the silicon waveguide as the absorption layer. While tuning the gate voltage, the absorption of graphene will change due to the rather strong electroabsorption effect, resulting in the modulation of light transmission (Figure 17d).

10.4. Polarizers

A polarizer converts undefined light into well-polarized light, and has broad applications in areas ranging from optical circuits to car mirrors and sunglasses. In-line fiber-based polarizers that use an evanescent field substrate processing technology, allow fabrication directly onto the fiber itself. Compared with traditional absorption or beam-splitting polarizers, this technique shows great advantages in device integration with most optical systems. However, the current in-line fiber polarizers are made with materials such as metals or crystals, which limit their optical bandwidth, as well as cause difficulty in changing between transverse electric (TE) and transverse magnetic (TM) pass modes. Graphene can function as an efficient polarizing material by selective attenuation of one polarization mode. It can select which mode to pass and which mode to damp by simply changing its Fermi level, in contrast to metal-based polarizers. Additionally, graphene can be used for polarizers in an ultrawide range of wavelengths, from ultraviolet to far-IR. The broadband graphene polarizer demonstrated by Bao et al. shows the apparent advantages over traditional devices.^[602] This simple structure easily integrates graphene within the fiber (Figure 17e) and works well in a wavelength range from 800 nm to 1650 nm. A strong s-polarization extinction ratio up to 27 dB (Figure 17f) is comparable with metal structures. The TE and TM modes can easily be tuned by changing the gate voltage ($|\mu| < \hbar\omega/2$ to support TE mode and $|\mu| > \hbar\omega/2$ to support TM mode), resulting in a low-cost, broadband, mode-tunable polarizer.

11. Chemical and Biological Sensors

Graphene is of increasing interest for the development of highly sensitive label-free chemical and biological sensors due to its unique combination of several important characteristics. The single-atom thickness and inherently low electrical noise in graphene could enable ultrasensitive chemical and biological sensors.^[603,604] Additionally, the well developed carbon chemistry can be used to functionalize graphene with various organic and inorganic species including atoms, nanoparticles, small molecules, polypeptides,^[605] and nucleotides^[606] to provide an extensive means of tailoring sensing and bio-interfacing abilities.^[607] Aptamers, specific oligonucleotide or peptide strands for targeted binding, can improve selectivity and sensitivity in graphene-based sensors: so-called aptasensors.^[608–610] Bioimaging and targeting of cancer cells with label-functionalized graphene could influence medicine.^[611] The atomically thin structure can also enable many novel sensing schemes, such as nanoporous membranes for DNA probing and sequencing.^[612–614]

Significant work has been carried out to explore graphene-based chemical and biological sensors, with a number of recent reviews.^[615,616] These devices are generally classified into two main categories: GFET-based, with the conductivity responding to nearby charge fluctuation brought by molecular binding near or on graphene; and graphene or graphene-derivative-based electrochemical sensors that detect redox potential and the current of certain species. Graphene is also involved in other sensing schemes such as fluorescence resonance energy transfer sensing^[617] and surface acoustic wave transducer-based gas sensors.^[618] Here we give a brief account of GFET-based chemical and biological sensors.

11.1. Chemical Sensors

Physical or chemical absorption of molecules that dope graphene generally constitutes the underlying principle for chemical sensing. Electron withdrawing groups contribute additional holes to the valence band of the p-type chemically derived graphene and increase the conductivity, which is decreased by electron donors that deplete holes. Various graphene molecular sensors have been reported with targets ranging from gases such as NO₂, NH₃, H₂ and CO and vapors such as alcohols, to biomolecules such as DNA and proteins. The exceptional electronic properties of graphene can allow extreme sensitivity not otherwise possible; an early demonstration showed that a graphene device made from mechanically peeled graphene can detect individual gas molecules (Figure 18b–g).^[619] Typical gas and vapor sensors showed fast response time and high sensitivity, up to approximately one part per billion (ppb). Measuring the Hall conductivity shows that NO₂, H₂O and iodine can function as p-type dopants, while NH₃, CO and ethanol are n-type dopants. Both an experimental and theoretical investigation of adsorbate doping of graphene determine that individual open shell NO₂ molecules are strong acceptors, while closed shell N₂O₄ dimers are weak dopants.^[620] It was also found that lithography residues on graphene could not only chemically dope and increases scattering in the graphene channel, but

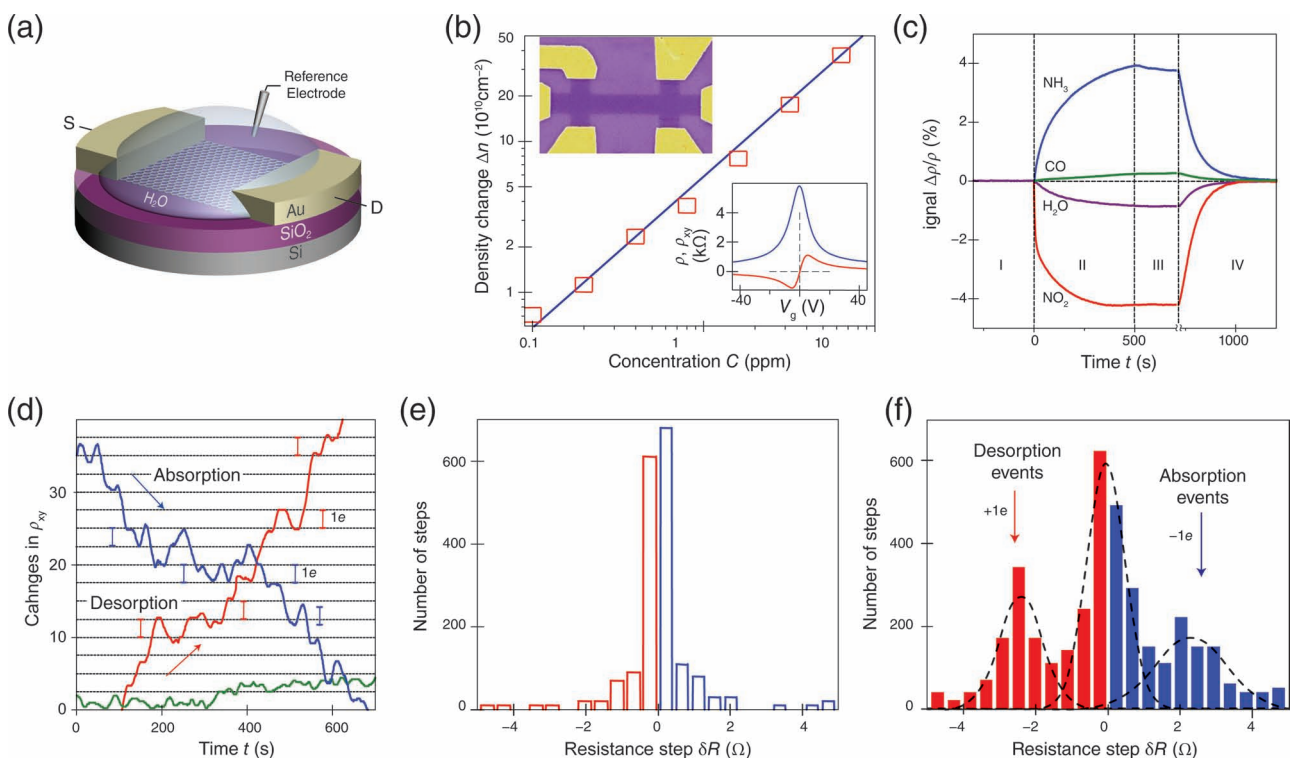


Figure 18. Sensors. a) Schematic of a GFET-based sensor, showing solution making contact with the graphene channel, and a reference electrode. b) Carrier concentration changes, Δn , of graphene as a function of the concentration of the exposed NO_2 source. Upper inset: False-color SEM of the Hall bar device; Lower inset: Field-effect characterization of the device. c) Changes in resistivity, ρ , at zero magnetic field, B , caused by graphene's exposure to various gases diluted in concentration to 1 ppm. d) Observation of changes in the Hall resistivity near the Dirac point during adsorption (blue) and desorption (red) of diluted NO_2 and reference curve (green). e,f) Statistical distribution of step heights: without its exposure to (e) and during a slow desorption of (f) NO_2 . b–f) Reproduced with permission.^[619] Copyright 2007, Nature Publishing Group.

also enhance sensor response by concentrating analyte molecules on the surface.^[621] In contrast, the intrinsic chemical responses of graphene after cleaning off the residue are surprisingly small. Graphene foams have shown parts per million (ppm) sensitivity towards NH_3 and NO_2 , which are reversible, operate at low power, and can be more practical as macroscopic devices.^[355] Chemically derived graphene devices demonstrated good sensitivity towards NO_2 , NH_3 , and dinitrotoluene under ambient conditions.^[622] Molecular sensors based on rGO can detect trace components of explosives and chemical warfare agents with sensitivity as high as ppb.^[623] Inkjet-printed rGO films on a PET substrate are fabricated into flexible and rugged sensors that reversibly detect ppb levels of NO_2 and Cl_2 vapors in air.^[624] Biofunctionalized GFETs can enhance chemical sensitivity: graphene decorated with single stranded DNA is sensitized towards vapor analytes.^[625] Palladium decorated rGO-based GFETs were used for highly sensitive and recoverable NO gas sensing.^[626] Sensors based on rGO films with micropatterned protein-functionalization have demonstrated highly sensitive, real-time detection of various metal ions.^[627]

11.2. Biosensors

Graphene-based biosensors can detect various biological species under physiological conditions. Research of graphene sensors

working in solution started with pH sensing tests, with a solution-gated GFET.^[628] A narrow p-n plateau region near the Dirac point was observed, while capacitive charging of the graphene/solution interface can induce both electron and hole conduction. As pH increases, OH^- adsorption p-dopes the channel, shifting the Dirac point towards positive potential. Charge transport in solution can be significantly affected by aqueous ions that screen impurity charges in the device.^[629,630] A solution-gated GFET showed high transconductance and electronic detection of pH and protein adsorption with a linear dependence of conductance with electrolyte pH.^[631] Additionally, the conductance increased with exposure to picomolar concentrations of a protein through non-specific absorption. Suspended graphene was found to exhibit higher transconductance in the linear operating modes and less low-frequency noise than GFETs supported on SiO_2 substrates.^[632] The rGO-based sensor devices have also demonstrated real-time, label-free detection of the hormonal catecholamine molecules secreted from living cells.^[633]

Although bare graphene devices showed high sensitivity toward biomolecules, there is usually a lack of specificity, which is necessary for any practical sensors. To this end, it is useful to functionalize graphene with receptors that selectively bind to specific target species. With the attachment of specific receptors, CMG biosensors are used to detect bacterium and DNA.^[634] Aptamer modified GFETs showed high sensitivity and

good selectivity toward immunoglobulin E (IgE) protein. The dissociation constant of IgE and the aptamer was calculated according to the calibration curve.^[635] By noncovalently immobilizing single-stranded DNA probes on CVD graphene devices, a DNA sensor can be created for the detection of specific target DNA with the capability to distinguish the mismatch of single-base pairs with a detection limit of 0.01×10^{-9} M.^[634] The sensing mechanism was attributed to n-doping based on interactions of the nucleotides with the graphene channel.

GFETs have also been used to interface with electrogenic cells to monitor the conductance signals resulting from spontaneously beating embryonic chicken cardiomyocytes.^[636] The devices yielded well-defined extracellular signals with signal-to-noise ratio >4 , which exceeded typical values for other planar devices. Additionally, by offsetting the solution gate voltage, both n- and p-type recording can be achieved from the same transistor. Flexible, low-cost, and label-free cancer marker biosensors using layer-by-layer self-assembled graphene on PET showed real-time detection of prostate-specific antigen in a large detection range, from 4 fg/mL to 4 μ g/mL.^[637]

12. Electromechanical Systems

An emerging field in nanoscience is the coupling of electronic and mechanical components into so-called micro- and nano-electromechanical systems (MEMS and NEMS). Utilizing conventional top-down microfabrication techniques as well as bottom-up assembly approaches, complex mechanical structures have been demonstrated at rather small scales. Graphene is an excellent candidate for this purpose, not only for its superior electronic properties as previously discussed, but also for its mechanical strength, flexibility and atomically thin membrane structure.^[638]

Actuators are devices that convert energy into mechanical work, triggering the active material in some form, often using electricity. The unique properties of graphene make it ideal for lightweight and thin film actuators at both macro and micro-mechanical scales. A thermally activated bimorph actuator utilizes the expansion coefficient mismatch of graphene on an organic film.^[639] Asymmetrically treated thin rGO papers work as macroscale electrochemical actuators in electrolyte solution: essentially, a supercapacitor that builds up charges which change bond lengths.^[640] Graphene has been implemented into a crude speaker device using rGO printed on a polymer film,^[641] and has also been suspended into a drum like structures.^[642] A bubble or blister formed by trapping air inside graphene can be tuned using electrostatic forces, and could be used as an adjustable microlens.^[643]

The pioneering work on graphene-based electromechanical devices is a microwave frequency resonator: a suspended monolayer that vibrates out of plane when electrically or optically actuated (**Figure 19a,b**),^[644] and later with multilayers,^[645] with suspended EG,^[249] at radio frequencies,^[646] and expanded to scalable arrays.^[647,648] Resonators of this nature could be useful in detecting minute mass,^[649] temperature, and quantum effects,^[650] which benefit from graphene's high resonant frequencies and lightweight membrane structure. Such devices have been limited by considerable damping effects which are not well understood.^[651]

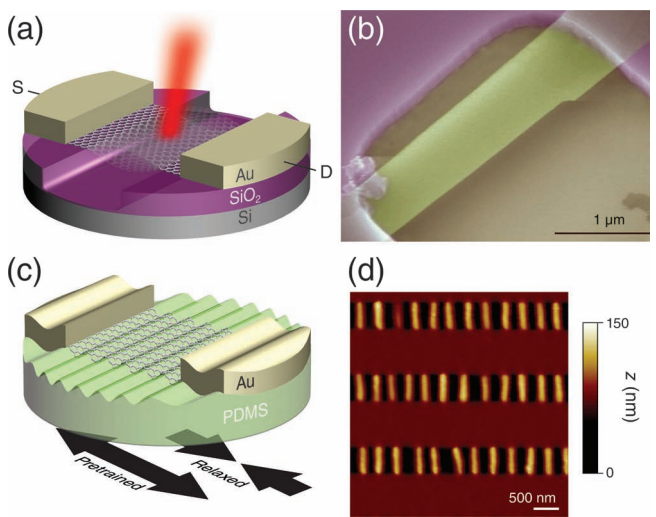


Figure 19. M/NEMS. Graphene nanoresonator, suspended over a trench: schematic (a) and false-color SEM (b). Rippled graphene on a prestrained PDMS substrate, up to 30% strain: schematic of the device (c), and AFM of the periodically buckled ripples along the graphene strips on the relaxed substrate (d). a) Redrawn.^[651] b) Reproduced with permission.^[644] Copyright 2007, American Association for the Advancement of Science. c) Redrawn.^[57] d) Reproduced with permission.^[57] Copyright 2011, American Chemical Society.

These studies have sparked further research in exploring the unique mechanical properties of graphene in novel electromechanical devices, such as mechanically based sensors. NEMS could be utilized to tune the electronic properties with strain. The graphene-based strain gauge is in essence an electromechanical system.^[557] Integrating MEMS and NEMS devices with graphene could prove useful for tunable strain engineering (Figure 19c,d). Non-volatile memory electromechanical switches have been made using suspended, few layer graphene beams as an electromechanical switch, utilizing electrostatic forces to pull the beam towards the silicon substrate until it connects, closing the circuit.^[652,653]

13. Conclusion and Outlook

With a relatively short history, graphene has quickly risen to take center stage of materials science today, exhibiting exciting potential for a wide variety of electronic technologies. New and unorthodox device designs that exploit the unique and remarkable properties of graphene are constantly being developed. A broad range of proof-of-concept devices have been proposed and explored that demonstrate the exciting possibilities of carbon-based electronics.^[654] The spark of graphene has also ignited interest in other inorganic layered materials such as insulating hBN, semiconducting MoS₂,^[655] and topological insulators such as Bi₂Te₃, among others.^[57] Even two-dimensional silica^[656] and experimental evidence of silicene,^[657] an atomically thin honeycomb lattice of silicon, have been synthesized. These can all be combined together into more complex heterostructures^[7,51,658–660] to enable new concepts of devices such as a vertically stacked tunneling transistor^[14] or graphene base

transistors.^[16] Other stable, allotropes of carbon may also prove useful, such as planar graphyne, which introduces *sp*-hybridized triple bonds.^[661–663] Artificial graphene-like electronic materials have been made by designing honeycomb lattices out of molecules and nanostructures with analogous properties.^[664–667]

Graphene has the potential for a new generation of electronic devices; however, many technological complications remain. The application of graphene into functional devices requires close integration with many functional components, often made of strikingly different materials. As a molecular scale material with single atomic thickness, the intrinsic physical properties of graphene can be easily (and often negatively) impacted by these material integration, device fabrication, and processing steps. Improving control, quality, scalability, and durability are all major challenges before graphene can be successfully implemented into various, commercially significant devices. Unconventional processing strategies are clearly necessary to mitigate these challenges and enable devices that can truly capture the intrinsic merits of graphene.

Early startups have focused on synthesizing graphene either as powder in solution, GO or rGO, conductive inks, and wafer scale CVD graphene on metal foil. Others are marketing academic prototypes, while larger corporations have shown their own interest; commercial products implementing graphene are just beyond the horizon. Some technologies are closer to market, such as graphene as printable, flexible, transparent conducting films, or simply as superior electrodes in energy storage applications. Niche applications like mode-lock lasers and radio-frequency switches and amplifiers could all be successful. Many concepts will prove impractical, but are crucial to the advancement of graphene science and engineering. The purpose is not necessarily to replace silicon,^[668] but rather more focused towards novel technologies that were previously inconceivable. For instance foldable, transparent electronics have been shown conceptually, yet remain elusive to consumers.

It could be a while before carbon-based nanoprocessors become technologically and financially feasible; an industrial setting requires an economical perspective in designing and manufacturing high-performance electronics. But undoubtedly, a deep understanding of graphene and similar nanomaterials help enable advanced devices. The far future will likely diverge into completely different technologies that supersede contemporary ideology, such as quantum computing^[669] or light-based circuitry in metatronics.^[670,671] They are built on the shoulders of today's achievements. Laboratory scale investigations play a major role in these innovations and establish indispensable milestones, whether particular experiments lead anywhere directly or not. Continued research and development of advanced devices utilizing graphene is critical in furthering nanoelectronics beyond existing capabilities.

Acknowledgements

X.D. acknowledges financial support by the NSF CAREER award 0956171 and the NIH Director's New Innovator Award 1DP2OD004342-01; Y.H. acknowledges support by the NIH Director's New Innovator Award 1DP2OD007279. N.O.W. acknowledges support by the NSF IGERT: Materials Creation Training Program (MCTP)-DGE-0654431 and the California NanoSystems Institute; H.Z. is grateful to the Camille and

Henry Dreyfus Foundation for financial support through the Camille and Henry Dreyfus Postdoctoral Program in Environmental Chemistry.

Received: April 12, 2012

Revised: June 14, 2012

Published online: August 29, 2012

- [1] K. S. Novoselov, A. K. Geim, S. Morozov, D. Jiang, Y. Zhang, S. V. Dubonos, I. V. Grigorieva, A. A. Firsov, *Science* **2004**, *306*, 666.
- [2] K. Novoselov, A. Geim, S. Morozov, D. Jiang, M. Katsnelson, I. Grigorieva, S. Dubonos, A. Firsov, *Nature* **2005**, *438*, 197.
- [3] A. K. Geim, K. S. Novoselov, *Nat. Mater.* **2007**, *6*, 183.
- [4] A. K. Geim, *Science* **2009**, *324*, 1530.
- [5] G. E. Moore, *Electronics* **1965**, *38*, 114.
- [6] F. Schwierz, *Nat. Nanotechnol.* **2010**, *5*, 487.
- [7] K. S. Novoselov, *Angew. Chem. Int. Ed.* **2011**, *50*, 6986.
- [8] A. K. Geim, *Angew. Chem. Int. Ed.* **2011**, *50*, 6966.
- [9] S. Iijima, *Nature* **1991**, *354*, 56.
- [10] H. W. Kroto, J. R. Heath, S. C. O'Brien, R. F. Curl, R. E. Smalley, *Nature* **1985**, *318*, 162.
- [11] P. Avouris, Z. Chen, V. Perebeinos, *Nat. Nanotechnol.* **2007**, *2*, 605.
- [12] E. V. Castro, H. Ochoa, M. I. Katsnelson, R. V. Gorbachev, D. C. Elias, K. S. Novoselov, A. K. Geim, F. Guinea, *Phys. Rev. Lett.* **2010**, *105*, 266601.
- [13] X. L. Wang, S. X. Dou, C. Zhang, *NPG Asia Mater.* **2010**, *2*, 31.
- [14] L. Britnell, R. V. Gorbachev, R. Jalil, B. D. Belle, F. Schedin, A. Mishchenko, T. Georgiou, M. I. Katsnelson, L. Eaves, S. V. Morozov, N. M. R. Peres, J. Leist, A. K. Geim, K. S. Novoselov, L. A. Ponomarenko, *Science* **2012**, *335*, 947.
- [15] C.-Y. Sung, J. U. Lee, *IEEE Spectr.* **2012**, *49*, 32.
- [16] W. Mehr, J. C. Scheytt, J. Dabrowski, G. Lippert, Y.-H. Xie, M. C. Lemme, M. Ostling, G. Lupina, *IEEE Electron Device Lett.* **2012**, *33*, 691.
- [17] H. Yang, J. Heo, S. Park, H. J. Song, D. H. Seo, K.-E. Byun, P. Kim, I. Yoo, H.-J. Chung, K. Kim, *Science* **2012**.
- [18] Q. Yan, B. Huang, J. Yu, F. W. Zheng, J. Zang, J. Wu, B.-L. Gu, F. Liu, W. H. Duan, *Nano Lett.* **2007**, *7*, 1469.
- [19] W. J. Yu, S. Y. Lee, S. H. Chae, D. Perello, G. H. Han, M. Yun, Y. H. Lee, *Nano Lett.* **2011**, *11*, 1344.
- [20] K. Kim, J.-Y. Choi, T. Kim, S.-H. Cho, H.-J. Chung, *Nature* **2011**, *479*, 338.
- [21] R. R. Nair, P. Blake, A. N. Grigorenko, K. S. Novoselov, T. J. Booth, T. Stauber, N. M. R. Peres, A. K. Geim, *Science* **2008**, *320*, 1308.
- [22] J. P. Reed, B. Uchoa, Y. I. Joe, Y. Gan, D. Casa, E. Fradkin, P. Abbamonte, *Science* **2010**, *330*, 805.
- [23] R. A. Suleimanov, N. A. Abdullaev, *Carbon* **1993**, *31*, 1011.
- [24] D. Yoon, Y.-W. Son, H. Cheong, *Nano Lett.* **2011**, *11*, 3227.
- [25] A. A. Balandin, S. Ghosh, W. Bao, I. Calizo, D. Teweldebrhan, F. Miao, C. N. Lau, *Nano Lett.* **2008**, *8*, 902.
- [26] S. Ghosh, I. Calizo, D. Teweldebrhan, E. P. Pokatilov, D. L. Nika, A. A. Balandin, W. Bao, F. Miao, C. N. Lau, *Appl. Phys. Lett.* **2008**, *92*, 151911.
- [27] Q. Liang, X. Yao, W. Wang, Y. Liu, C. P. Wong, *ACS Nano* **2011**, *5*, 2392.
- [28] K. M. F. Shahil, A. A. Balandin, *Nano Lett.* **2012**, *12*, 861.
- [29] K. L. Grosse, M.-H. Bae, F. Lian, E. Pop, W. P. King, *Nat. Nanotechnol.* **2011**, *6*, 287.
- [30] I. W. Frank, D. M. Tanenbaum, A. M. Van der Zande, P. L. McEuen, *J. Vac. Sci. Technol. B* **2007**, *25*, 2558.
- [31] C. Lee, X. Wei, J. W. Kysar, J. Hone, *Science* **2008**, *321*, 385.
- [32] X. Liu, T. H. Metcalf, J. T. Robinson, B. H. Houston, F. Scarpa, *Nano Lett.* **2012**, *12*, 1013.

- [33] S. Stankovich, D. A. Dikin, G. H. B. Dommett, K. M. Kohlhaas, E. J. Zimney, E. A. Stach, R. D. Piner, S. T. Nguyen, R. S. Ruoff, *Nature* **2006**, *442*, 282.
- [34] T. Ramanathan, A. A. Abdala, S. Stankovich, D. A. Dikin, M. Herrera Alonso, R. D. Piner, D. H. Adamson, H. C. Schniepp, X. Chen, R. S. Ruoff, S. T. Nguyen, I. A. Aksay, R. K. Prud'Homme, L. C. Brinson, *Nat. Nanotechnol.* **2008**, *3*, 327.
- [35] X. Huang, X. Qi, F. Boey, H. Zhang, *Chem. Soc. Rev.* **2012**, *41*, 666.
- [36] M. K. Shin, B. Lee, S. H. Kim, J. A. Lee, G. M. Spinks, S. Gambhir, G. G. Wallace, M. E. Kozlov, R. H. Baughman, S. J. Kim, *Nat. Commun.* **2012**, *3*, 650.
- [37] J. R. Potts, D. R. Dreyer, C. W. Bielawski, R. S. Ruoff, *Polymer* **2011**, *52*, 5.
- [38] L. Gong, R. J. Young, I. A. Kinloch, I. Riaz, R. Jalil, K. S. Novoselov, *ACS Nano* **2012**, *6*, 2086.
- [39] S. P. Koenig, N. G. Boddeti, M. L. Dunn, J. S. Bunch, *Nat. Nanotechnol.* **2011**, *6*, 543.
- [40] T. Yoon, W. C. Shin, T. Y. Kim, J. H. Mun, T.-S. Kim, B. J. Cho, *Nano Lett.* **2012**, *12*, 1448.
- [41] L. Spanu, S. Sorella, G. Galli, *Phys. Rev. Lett.* **2009**, *103*, 196401.
- [42] S. Wang, Y. Zhang, N. Abidi, L. Cabrales, *Langmuir* **2009**, *25*, 11078.
- [43] J. Rafiee, X. Mi, H. Gullapalli, A. V. Thomas, F. Yavari, Y. Shi, P. M. Ajayan, N. A. Koratkar, *Nat. Mater.* **2012**, *11*, 217.
- [44] D. Prasai, J. C. Tuberquia, R. R. Harl, G. K. Jennings, K. I. Bolotin, *ACS Nano* **2012**, *6*, 1102.
- [45] P. R. Wallace, *Phys. Rev.* **1947**, *71*, 622.
- [46] A. H. Castro Neto, F. Guinea, N. M. R. Peres, K. S. Novoselov, A. K. Geim, *Rev. Mod. Phys.* **2009**, *81*, 109.
- [47] D. S. L. Abergel, V. Apalkov, J. Berashevich, K. Ziegler, T. Chakraborty, *Adv. Phys.* **2010**, *59*, 261.
- [48] S. Das Sarma, S. Adam, E. H. Hwang, E. Rossi, *Rev. Mod. Phys.* **2011**, *83*, 407.
- [49] N. M. R. Peres, *Rev. Mod. Phys.* **2010**, *82*, 2673.
- [50] J. Slonczewski, P. Weiss, *Phys. Rev.* **1958**, *109*, 272.
- [51] A. S. Mayorov, R. V. Gorbachev, S. V. Morozov, L. Britnell, R. Jalil, L. A. Ponomarenko, P. Blake, K. S. Novoselov, K. Watanabe, T. Taniguchi, A. K. Geim, *Nano Lett.* **2011**, *11*, 2396.
- [52] H. B. Heersche, P. Jarillo-Herrero, J. B. Oostinga, L. M. K. Vandersypen, A. F. Morpurgo, *Nature* **2007**, *446*, 56.
- [53] A. Bostwick, T. Ohta, T. Seyller, K. Horn, E. Rotenberg, *Nat. Phys.* **2007**, *3*, 36.
- [54] D. C. Elias, R. V. Gorbachev, A. S. Mayorov, S. V. Morozov, A. A. Zhukov, P. Blake, K. S. Novoselov, A. K. Geim, F. Guinea, *Nat. Phys.* **2011**, *7*, 701.
- [55] A. Bostwick, T. Ohta, J. L. McChesney, K. V. Emtsev, F. Speck, T. Seyller, K. Horn, S. D. Kevan, E. Rotenberg, *New J. Phys.* **2010**, *12*, 125014.
- [56] Y. Mimura, S. Hiyamizu, T. Fujii, K. Nanbu, *Jpn. J. Appl. Phys.* **1980**, *19*, L225.
- [57] J. E. Moore, *Nature* **2010**, *464*, 194.
- [58] M. Z. Hasan, C. L. Kane, *Rev. Mod. Phys.* **2010**, *82*, 3045.
- [59] Y. Zhang, Y. Tan, H. Stormer, P. Kim, *Nature* **2005**, *438*, 201.
- [60] Z. Jiang, Y. Zhang, Y.-W. Tan, H. L. Stormer, P. Kim, *Solid State Commun.* **2007**, *143*, 14.
- [61] G. Li, E. Y. Andrei, *Nat. Phys.* **2007**, *3*, 623.
- [62] C. R. Dean, A. F. Young, P. Cadden-Zimansky, L. Wang, H. Ren, K. Watanabe, T. Taniguchi, P. Kim, J. Hone, K. L. Shepard, *Nat. Phys.* **2011**, *7*, 693.
- [63] D. L. Miller, K. D. Kubista, G. M. Rutter, M. Ruan, W. A. de Heer, P. N. First, J. A. Stroscio, *Science* **2009**, *324*, 924.
- [64] K. I. Bolotin, F. Ghahari, M. D. Shulman, H. L. Stormer, P. Kim, *Nature* **2009**, *462*, 196.
- [65] D. A. Abanin, S. V. Morozov, L. A. Ponomarenko, R. V. Gorbachev, A. S. Mayorov, M. I. Katsnelson, K. Watanabe, T. Taniguchi, K. S. Novoselov, L. S. Levitov, A. K. Geim, *Science* **2011**, *332*, 328.
- [66] M. I. Katsnelson, K. S. Novoselov, A. K. Geim, *Nat. Phys.* **2006**, *2*, 620.
- [67] A. F. Young, P. Kim, *Nat. Phys.* **2009**, *5*, 222.
- [68] N. Stander, B. Huard, D. Goldhaber-Gordon, *Phys. Rev. Lett.* **2009**, *102*, 026807.
- [69] D. A. Abanin, L. S. Levitov, *Science* **2007**, *317*, 641.
- [70] J. R. Williams, L. DiCarlo, C. M. Marcus, *Science* **2007**, *317*, 638.
- [71] V. V. Cheianov, V. I. Fal'ko, *Phys. Rev. B* **2006**, *74*, 041403.
- [72] H.-C. Cheng, R.-J. Shiue, C.-C. Tsai, W.-H. Wang, Y.-T. Chen, *ACS Nano* **2011**, *5*, 2051.
- [73] G. Liu, J. J. Velasco, W. Bao, C. N. Lau, *Appl. Phys. Lett.* **2008**, *92*, 203103.
- [74] J. Velasco, G. Liu, W. Bao, C. N. Lau, *New J. Phys.* **2009**, *11*, 095008.
- [75] R. V. Gorbachev, A. S. Mayorov, A. K. Savchenko, D. W. Horsell, F. Guinea, *Nano Lett.* **2008**, *8*, 1995.
- [76] V. V. Cheianov, V. Fal'ko, B. L. Altshuler, *Science* **2007**, *315*, 1252.
- [77] A. Vakil, N. Engheta, *Science* **2011**, *332*, 1291.
- [78] J. R. Williams, T. Low, M. S. Lundstrom, C. M. Marcus, *Nat. Nanotechnol.* **2011**, *6*, 222.
- [79] R. Nandkishore, L. S. Levitov, A. V. Chubukov, *Nat. Phys.* **2012**, *8*, 158.
- [80] J. L. McChesney, A. Bostwick, T. Ohta, T. Seyller, K. Horn, J. González, E. Rotenberg, *Phys. Rev. Lett.* **2010**, *104*, 136803.
- [81] K. I. Bolotin, K. J. Sikes, J. Hone, H. L. Stormer, P. Kim, *Phys. Rev. Lett.* **2008**, *101*, 096802.
- [82] X. Du, I. Skachko, A. Barker, E. Y. Andrei, *Nat. Nanotechnol.* **2008**, *3*, 491.
- [83] C. R. Dean, A. F. Young, I. Meric, C. Lee, L. Wang, S. Sorgenfrei, K. Watanabe, T. Taniguchi, P. Kim, K. L. Shepard, J. Hone, *Nat. Nanotechnol.* **2010**, *5*, 722.
- [84] S.-Y. Chen, P.-H. Ho, R.-J. Shiue, C.-W. Chen, W.-H. Wang, *Nano Lett.* **2012**, *12*, 964.
- [85] J.-H. Chen, C. Jang, S. Xiao, M. Ishigami, M. S. Fuhrer, *Nat. Nanotechnol.* **2008**, *3*, 206.
- [86] L. Liao, J. Bai, Y. Qu, Y.-C. Lin, Y. Li, Y. Huang, X. Duan, *Proc. Natl. Acad. Sci. USA* **2010**, *107*, 6711.
- [87] N. Petrone, C. R. Dean, I. Meric, A. M. van der Zande, P. Y. Huang, L. Wang, D. Muller, K. L. Shepard, J. Hone, *Nano Lett.* **2012**, *12*, 2751.
- [88] C. Berger, Z. Song, X. B. Li, X. S. Wu, N. Brown, C. Naud, D. Mayou, T. B. Li, J. Hass, A. N. Marchenkov, E. H. Conrad, P. N. First, W. A. de Heer, *Science* **2006**, *312*, 1191.
- [89] K. V. Emtsev, A. Bostwick, K. Horn, J. Jobst, G. L. Kellogg, L. Ley, J. L. McChesney, T. Ohta, S. A. Reshanov, J. Roehrl, E. Rotenberg, A. K. Schmid, D. Waldmann, H. B. Weber, T. Seyller, *Nat. Mater.* **2009**, *8*, 203.
- [90] J. A. Robinson, M. Wetherington, J. L. Tedesco, P. M. Campbell, X. Weng, J. Stitt, M. A. Fanton, E. Frantz, D. Snyder, B. L. VanMil, G. G. Jernigan, R. L. Myers-Ward, C. R. Eddy, D. K. Gaskill, *Nano Lett.* **2009**, *9*, 2873.
- [91] G. Jo, S.-I. Na, S.-H. Oh, S. Lee, T.-S. Kim, G. Wang, M. Choe, W. Park, J. Yoon, D.-Y. Kim, Y. H. Kahng, T. Lee, *Appl. Phys. Lett.* **2010**, *97*, 213301.
- [92] S. Kim, J. Nah, I. Jo, D. Shahrjerdi, L. Colombo, Z. Yao, E. Tutuc, S. K. Banerjee, *Appl. Phys. Lett.* **2009**, *94*, 062107.
- [93] M. Sprinkle, M. Ruan, Y. Hu, J. Hankinson, M. Rubio-Roy, B. Zhang, X. Wu, C. Berger, W. A. de Heer, *Nat. Nanotechnol.* **2010**, *5*, 727.
- [94] S. Y. Zhou, G.-H. Gweon, A. V. Fedorov, P. N. First, W. A. de Heer, D.-H. Lee, F. Guinea, A. H. C. Neto, A. Lanzara, *Nat. Mater.* **2007**, *6*, 770.

- [95] H. Liu, Y. Liu, D. Zhu, *J. Mater. Chem.* **2011**, *21*, 3335.
- [96] Y. Wang, C. Miao, B.-c. Huang, J. Zhu, W. Liu, Y. Park, Y.-h. Xie, J. C. S. Woo, *IEEE Trans. Electron Devices* **2010**, *57*, 3472.
- [97] F. Yavari, C. Kritzinger, C. Gaire, L. Song, H. Gullapalli, T. Borca-Tasciuc, P. M. Ajayan, N. Koratkar, *Small* **2010**, *6*, 2535.
- [98] Y.-C. Lin, C.-C. Lu, C.-H. Yeh, C. Jin, K. Suenaga, P.-W. Chiu, *Nano Lett.* **2011**, *12*, 414.
- [99] W. Bao, G. Liu, Z. Zhao, H. Zhang, D. Yan, A. Deshpande, B. J. LeRoy, C. N. Lau, *Nano Res.* **2010**, *3*, 98.
- [100] N. Staley, H. Wang, C. Puls, J. Forster, T. N. Jackson, K. McCarthy, B. Clouser, Y. Liu, *Appl. Phys. Lett.* **2007**, *90*, 143518.
- [101] Z. H. Ni, H. M. Wang, Z. Q. Luo, Y. Y. Wang, T. Yu, Y. H. Wu, Z. X. Shen, *J. Raman Spectrosc.* **2010**, *41*, 479.
- [102] X. Jia, M. Hofmann, V. Meunier, B. G. Sumpter, J. Campos-Delgado, J. M. Romo-Herrera, H. Son, Y.-P. Hsieh, A. Reina, J. Kong, M. Terrones, M. S. Dresselhaus, *Science* **2009**, *323*, 1701.
- [103] J. Moser, A. Barreiro, A. Bachtold, *Phys. Rev. Lett.* **2007**, *91*, 163513.
- [104] A. M. Goossens, V. E. Calado, A. Barreiro, K. Watanabe, T. Taniguchi, L. M. K. Vandersypen, *Appl. Phys. Lett.* **2012**, *100*, 073110.
- [105] P. Blake, E. W. Hill, A. H. Castro Neto, K. S. Novoselov, D. Jiang, R. Yang, T. J. Booth, A. K. Geim, *Appl. Phys. Lett.* **2007**, *91*, 063124.
- [106] C. H. Lui, L. Liu, K. F. Mak, G. W. Flynn, T. F. Heinz, *Nature* **2009**, *462*, 339.
- [107] M. Ishigami, J. H. Chen, W. G. Cullen, M. S. Fuhrer, E. D. Williams, *Nano Lett.* **2007**, *7*, 1643.
- [108] A. Deshpande, W. Bao, Z. Zhao, C. N. Lau, B. J. LeRoy, *Phys. Rev. B* **2011**, *83*, 155409.
- [109] J. Martin, N. Akerman, G. Ulbricht, T. Lohmann, J. H. Smet, K. von Klitzing, A. Yacoby, *Nat. Phys.* **2008**, *4*, 144.
- [110] L. A. Ponomarenko, A. K. Geim, A. A. Zhukov, R. Jalil, S. V. Morozov, K. S. Novoselov, I. V. Grigorieva, E. H. Hill, V. V. Cheianov, V. I. Fal'ko, K. Watanabe, T. Taniguchi, R. V. Gorbachev, *Nat. Phys.* **2011**, *7*, 958.
- [111] L. Liao, J. Bai, Y. Qu, Y. Huang, X. Duan, *Nanotechnology* **2010**, *21*, 015705.
- [112] Q. Liu, Z. Liu, X. Zhong, L. Yang, N. Zhang, G. Pan, S. Yin, Y. Chen, J. Wei, *Adv. Funct. Mater.* **2009**, *19*, 894.
- [113] X. Hong, J. Hoffman, A. Posadas, K. Zou, C. H. Ahn, J. Zhu, *Appl. Phys. Lett.* **2010**, *97*, 033114.
- [114] E. B. Song, B. Lian, S. M. Kim, S. Lee, T.-K. Chung, M. Wang, C. Zeng, G. Xu, K. Wong, Y. Zhou, H. I. Rasool, D. H. Seo, H.-J. Chung, J. Heo, S. Seo, K. L. Wang, *Appl. Phys. Lett.* **2011**, *99*, 042109.
- [115] L. Liao, J. Bai, R. Cheng, Y.-C. Lin, S. Jiang, Y. Huang, X. Duan, *Nano Lett.* **2010**, *10*, 1917.
- [116] L. Liao, J. Bai, Y.-C. Lin, Y. Qu, Y. Huang, X. Duan, *Adv. Mater.* **2010**, *22*, 1941.
- [117] Z. Wang, H. Xu, Z. Zhang, S. Wang, L. Ding, Q. Zeng, L. Yang, T. Pei, X. Liang, M. Gao, L.-M. Peng, *Nano Lett.* **2010**, *10*, 2024.
- [118] W. Zhu, D. Neumayer, V. Perebeinos, P. Avouris, *Nano Lett.* **2010**, *10*, 3572.
- [119] J. Xue, J. Sanchez-Yamagishi, D. Bulmash, P. Jacquod, A. Deshpande, K. Watanabe, T. Taniguchi, P. Jarillo-Herrero, B. J. Leroy, *Nat. Mater.* **2011**, *10*, 282.
- [120] I. Meric, C. Dean, A. Young, J. Hone, P. Kim, K. L. Shepard, presented at *IEEE Int. Electron Devices Meeting*, San Francisco, CA, 6–8 December **2010**.
- [121] I. Meric, C. R. Dean, H. Shu-Jen, W. Lei, K. A. Jenkins, J. Hone, K. L. Shepard, presented at *IEEE Int. Electron Devices Meeting*, Washington, DC, 5–7 December **2011**.
- [122] K. H. Lee, H.-J. Shin, J. Lee, I.-y. Lee, G.-H. Kim, J.-Y. Choi, S.-W. Kim, *Nano Lett.* **2012**, *12*, 714.
- [123] W. Gannett, W. Regan, K. Watanabe, T. Taniguchi, M. F. Crommie, A. Zettl, *Appl. Phys. Lett.* **2011**, *98*, 242105.
- [124] W. Han, T. Taychatanapat, A. Hsu, K. Watanabe, T. Taniguchi, P. Jarillo-Herrero, T. Palacios, *IEEE Electron Device Lett.* **2011**, *32*, 1209.
- [125] M. Yankowitz, J. Xue, D. Cormode, J. D. Sanchez-Yamagishi, K. Watanabe, T. Taniguchi, P. Jarillo-Herrero, P. Jacquod, B. J. LeRoy, *Nat. Phys.* **2012**, *8*, 382.
- [126] J. M. Garcia, U. Wurstbauer, A. Levy, L. N. Pfeiffer, A. Pinczuk, A. S. Plaut, L. Wang, C. R. Dean, R. Buizza, A. Van Der Zande, J. Hone, K. Watanabe, T. Taniguchi, *Solid State Commun.* **2012**, *152*, 975.
- [127] A. K. M. Newaz, Y. S. Puzyrev, B. Wang, S. T. Pantelides, K. I. Bolotin, *Nat. Commun.* **2012**, *3*, 734.
- [128] J. Yu, G. Liu, A. V. Sumant, V. Goyal, A. A. Balandin, *Nano Lett.* **2012**, *12*, 1603.
- [129] E.-A. Kim, A. H. C. Neto, *Europhys. Lett.* **2008**, *84*, 57007.
- [130] A. Fasolino, J. H. Los, M. I. Katsnelson, *Nat. Mater.* **2007**, *6*, 858.
- [131] J. C. Meyer, A. K. Geim, M. I. Katsnelson, K. S. Novoselov, T. J. Booth, S. Roth, *Nature* **2007**, *446*, 60.
- [132] W. Bao, F. Miao, Z. Chen, H. Zhang, W. Jang, C. Dames, C. N. Lau, *Nat. Nanotechnol.* **2009**, *4*, 562.
- [133] J. C. Meyer, A. K. Geim, M. I. Katsnelson, K. S. Novoselov, D. Obergfell, S. Roth, C. Girit, A. Zettl, *Solid State Commun.* **2007**, *143*, 101.
- [134] X. Xie, L. Ju, X. Feng, Y. Sun, R. Zhou, K. Liu, S. Fan, Q. Li, K. Jiang, *Nano Lett.* **2009**, *9*, 2565.
- [135] K. Kim, Z. Lee, B. D. Malone, K. T. Chan, B. Aleman, W. Regan, W. Gannett, M. F. Crommie, M. L. Cohen, A. Zettl, *Phys. Rev. B* **2011**, *83*, 245433.
- [136] M. J. Allen, M. Wang, S. A. V. Jannuzzi, Y. Yang, K. L. Wang, R. B. Kaner, *Chem. Commun.* **2009**, *41*, 6285.
- [137] K. I. Bolotin, K. J. Sikes, Z. Jiang, M. Klima, G. Fudenberg, J. Hone, P. Kim, H. L. Stormer, *Solid State Commun.* **2008**, *146*, 351.
- [138] K. Kim, V. I. Artyukhov, W. Regan, Y. Liu, M. F. Crommie, B. I. Yakobson, A. Zettl, *Nano Lett.* **2011**, *12*, 293.
- [139] J. S. Bunch, S. S. Verbridge, J. S. Alden, A. M. van der Zande, J. M. Parpia, H. G. Craighead, P. L. McEuen, *Nano Lett.* **2008**, *8*, 2458.
- [140] R. R. Nair, H. A. Wu, P. N. Jayaram, I. V. Grigorieva, A. K. Geim, *Science* **2012**, *335*, 442.
- [141] K. Nagashio, T. Nishimura, K. Kita, A. Toriumi, *Appl. Phys. Lett.* **2010**, *97*.
- [142] S. Russo, M. F. Craciun, M. Yamamoto, A. F. Morpurgo, S. Tarucha, *Physica E* **2010**, *42*, 677.
- [143] E. J. H. Lee, K. Balasubramanian, R. T. Weitz, M. Burghard, K. Kern, *Nat. Nanotechnol.* **2008**, *3*, 486.
- [144] T. Mueller, F. Xia, M. Freitag, J. Tsang, P. Avouris, *Phys. Rev. B* **2009**, *79*, 245430.
- [145] A. D. Franklin, H. Shu-Jen, A. A. Bol, W. Haensch, *IEEE Electron Device Lett.* **2011**, *32*, 1035.
- [146] G. Giovannetti, P. A. Khomyakov, G. Brocks, V. M. Karpan, J. van den Brink, P. J. Kelly, *Phys. Rev. Lett.* **2008**, *101*, 026803.
- [147] H. Xu, S. Wang, Z. Zhang, Z. Wang, H. Xu, L.-M. Peng, *Appl. Phys. Lett.* **2012**, *100*, 103501.
- [148] F. Xia, V. Perebeinos, Y.-M. Lin, Y. Wu, P. Avouris, *Nat. Nanotechnol.* **2011**, *6*, 179.
- [149] L. Liao, Y.-C. Lin, M. Bao, R. Cheng, J. Bai, Y. Liu, Y. Qu, K. L. Wang, Y. Huang, X. Duan, *Nature* **2010**, *467*, 305.
- [150] J. A. Robinson, M. LaBella, M. Zhu, M. Hollander, R. Kasarda, Z. Hughes, K. Trumbull, R. Cavalero, D. Snyder, *Appl. Phys. Lett.* **2011**, *98*, 053103.
- [151] K. Nagashio, T. Nishimura, K. Kita, A. Toriumi, presented at *IEEE Int. Electron Devices Meeting*, Baltimore, MD, 7–9 December **2009**.
- [152] F. Xia, T. Mueller, R. Golizadeh-Mojarad, M. Freitag, Y.-M. Lin, J. Tsang, V. Perebeinos, P. Avouris, *Nano Lett.* **2009**, *9*, 1039.

- [153] N. Tombros, C. Jozsa, M. Popinciuc, H. T. Jonkman, B. J. v. Wees, *Nature* **2007**, *448*, 571.
- [154] H. B. Heersche, P. Jarillo-Herrero, J. B. Oostinga, L. M. K. Vandersypen, A. F. Morpurgo, *Solid State Commun.* **2007**, *143*, 72.
- [155] X. Du, I. Skachko, E. Y. Andrei, *Phys. Rev. B* **2008**, *77*, 184507.
- [156] F. Guinea, M. I. Katsnelson, A. K. Geim, *Nat. Phys.* **2010**, *6*, 30.
- [157] N. Levy, S. A. Burke, K. L. Meaker, M. Panlasigui, A. Zettl, F. Guinea, A. H. C. Neto, M. F. Crommie, *Science* **2010**, *329*, 544.
- [158] R. R. Nair, M. Sepioni, I. L. Tsai, O. Lehtinen, J. Keinonen, A. V. Krasheninnikov, T. Thomson, A. K. Geim, I. V. Grigorieva, *Nat. Phys.* **2012**, *8*, 199.
- [159] J.-H. Chen, L. Li, W. G. Cullen, E. D. Williams, M. S. Fuhrer, *Nat. Phys.* **2011**, *7*, 535.
- [160] S. Chandratre, P. Sharma, *Appl. Phys. Lett.* **2012**, *100*, 023114.
- [161] M. T. Ong, E. J. Reed, *ACS Nano* **2011**, *6*, 1387.
- [162] Y.-J. Hu, J. Jin, H. Zhang, P. Wu, C.-X. Cai, *Acta Phys.-Chim. Sin.* **2010**, *26*, 2073.
- [163] L. Yan, Y. B. Zheng, F. Zhao, S. Li, X. Gao, B. Xu, P. S. Weiss, Y. Zhao, *Chem. Soc. Rev.* **2012**, *41*, 97.
- [164] S. Ryu, M. Y. Han, J. Maultzsch, T. F. Heinz, P. Kim, M. L. Steigerwald, L. E. Brus, *Nano Lett.* **2008**, *8*, 4597.
- [165] D. C. Elias, R. R. Nair, T. M. G. Mohiuddin, S. V. Morozov, P. Blake, M. P. Halsall, A. C. Ferrari, D. W. Boukhvalov, M. I. Katsnelson, A. K. Geim, K. S. Novoselov, *Science* **2009**, *323*, 610.
- [166] M. Jaiswal, C. H. Y. X. Lim, Q. Bao, C. T. Toh, K. P. Loh, B. Özyilmaz, *ACS Nano* **2011**, *5*, 888.
- [167] J. Zhou, Q. Wang, Q. Sun, X. S. Chen, Y. Kawazoe, P. Jena, *Nano Lett.* **2009**, *9*, 3867.
- [168] L. W. Wei, K. Efthimios, *New J. Phys.* **2010**, *12*, 125012.
- [169] R. R. Nair, W. Ren, R. Jalil, I. Riaz, V. G. Kravets, L. Britnell, P. Blake, F. Schedin, A. S. Mayorov, S. Yuan, M. I. Katsnelson, H.-M. Cheng, W. Strupinski, L. G. Bulusheva, A. V. Okotrub, I. V. Grigorieva, A. N. Grigorenko, K. S. Novoselov, A. K. Geim, *Small* **2010**, *6*, 2773.
- [170] F. Withers, M. Dubois, A. K. Savchenko, *Phys. Rev. B* **2010**, *82*, 073403.
- [171] S. H. Cheng, K. Zou, F. Okino, H. R. Gutierrez, A. Gupta, N. Shen, P. C. Eklund, J. O. Sofo, J. Zhu, *Phys. Rev. B* **2010**, *81*, 205435.
- [172] M. Yang, A. Nurbawono, C. Zhang, Y. P. Feng, Ariando, *Appl. Phys. Lett.* **2010**, *96*, 193115.
- [173] R. Balog, B. Jorgensen, L. Nilsson, M. Andersen, E. Rienks, M. Bianchi, M. Fanetti, E. Laegsgaard, A. Baraldi, S. Lizzit, Z. Sljivancanin, F. Besenbacher, B. Hammer, T. G. Pedersen, P. Hofmann, L. Hornekaer, *Nat. Mater.* **2010**, *9*, 315.
- [174] Z. Sun, C. L. Pint, D. C. Marcano, C. Zhang, J. Yao, G. Ruan, Z. Yan, Y. Zhu, R. H. Haage, J. M. Tour, *Nat. Commun.* **2011**, *2*, 559.
- [175] T. Xue, S. Jiang, Y. Qu, Q. Su, R. Cheng, S. Dubin, C.-Y. Chiu, R. Kaner, Y. Huang, X. Duan, *Angew. Chem. Int. Ed.* **2012**, *51*, 3822.
- [176] Q. Xiang, J. Yu, M. Jaroniec, *Chem. Soc. Rev.* **2012**, *41*, 782.
- [177] Y. Choi, I. S. Moody, P. C. Sims, S. R. Hunt, B. L. Corso, I. Perez, G. A. Weiss, P. G. Collins, *Science* **2012**, *335*, 319.
- [178] Y. Wang, M. Jaiswal, M. Lin, S. Saha, B. Özyilmaz, K. P. Loh, *ACS Nano* **2012**, *6*, 1018.
- [179] M. Deifallah, P. F. McMillan, F. Cora, *J. Phys. Chem. C* **2008**, *112*, 5447.
- [180] T. B. Martins, R. H. Miwa, A. J. R. da Silva, A. Fazzio, *Phys. Rev. Lett.* **2007**, *98*, 196803.
- [181] F. Cervantes-Sodi, G. Csanyi, S. Piscanec, A. C. Ferrari, *Phys. Rev. B* **2008**, *77*, 165427.
- [182] A. Lherbier, X. Blase, Y.-M. Niquet, F. Triozon, S. Roche, *Phys. Rev. Lett.* **2008**, *101*, 036808.
- [183] Z.-H. Sheng, H.-L. Gao, W.-J. Bao, F.-B. Wang, X.-H. Xia, *J. Mater. Chem.* **2012**, *22*, 390.
- [184] D. Wei, Y. Liu, Y. Wang, H. Zhang, L. Huang, G. Yu, *Nano Lett.* **2009**, *9*, 1752.
- [185] L. Qu, Y. Liu, J.-B. Baek, L. Dai, *ACS Nano* **2010**, *4*, 1321.
- [186] L. Ci, L. Song, C. Jin, D. Jariwala, D. Wu, Y. Li, A. Srivastava, Z. F. Wang, K. Storr, L. Balicas, F. Liu, P. M. Ajayan, *Nat. Mater.* **2010**, *9*, 430.
- [187] G. Fiori, A. Betti, S. Bruzzone, G. Iannaccone, *ACS Nano* **2012**, *6*, 2642.
- [188] X. Li, W. Cai, L. Colombo, R. S. Ruoff, *Nano Lett.* **2009**, *9*, 4268.
- [189] S. Chen, Q. Wu, C. Mishra, J. Kang, H. Zhang, K. Cho, W. Cai, A. A. Balandin, R. S. Ruoff, *Nat. Mater.* **2012**, *11*, 203.
- [190] D. R. Dreyer, R. S. Ruoff, C. W. Bielawski, *Angew. Chem. Int. Ed.* **2010**, *49*, 9336.
- [191] N. D. Mermin, *Phys. Rev.* **1968**, *176*, 250.
- [192] M. S. Dresselhaus, G. Dresselhaus, *Adv. Phys.* **1981**, *30*, 139.
- [193] V. H. P. Boehm, A. Clauss, G. O. Fischer, U. Hofmann, *Z. Naturforsch.* **1962**, *17*, 150.
- [194] H. P. Boehm, R. Setton, E. Stumpp, *Carbon* **1986**, *24*, 241.
- [195] H. P. Boehm, R. Setton, E. Stumpp, *Pure Appl. Chem.* **1994**, *66*, 1893.
- [196] P. M. Stefan, M. L. Shek, I. Lindau, W. E. Spicer, L. I. Johansson, F. Herman, R. V. Kasowski, G. Brogen, *Phys. Rev. B* **1984**, *29*, 5423.
- [197] T. Aizawa, R. Souda, S. Otani, Y. Ishizawa, C. Oshima, *Phys. Rev. Lett.* **1990**, *64*, 768.
- [198] A. Nagashima, K. Nuka, H. Itoh, T. Ichinokawa, C. Oshima, S. Otani, *Surf. Sci.* **1993**, *291*, 93.
- [199] C. Oshima, E. Bannai, T. Tanaka, S. Kawai, *Jpn. J. Appl. Phys.* **1977**, *16*, 965.
- [200] R. Rosei, M. De Crescenzi, F. Sette, C. Quaresima, A. Savoia, P. Perfetti, *Phys. Rev. B* **1983**, *28*, 1161.
- [201] N. A. Kholin, E. V. Rut'kov, A. Y. Tontegode, *Surf. Sci.* **1984**, *139*, 155.
- [202] N. R. Gall, S. N. Mikhailov, E. V. Rut'kov, A. Y. Tontegode, *Sov. Phys. Solid State* **1985**, *27*, 1410.
- [203] H. Zi-Pu, D. F. Ogletree, M. A. Van Hove, G. A. Somorjai, *Surf. Sci.* **1987**, *180*, 433.
- [204] A. J. Van Bommel, J. E. Crombeen, A. Van Tooren, *Surf. Sci.* **1975**, *48*, 463.
- [205] C. Berger, Z. M. Song, T. B. Li, X. Li, A. Y. Ogbazghi, R. Feng, Z. T. Dai, A. N. Marchenkov, E. H. Conrad, P. N. First, W. A. de Heer, *J. Phys. Chem. B* **2004**, *108*, 19912.
- [206] Y. Zhang, J. Small, W. Pontius, P. Kim, *Appl. Phys. Lett.* **2005**, *86*, 073104.
- [207] D. D. L. Chung, *J. Mater. Sci.* **1987**, *22*, 4190.
- [208] X. Lu, M. Yu, H. Huang, R. Ruoff, *Nanotechnology* **1999**, *10*, 269.
- [209] S. V. Morozov, K. S. Novoselov, M. I. Katsnelson, F. Schedin, D. C. Elias, J. A. Jaszcak, A. K. Geim, *Phys. Rev. Lett.* **2008**, *100*, 016602.
- [210] S. Berciaud, S. Ryu, L. E. Brus, T. F. Heinz, *Nano Lett.* **2009**, *9*, 346.
- [211] C. Soldano, A. Mahmood, E. Dujardin, *Carbon* **2010**, *48*, 2127.
- [212] X. L. Li, G. Y. Zhang, X. D. Bai, X. M. Sun, X. R. Wang, E. G. Wang, H. J. Dai, *Nat. Nanotechnol.* **2008**, *3*, 538.
- [213] Y. Hernandez, V. Nicolosi, M. Lotya, F. M. Blighe, Z. Sun, S. De, I. T. McGovern, B. Holland, M. Byrne, Y. K. Gun'ko, J. J. Boland, P. Niraj, G. Duesberg, S. Krishnamurthy, R. Goodhue, J. Hutchison, V. Scardaci, A. C. Ferrari, J. N. Coleman, *Nat. Nanotechnol.* **2008**, *3*, 563.
- [214] M. Lotya, Y. Hernandez, P. J. King, R. J. Smith, V. Nicolosi, L. S. Karlsson, F. M. Blighe, S. De, Z. Wang, I. T. McGovern, G. S. Duesberg, J. N. Coleman, *J. Am. Chem. Soc.* **2009**, *131*, 3611.
- [215] A. B. Bourlinos, V. Georgakilas, R. Zboril, T. A. Steriotis, A. K. Stubos, *Small* **2009**, *5*, 1841.

- [216] U. Khan, A. O'Neill, M. Lotya, S. De, J. N. Coleman, *Small* **2010**, *6*, 864.
- [217] C. Valles, C. Drummond, H. Saadaoui, C. A. Furtado, M. He, O. Roubeau, L. Ortolani, M. Monthoux, A. Penicaud, *J. Am. Chem. Soc.* **2008**, *130*, 15802.
- [218] J. S. Moon, D. Curtis, M. Hu, D. Wong, C. McGuire, P. M. Campbell, G. Jernigan, J. L. Tedesco, B. VanMil, R. Myers-Ward, C. J. Eddy, D. K. Gaskill, *IEEE Electron. Device Lett.* **2009**, *30*, 650.
- [219] O. C. Compton, S. T. Nguyen, *Small* **2010**, *6*, 711.
- [220] Y. Si, E. T. Samulski, *Nano Lett.* **2008**, *8*, 1679.
- [221] D. R. Dreyer, S. Park, C. W. Bielawski, R. S. Ruoff, *Chem. Soc. Rev.* **2010**, *39*, 228.
- [222] S. Park, J. An, I. Jung, R. D. Piner, S. J. An, X. Li, A. Velamakanni, R. S. Ruoff, *Nano Lett.* **2009**, *9*, 1593.
- [223] M. A. Rafiee, J. Rafiee, Z. Wang, H. Song, Z.-Z. Yu, N. Koratkar, *ACS Nano* **2009**, *3*, 3884.
- [224] Y. Shao, J. Wang, M. Engelhard, C. Wang, Y. Lin, *J. Mater. Chem.* **2010**, *20*, 743.
- [225] L. J. Cote, R. Cruz-Silva, J. Huang, *J. Am. Chem. Soc.* **2009**, *131*, 11027.
- [226] V. Strong, S. Dubin, M. F. El-Kady, A. Lech, Y. Wang, B. H. Weiller, R. B. Kaner, *ACS Nano* **2012**, *6*, 1395.
- [227] G. Wang, J. Yang, J. Park, X. Gou, B. Wang, H. Liu, J. Yao, *J. Phys. Chem. C* **2008**, *112*, 8192.
- [228] S. Stankovich, D. A. Dikin, R. D. Piner, K. A. Kohlhaas, A. Kleinhammes, Y. Jia, Y. Wu, S. T. Nguyen, R. S. Ruoff, *Carbon* **2007**, *45*, 1558.
- [229] D. Li, M. B. Mueller, S. Gilje, R. B. Kaner, G. G. Wallace, *Nat. Nanotechnol.* **2008**, *3*, 101.
- [230] V. C. Tung, M. J. Allen, Y. Yang, R. B. Kaner, *Nat. Nanotechnol.* **2009**, *4*, 25.
- [231] J. Gao, F. Liu, Y. Liu, N. Ma, Z. Wang, X. Zhang, *Chem. Mater.* **2010**, *22*, 2213.
- [232] O. Akhavan, E. Ghaderi, *Carbon* **2012**, *50*, 1853.
- [233] S. Gilje, S. Han, M. Wang, K. L. Wang, R. B. Kaner, *Nano Lett.* **2007**, *7*, 3394.
- [234] Z.-J. Fan, W. Kai, J. Yan, T. Wei, L.-J. Zhi, J. Feng, Y.-m. Ren, L.-P. Song, F. Wei, *ACS Nano* **2011**, *5*, 191.
- [235] H.-L. Guo, X.-F. Wang, Q.-Y. Qian, F.-B. Wang, X.-H. Xia, *ACS Nano* **2009**, *3*, 2653.
- [236] X. Fan, W. Peng, Y. Li, X. Li, S. Wang, G. Zhang, F. Zhang, *Adv. Mater.* **2008**, *20*, 4490.
- [237] W. Chen, L. Yan, P. R. Bangal, *Carbon* **2010**, *48*, 1146.
- [238] X. Wang, L. Zhi, K. Müllen, *Nano Lett.* **2008**, *8*, 323.
- [239] H. A. Becerril, J. Mao, Z. Liu, R. M. Stoltenberg, Z. Bao, Y. Chen, *ACS Nano* **2008**, *2*, 463.
- [240] J. Wu, H. A. Becerril, Z. Bao, Z. Liu, Y. Chen, P. Peumans, *Appl. Phys. Lett.* **2008**, *92*, 263302.
- [241] S. Gilje, S. Dubin, A. Badakhshan, J. Farrar, S. A. Danczyk, R. B. Kaner, *Adv. Mater.* **2010**, *22*, 419.
- [242] G. Williams, B. Seger, P. V. Kamat, *ACS Nano* **2008**, *2*, 1487.
- [243] S. Guo, S. Dong, *Chem. Soc. Rev.* **2011**, *40*, 2644.
- [244] W. A. de Heer, C. Berger, X. Wu, M. Sprinkle, Y. Hu, M. Ruan, J. A. Stroscio, P. N. First, R. Haddon, B. Piot, C. Faugeras, M. Potemski, J.-S. Moon, *J. Phys. D: Appl. Phys.* **2010**, *43*, 374007.
- [245] E. Rollings, G.-H. Gweon, S. Y. Zhou, B. S. Mun, J. L. McChesney, B. S. Hussain, A. Fedorov, P. N. First, W. A. de Heer, A. Lanzara, *J. Phys. Chem. Solids* **2006**, *67*, 2172.
- [246] J. Robinson, X. Weng, K. Trumbull, R. Cavalero, M. Wetherington, E. Frantz, M. LaBella, Z. Hughes, M. Fanton, D. Snyder, *ACS Nano* **2010**, *4*, 153.
- [247] G. L. Creeth, A. J. Strudwick, J. T. Sadowski, C. H. Marrows, *Phys. Rev. B* **2011**, *83*, 195440.
- [248] J. K. Hite, M. E. Twigg, J. L. Tedesco, A. L. Friedman, R. L. Myers-Ward, C. R. J. Eddy, D. K. Gaskill, *Nano Lett.* **2011**, *11*, 1190.
- [249] S. Shivaraman, R. A. Barton, X. Yu, J. Alden, L. Herman, M. V. S. Chandrashekhar, J. Park, P. L. McEuen, J. M. Parpia, H. G. Craighead, M. G. Spencer, *Nano Lett.* **2009**, *9*, 3100.
- [250] J. Hass, W. A. de Heer, E. H. Conrad, *J. Phys.: Condens. Matter* **2008**, *20*, 323202.
- [251] N. Camara, G. Rius, J.-R. Huntzinger, A. Tiberj, N. Mestres, P. Godignon, J. Camassel, *Appl. Phys. Lett.* **2008**, *93*, 123503.
- [252] M. Rubio-Roy, F. Zaman, Y. Hu, C. Berger, M. W. Moseley, J. D. Meindl, W. A. de Heer, *Appl. Phys. Lett.* **2010**, *96*, 082112.
- [253] V. Y. Aristov, G. Urbanik, K. Kummer, D. V. Vyalikh, O. V. Molodtsova, A. B. Preobrazhenski, A. A. Zakharov, C. Hess, T. Haenke, B. Buechner, I. Vobornik, J. Fujii, G. Panaccione, Y. A. Ossipyan, M. Knupfer, *Nano Lett.* **2010**, *10*, 992.
- [254] J. D. Caldwell, T. J. Anderson, J. C. Culbertson, G. G. Jernigan, K. D. Hobart, F. J. Kub, M. J. Tadjer, J. L. Tedesco, J. K. Hite, M. A. Mastro, R. L. Myers-Ward, C. R. Eddy, P. M. Campbell, D. K. Gaskill, *ACS Nano* **2010**, *4*, 1108.
- [255] Y. Dedkov, A. Shikin, V. Adamchuk, S. Molodtsov, C. Laubschat, A. Bauer, G. Kaindl, *Phys. Rev. B* **2001**, *64*, 035405.
- [256] P. W. Sutter, J.-I. Flege, E. A. Sutter, *Nat. Mater.* **2008**, *7*, 406.
- [257] T. A. Land, T. Michely, R. J. Behm, J. C. Hemminger, G. Comsa, *Surf. Sci.* **1992**, *264*, 261.
- [258] Y. S. Dedkov, M. Fonin, C. Laubschat, *Appl. Phys. Lett.* **2008**, *92*, 052506.
- [259] A. T. N'Diaye, J. Coraux, T. N. Plasa, C. Busse, T. Michely, *New J. Phys.* **2008**, *10*, 043033.
- [260] W. Cai, R. D. Piner, Y. Zhu, X. Li, Z. Tan, H. C. Floresca, C. Yang, L. Lu, M. J. Kim, R. S. Ruoff, *Nano Res.* **2009**, *2*, 851.
- [261] W. Liu, C.-H. Chung, C.-Q. Miao, Y.-J. Wang, B.-Y. Li, L.-Y. Ruan, K. Patel, Y.-J. Park, J. Woo, Y.-H. Xie, *Thin Solid Films* **2010**, *518*, S128.
- [262] A. Reina, X. Jia, J. Ho, D. Nezich, H. Son, V. Bulovic, M. S. Dresselhaus, J. Kong, *Nano Lett.* **2009**, *9*, 30.
- [263] G. Lopez, E. Mittermeier, *Scr. Mater.* **2004**, *51*, 1.
- [264] G. L. Selman, P. J. Ellison, A. s. Darling, *Platinum Metals Rev.* **1970**, *14*, 14.
- [265] S. Bhaviripudi, X. Jia, M. S. Dresselhaus, J. Kong, *Nano Lett.* **2010**, *10*, 4128.
- [266] L. Liu, H. Zhou, R. Cheng, Y. Chen, Y.-C. Lin, Y. Qu, J. Bai, I. A. Ivanov, G. Liu, Y. Huang, X. Duan, *J. Mater. Chem.* **2012**, *22*, 1498.
- [267] G. Jian-Hua, S. Keisuke, K. Masayo, X. Ming-Sheng, M. Satoru, F. Daisuke, *Nanotechnology* **2012**, *23*, 055704.
- [268] D. Usachov, A. M. Dobrovskii, A. Varykhhalov, O. Rader, W. Gudat, A. M. Shikin, V. K. Adamchuk, *Phys. Rev. B* **2008**, *78*, 085403.
- [269] H. I. Rasool, E. B. Song, M. Mecklenburg, B. C. Regan, K. L. Wang, B. H. Weiller, J. K. Gimzewski, *J. Am. Chem. Soc.* **2011**, *133*, 12536.
- [270] K. Yan, H. Peng, Y. Zhou, H. Li, Z. Liu, *Nano Lett.* **2011**, *11*, 1106.
- [271] S. Chen, W. Cai, R. D. Piner, J. W. Suk, Y. Wu, Y. Ren, J. Kang, R. S. Ruoff, *Nano Lett.* **2011**, *11*, 3519.
- [272] X. Li, C. W. Magnuson, A. Venugopal, J. An, J. W. Suk, B. Han, M. Borysiak, W. Cai, A. Velamakanni, Y. Zhu, L. Fu, E. M. Vogel, E. Voelkl, L. Colombo, R. S. Ruoff, *Nano Lett.* **2010**, *10*, 4328.
- [273] X. Li, C. W. Magnuson, A. Venugopal, R. M. Tromp, J. B. Hannon, E. M. Vogel, L. Colombo, R. S. Ruoff, *J. Am. Chem. Soc.* **2011**, *133*, 2816.
- [274] P. Y. Huang, C. S. Ruiz-Vargas, A. M. van der Zande, W. S. Whitney, M. P. Levendorf, J. W. Kevek, S. Garg, J. S. Alden, C. J. Hustadt, Y. Zhu, J. Park, P. L. McEuen, D. A. Muller, *Nature* **2011**, *469*, 389.

- [275] Q. Yu, L. A. Jauregui, W. Wu, R. Colby, J. Tian, Z. Su, H. Cao, Z. Liu, D. Pandey, D. Wei, T. F. Chung, P. Peng, N. P. Guisinger, E. A. Stach, J. Bao, S.-S. Pei, Y. P. Chen, *Nat. Mater.* **2011**, *10*, 443.
- [276] Z. Li, P. Wu, C. Wang, X. Fan, W. Zhang, X. Zhai, C. Zeng, Z. Li, J. Yang, J. Hou, *ACS Nano* **2011**, *5*, 3385.
- [277] J. Wang, M. Zhu, R. Outlaw, X. Zhao, D. Manos, B. Holloway, V. Mammana, *Appl. Phys. Lett.* **2004**, *85*, 1265.
- [278] R. Vitchev, A. Malesevic, R. H. Petrov, R. Kemps, M. Mertens, A. Vanhulsel, C. Van Haesendonck, *Nanotechnology* **2010**, *21*, 095602.
- [279] M. Zhu, J. Wang, B. C. Holloway, R. A. Outlaw, X. Zhao, K. Hou, V. Shutthanandan, D. M. Manos, *Carbon* **2007**, *45*, 2229.
- [280] J. B. Park, W. Xiong, Y. Gao, M. Qian, Z. Q. Xie, M. Mitchell, Y. S. Zhou, G. H. Han, L. Jiang, Y. F. Lu, *Appl. Phys. Lett.* **2011**, *98*, 123109.
- [281] G. Ruan, Z. Sun, Z. Peng, J. M. Tour, *ACS Nano* **2011**.
- [282] Z. Sun, Z. Yan, J. Yao, E. Beitler, Y. Zhu, J. M. Tour, *Nature* **2010**, *468*, 549.
- [283] X. Liang, B. A. Sperling, I. Calizo, G. Cheng, C. A. Hacker, Q. Zhang, Y. Obeng, K. Yan, H. Peng, Q. Li, X. Zhu, H. Yuan, A. R. Hight Walker, Z. Liu, L.-m. Peng, C. A. Richter, *ACS Nano* **2011**, *5*, 9144.
- [284] Z. Liu, L. Song, S. Zhao, J. Huang, L. Ma, J. Zhang, J. Lou, P. M. Ajayan, *Nano Lett.* **2011**, *11*, 2032.
- [285] X. Ding, G. Ding, X. Xie, F. Huang, M. Jiang, *Carbon* **2011**, *49*, 2522.
- [286] M. Son, H. Lim, M. Hong, H. C. Choi, *Nanoscale* **2011**, *3*, 3089.
- [287] A. Ismach, C. Druzgalski, S. Penwell, A. Schwartzberg, M. Zheng, A. Javey, J. Bokor, Y. Zhang, *Nano Lett.* **2010**, *10*, 1542.
- [288] C.-Y. Su, A.-Y. Lu, C.-Y. Wu, Y.-T. Li, K.-K. Liu, W. Zhang, S.-Y. Lin, Z.-Y. Juang, Y.-L. Zhong, F.-R. Chen, L.-J. Li, *Nano Lett.* **2011**, *11*, 3612.
- [289] M. P. Levendorf, C. S. Ruiz-Vargas, S. Garg, J. Park, *Nano Lett.* **2009**, *9*, 4479.
- [290] Z. Yan, Z. Peng, Z. Sun, J. Yao, Y. Zhu, Z. Liu, P. M. Ajayan, J. M. Tour, *ACS Nano* **2011**, *5*, 8187.
- [291] P.-Y. Teng, C.-C. Lu, K. Akiyama-Hasegawa, Y.-C. Lin, C.-H. Yeh, K. Suenaga, P.-W. Chiu, *Nano Lett.* **2012**, *12*, 1379.
- [292] J. Chen, Y. Wen, Y. Guo, B. Wu, L. Huang, Y. Xue, D. Geng, D. Wang, G. Yu, Y. Liu, *J. Am. Chem. Soc.* **2011**, *133*, 17548.
- [293] J. Mao, L. Huang, Y. Pan, M. Gao, J. He, H. Zhou, H. Guo, Y. Tian, Q. Zou, L. Zhang, H. Zhang, Y. Wang, S. Du, X. Zhou, A. H. C. Neto, H.-J. Gao, *Appl. Phys. Lett.* **2012**, *100*, 093101.
- [294] B. Guo, Q. Liu, E. Chen, H. Zhu, L. Fang, J. R. Gong, *Nano Lett.* **2010**, *10*, 4975.
- [295] J. Wu, W. Pisula, K. Muellen, *Chem. Rev.* **2007**, *107*, 718.
- [296] X. Yang, X. Dou, A. Rouhaniour, L. Zhi, H. J. Rader, K. Müllen, *J. Am. Chem. Soc.* **2008**, *130*, 4216.
- [297] J. Cai, P. Ruffieux, R. Jaafar, M. Bieri, T. Braun, S. Blankenburg, M. Muoth, A. P. Seitsonen, M. Saleh, X. Feng, K. Muellen, R. Fasel, *Nature* **2010**, *466*, 470.
- [298] X. Yan, X. Cui, L.-s. Li, *J. Am. Chem. Soc.* **2010**, *132*, 5944.
- [299] X. Yan, X. Cui, B. Li, L.-s. Li, *Nano Lett.* **2010**, *10*, 1869.
- [300] L. Ward, *The Optical Constants of Bulk Materials and Films*, Adam Hilger, Bristol, UK **1988**.
- [301] J. Inhwa, R. Jong-Soo, S. Jong Yeog, S. R. Rodney, R. Kyong-Yop, *Nanotechnology* **2012**, *23*, 025708.
- [302] D. W. Kim, Y. H. Kim, H. S. Jeong, H.-T. Jung, *Nat. Nanotechnol.* **2012**, *7*, 29.
- [303] G. Liu, D. Teweldebrhan, A. A. Balandin, *IEEE Trans. Nanotechnol.* **2011**, *10*, 865.
- [304] I. Vlassioul, M. Regmi, P. Fulvio, S. Dai, P. Datskos, G. Eres, S. Smirnov, *ACS Nano* **2011**, *5*, 6069.
- [305] X. Li, W. Cai, J. An, S. Kim, J. Nah, D. Yang, R. Piner, A. Velamakanni, I. Jung, E. Tutuc, S. K. Banerjee, L. Colombo, R. S. Ruoff, *Science* **2009**, *324*, 1312.
- [306] J. C. Meyer, C. Kisielowski, R. Erni, M. D. Rossell, M. F. Crommie, A. Zettl, *Nano Lett.* **2008**, *8*, 3582.
- [307] M. H. Gass, U. Bangert, A. L. Bleloch, P. Wang, R. R. Nair, A. K. Geim, *Nat. Nanotechnol.* **2008**, *3*, 676.
- [308] O. L. Krivanek, M. F. Chisholm, V. Nicolosi, T. J. Pennycook, G. J. Corbin, N. Dellby, M. F. Murfitt, C. S. Own, Z. S. Szilagyi, M. P. Oxley, S. T. Pantelides, S. J. Pennycook, *Nature* **2010**, *464*, 571.
- [309] Z. Lee, K.-J. Jeon, A. Dato, R. Erni, T. J. Richardson, M. Frenklach, V. Radmilovic, *Nano Lett.* **2009**, *9*, 3365.
- [310] R. R. Nair, P. Blake, J. R. Blake, R. Zan, S. Anissimova, U. Bangert, A. P. Golovanov, S. V. Morozov, A. K. Geim, K. S. Novoselov, T. Latychevskaia, *Appl. Phys. Lett.* **2010**, *97*, 153102.
- [311] J. M. Yuk, J. Park, P. Ercius, K. Kim, D. J. Hellebusch, M. F. Crommie, J. Y. Lee, A. Zettl, A. P. Alivisatos, *Science* **2012**, *336*, 61.
- [312] M. R. Connolly, C. G. Smith, *Phil. Trans. R. Soc. A* **2010**, *368*, 5379.
- [313] A. Deshpande, B. J. LeRoy, *Physica E* **2012**, *44*, 743.
- [314] J. I. Paredes, S. Villar-Rodil, P. Solis-Fernandez, A. Martinez-Alonso, J. M. D. Tascon, *Langmuir* **2009**, *25*, 5957.
- [315] J. P. Rabe, S. Buchholz, *Science* **1991**, *253*, 424.
- [316] L. Gao, J. R. Guest, N. P. Guisinger, *Nano Lett.* **2010**, *10*, 3512.
- [317] Y. Murata, V. Petrova, B. B. Kappes, A. Ebnnnasir, I. Petrov, Y.-H. Xie, C. V. Ciobanu, S. Kodambaka, *ACS Nano* **2010**, *4*, 6509.
- [318] D. L. Miller, K. D. Kubista, G. M. Rutter, M. Ruan, W. A. de Heer, P. N. First, J. A. Stroscio, *Phys. Rev. B* **2010**, *81*, 125427.
- [319] L. M. Malard, M. A. Pimenta, G. Dresselhaus, M. S. Dresselhaus, *Phys. Rep.* **2009**, *473*, 51.
- [320] A. C. Ferrari, J. C. Meyer, V. Scardaci, C. Casiraghi, M. Lazzeri, F. Mauri, S. Piscanec, D. Jiang, K. S. Novoselov, S. Roth, A. K. Geim, *Phys. Rev. Lett.* **2006**, *97*, 187401.
- [321] Z. H. Ni, W. Chen, X. F. Fan, J. L. Kuo, T. Yu, A. T. S. Wee, Z. X. Shen, *Phys. Rev. B* **2008**, *77*, 115416.
- [322] T. M. G. Mohiuddin, A. Lombardo, R. R. Nair, A. Bonetti, G. Savini, R. Jalil, N. Bonini, D. M. Basko, C. Galotis, N. Marzari, K. S. Novoselov, A. K. Geim, A. C. Ferrari, *Phys. Rev. B* **2009**, *79*, 205433.
- [323] T. Yu, Z. Ni, C. Du, Y. You, Y. Wang, Z. Shen, *J. Phys. Chem. C* **2008**, *112*, 12602.
- [324] A. Das, S. Pisana, B. Chakraborty, S. Piscanec, S. K. Saha, U. V. Waghmare, K. S. Novoselov, H. R. Krishnamurthy, A. K. Geim, A. C. Ferrari, A. K. Sood, *Nat. Nanotechnol.* **2008**, *3*, 210.
- [325] C. Casiraghi, A. Hartschuh, H. Qian, S. Piscanec, *Nano Lett.* **2009**, *9*, 1433.
- [326] L. Zhao, R. He, K. T. Rim, T. Schiros, K. S. Kim, H. Zhou, C. Gutierrez, S. P. Chockalingam, C. J. Arguello, L. Pálová, D. Nordlund, M. S. Hybertsen, D. R. Reichman, T. F. Heinz, P. Kim, A. Pinczuk, G. W. Flynn, A. N. Pasupathy, *Science* **2011**, *333*, 999.
- [327] Y. Wang, Y. Shao, D. W. Matson, J. Li, Y. Lin, *ACS Nano* **2010**, *4*, 1790.
- [328] M.-C. Hsiao, S.-H. Liao, M.-Y. Yen, P.-I. Liu, N.-W. Pu, C.-A. Wang, C.-C. M. Ma, *ACS Appl. Mater. Interfaces* **2010**, *2*, 3092.
- [329] D. Yang, A. Velamakanni, G. Bozoklu, S. Park, M. Stoller, R. D. Piner, S. Stankovich, I. Jung, D. A. Field, C. A. Ventrice, R. S. Ruoff, *Carbon* **2009**, *47*, 145.
- [330] X. Gao, S. Chen, T. Liu, W. Chen, A. T. S. Wee, T. Nomoto, S. Yagi, K. Soda, J. Yuhara, *Phys. Rev. B* **2008**, *78*, 201404.
- [331] S. Y. Zhou, G.-H. Gweon, J. Graf, A. V. Fedorov, C. D. Spataru, R. D. Diehl, Y. Kopelevich, D.-H. Lee, S. G. Louie, A. Lanzara, *Nat. Phys.* **2006**, *2*, 595.
- [332] K. R. Knox, A. Locatelli, M. B. Yilmaz, D. Cvetko, T. O. Mentes, M. Á. Niño, P. Kim, A. Morgante, R. M. Osgood Jr., *Phys. Rev. B* **2011**, *84*, 115401.

- [333] D. A. Siegel, C.-H. Park, C. Hwang, J. Deslippe, A. V. Fedorov, S. G. Louie, A. Lanzara, *Proc. Natl. Acad. Sci. USA* **2011**, *108*, 11365.
- [334] C. Hwang, C.-H. Park, D. A. Siegel, A. V. Fedorov, S. G. Louie, A. Lanzara, *Phys. Rev. B* **2011**, *84*, 125422.
- [335] Y. Liu, G. Bian, T. Miller, T.-C. Chiang, *Phys. Rev. Lett.* **2011**, *107*, 166803.
- [336] P. N. First, W. A. de Heer, T. Seyller, C. Berger, J. A. Stroscio, J. S. Moon, *MRS Bull.* **2010**, *35*, 296.
- [337] G. Jo, M. Choe, S. Lee, W. Park, Y. H. Kahng, T. Lee, *Nanotechnology* **2012**, *23*, 112001.
- [338] D. S. Hecht, L. Hu, G. Irvin, *Adv. Mater.* **2011**, *23*, 1482.
- [339] A. B. Kaiser, V. Skakalova, *Chem. Soc. Rev.* **2011**, *40*, 3786.
- [340] I. Khrapach, F. Withers, T. H. Bointon, D. K. Polyushkin, W. L. Barnes, S. Russo, M. F. Craciun, *Adv. Mater.* **2012**, *24*, 2844.
- [341] S. De, P. J. King, M. Lotya, A. O'Neill, E. M. Doherty, Y. Hernandez, G. S. Duesberg, J. N. Coleman, *Small* **2010**, *6*, 458.
- [342] L. J. Cote, F. Kim, J. Huang, *J. Am. Chem. Soc.* **2009**, *131*, 1043.
- [343] Y. Zhu, W. Cai, R. D. Piner, A. Velamakanni, R. S. Ruoff, *Appl. Phys. Lett.* **2009**, *95*, 103104.
- [344] Q. Zheng, W. Ip, X. Lin, N. Yousefi, K. Yeung, Z. Li, *ACS Nano* **2011**, *5*, 6039.
- [345] L. Huang, Y. Huang, J. Liang, X. Wan, Y. Chen, *Nano Res.* **2011**, *4*, 675.
- [346] F. Torrisi, T. Hasan, W. Wu, Z. Sun, A. Lombardo, T. S. Kulmala, G.-W. Hsieh, S. Jung, F. Bonaccorso, P. J. Paul, D. Chu, A. C. Ferrari, *ACS Nano* **2012**, *6*, 2992.
- [347] G. Eda, G. Fanchini, M. Chhowalla, *Nat. Nanotechnol.* **2008**, *3*, 270.
- [348] D. A. Dikin, S. Stankovich, E. J. Zimney, R. D. Piner, G. H. B. Dommett, G. Evmenenko, S. T. Nguyen, R. S. Ruoff, *Nature* **2007**, *448*, 457.
- [349] C. Vallés, J. D. Núñez, A. M. Benito, W. K. Maser, *Carbon* **2011**, *50*, 835.
- [350] A. R. Ranjbarzadeh, B. Wang, X. Shen, G. Wang, *J. Appl. Phys.* **2011**, *109*, 014306.
- [351] X. Zhou, Z. Liu, *IOP Conf. Ser.: Mater. Sci.* **2011**, *18*, 062006.
- [352] H.-P. Cong, X.-C. Ren, P. Wang, S.-H. Yu, *ACS Nano* **2012**, *6*, 2693.
- [353] M. A. Worsley, P. J. Pauzauskis, T. Y. Olson, J. Biener, J. H. Satcher, T. F. Baumann, *J. Am. Chem. Soc.* **2010**, *132*, 14067.
- [354] Z. Chen, W. Ren, L. Gao, B. Liu, S. Pei, H.-M. Cheng, *Nat. Mater.* **2011**, *10*, 424.
- [355] F. Yavari, Z. Chen, A. V. Thomas, W. Ren, H.-M. Cheng, N. Koratkar, *Sci. Rep.* **2011**, *1*, 166.
- [356] S. Watcharotone, D. A. Dikin, S. Stankovich, R. Piner, I. Jung, G. H. B. Dommett, G. Evmenenko, S.-E. Wu, S.-F. Chen, C.-P. Liu, S. T. Nguyen, R. S. Ruoff, *Nano Lett.* **2007**, *7*, 1888.
- [357] Y. Zhu, Z. Sun, Z. Yan, Z. Jin, J. M. Tour, *ACS Nano* **2011**, *5*, 6472.
- [358] V. C. Tung, L.-M. Chen, M. J. Allen, J. K. Wasai, K. Nelson, R. B. Kaner, Y. Yang, *Nano Lett.* **2009**, *9*, 1949.
- [359] L. Peng, Y. Feng, P. Lv, D. Lei, Y. Shen, Y. Li, W. Feng, *J. Phys. Chem. C* **2012**, *116*, 4970.
- [360] B. Chandra, J. Bhattacharjee, M. Purewal, Y.-W. Son, Y. Wu, M. Huang, H. Yan, T. F. Heinz, P. Kim, J. B. Neaton, J. Hone, *Nano Lett.* **2009**, *9*, 1544.
- [361] A. Reina, H. Son, L. Jiao, B. Fan, M. S. Dresselhaus, Z. Liu, J. Kong, *J. Phys. Chem. C* **2008**, *112*, 17741.
- [362] X. Li, Y. Zhu, W. Cai, M. Borysiak, B. Han, D. Chen, R. D. Piner, L. Colombo, R. S. Ruoff, *Nano Lett.* **2009**, *9*, 4359.
- [363] Y. Lee, S. Bae, H. Jang, S. Jang, S.-E. Zhu, S. H. Sim, Y. I. Song, B. H. Hong, J.-H. Ahn, *Nano Lett.* **2010**, *10*, 490.
- [364] S. Bae, H. Kim, Y. Lee, X. Xu, J.-S. Park, Y. Zheng, J. Balakrishnan, T. Lei, H. Ri Kim, Y. I. Song, Y.-J. Kim, K. S. Kim, B. Ozilmez, J.-H. Ahn, B. H. Hong, S. Iijima, *Nat. Nanotechnol.* **2010**, *5*, 574.
- [365] W. Liu, B. L. Jackson, J. Zhu, C.-Q. Miao, C.-H. Chung, Y. J. Park, K. Sun, J. Woo, Y.-H. Xie, *ACS Nano* **2010**, *4*, 3927.
- [366] W. H. Lee, J. Park, S. H. Sim, S. B. Jo, K. S. Kim, B. H. Hong, K. Cho, *Adv. Mater.* **2011**, *23*, 1752.
- [367] W. J. Yu, S. H. Chae, S. Y. Lee, D. L. Duong, Y. H. Lee, *Adv. Mater.* **2011**, *23*, 1889.
- [368] R.-H. Kim, M.-H. Bae, D. G. Kim, H. Cheng, B. H. Kim, D.-H. Kim, M. Li, J. Wu, F. Du, H.-S. Kim, S. Kim, D. Estrada, S. W. Hong, Y. Huang, E. Pop, J. A. Rogers, *Nano Lett.* **2011**, *11*, 3881.
- [369] L. Gomez De Arco, Y. Zhang, C. W. Schlenker, K. Ryu, M. E. Thompson, C. Zhou, *ACS Nano* **2010**, *4*, 2865.
- [370] C. Sire, F. Ardaci, S. Lepilliet, J.-W. T. Seo, M. C. Hersam, G. Dambrine, H. Happy, V. Derycke, *Nano Lett.* **2012**, *12*, 1184.
- [371] Y. Ji, S. Lee, B. Cho, S. Song, T. Lee, *ACS Nano* **2011**, *5*, 5995.
- [372] H. Y. Jeong, J. Y. Kim, J. W. Kim, J. O. Hwang, J.-E. Kim, J. Y. Lee, T. H. Yoon, B. J. Cho, S. O. Kim, R. S. Ruoff, S.-Y. Choi, *Nano Lett.* **2010**, *10*, 4381.
- [373] L. Hu, J. Li, J. Liu, G. Gruener, T. Marks, *Nanotechnology* **2010**, *21*, 155202.
- [374] S.-K. Lee, B. J. Kim, H. Jang, S. C. Yoon, C. Lee, B. H. Hong, J. A. Rogers, J. H. Cho, J.-H. Ahn, *Nano Lett.* **2011**, *11*, 4642.
- [375] P. Blake, P. D. Brimicombe, R. R. Nair, T. J. Booth, D. Jiang, F. Schedin, L. A. Ponomarenko, S. V. Morozov, H. F. Gleeson, E. W. Hill, A. K. Geim, K. S. Novoselov, *Nano Lett.* **2008**, *8*, 1704.
- [376] F. Bonaccorso, Z. Sun, T. Hasan, A. C. Ferrari, *Nat. Photonics* **2010**, *4*, 611.
- [377] L. Zhao, L. Zhao, Y. Xu, T. Qiu, L. Zhi, G. Shi, *Electrochim. Acta* **2009**, *55*, 491.
- [378] G. Jo, M. Choe, C.-Y. Cho, J. H. Kim, W. Park, S. Lee, W.-K. Hong, T.-W. Kim, S.-J. Park, B. H. Hong, Y. H. Kahng, T. Lee, *Nanotechnology* **2010**, *21*, 175201.
- [379] D. Zhang, K. Ryu, X. Liu, E. Polikarpov, J. Ly, M. E. Tompson, C. Zhou, *Nano Lett.* **2006**, *6*, 1880.
- [380] J. Wu, M. Agrawal, H. A. Becerril, Z. Bao, Z. Liu, Y. Chen, P. Peumans, *ACS Nano* **2010**, *4*, 43.
- [381] H. Chang, G. Wang, A. Yang, X. Tao, X. Liu, *Adv. Funct. Mater.* **2010**, *20*, 2893.
- [382] J. M. Lee, J. W. Choung, J. Yi, D. H. Lee, M. Samal, D. K. Yi, C.-H. Lee, G.-C. Yi, U. Paik, J. A. Rogers, W. I. Park, *Nano Lett.* **2010**, *10*, 2783.
- [383] a) P. Matyba, H. Yamaguchi, G. Eda, M. Chhowalla, L. Edman, N. D. Robinson, *ACS Nano* **2010**, *4*, 637; b) P. Matyba, H. Yamaguchi, M. Chhowalla, N. D. Robinson, L. Edman, *ACS Nano* **2011**, *5*, 574.
- [384] J. O. Hwang, J. S. Park, D. S. Choi, J. Y. Kim, S. H. Lee, K. E. Lee, Y.-H. Kim, M. H. Song, S. Yoo, S. O. Kim, *ACS Nano* **2011**, *6*, 159.
- [385] Y.-J. Yu, Y. Zhao, S. Ryu, L. E. Brus, K. S. Kim, P. Kim, *Nano Lett.* **2009**, *9*, 3430.
- [386] J.-H. Huang, J.-H. Fang, C.-C. Liu, C.-W. Chu, *ACS Nano* **2011**, *5*, 6262.
- [387] Y. Lu, Y. Jiang, W. Wei, H. Wu, M. Liu, L. Niu, W. Chen, *J. Mater. Chem.* **2012**, *22*, 2929.
- [388] T. Gokus, R. R. Nair, A. Bonetti, M. Böhmler, A. Lombardo, K. S. Novoselov, A. K. Geim, A. C. Ferrari, A. Hartschuh, *ACS Nano* **2009**, *3*, 3963.
- [389] G. Eda, Y.-Y. Lin, C. Mattevi, H. Yamaguchi, H.-A. Chen, I. S. Chen, C.-W. Chen, M. Chhowalla, *Adv. Mater.* **2010**, *22*, 505.
- [390] B. Luo, S. Liu, L. Zhi, *Small* **2012**, *8*, 630.
- [391] S.-S. Li, K.-H. Tu, C.-C. Lin, C.-W. Chen, M. Chhowalla, *ACS Nano* **2010**, *4*, 3169.
- [392] F. Molitor, A. Jacobsen, C. Stampfer, J. Guettler, T. Ihn, K. Ensslin, *Phys. Rev. B* **2009**, *79*, 075426.
- [393] J.-P. Shim, M. Choe, S.-R. Jeon, D. Seo, T. Lee, D.-S. Lee, *Appl. Phys. Express* **2011**, *4*, 052302.
- [394] H. Park, J. A. Rowohl, K. K. Kim, V. Bulovic, J. Kong, *Nanotechnology* **2010**, *21*, 155202.

- [395] X. Wan, G. Long, L. Huang, Y. Chen, *Adv. Mater.* **2011**, *23*, 5342.
- [396] Y.-Y. Lee, K.-H. Tu, C.-C. Yu, S.-S. Li, J.-Y. Hwang, C.-C. Lin, K.-H. Chen, L.-C. Chen, H.-L. Chen, C.-W. Chen, *ACS Nano* **2011**, *5*, 6564.
- [397] Y. Wang, X. Chen, Y. Zhong, F. Zhu, K. P. Loh, *Appl. Phys. Lett.* **2009**, *95*, 063302.
- [398] M. Choe, B. H. Lee, G. Jo, J. Park, W. Park, S. Lee, W.-K. Hong, M.-J. Seong, Y. H. Kahng, K. Lee, T. Lee, *Org. Electron.* **2010**, *11*, 1864.
- [399] Z. Yin, S. Wu, X. Zhou, X. Huang, Q. Zhang, F. Boey, H. Zhang, *Small* **2010**, *6*, 307.
- [400] W. Hong, Y. Xu, G. Lu, C. Li, G. Shi, *Electrochem. Commun.* **2008**, *10*, 1555.
- [401] C.-C. Chen, M. Aykol, C.-C. Chang, A. F. J. Levi, S. B. Cronin, *Nano Lett.* **2011**, *11*, 1863.
- [402] X. Miao, S. Tongay, M. K. Petterson, K. Berke, A. G. Rinzler, B. R. Appleton, A. F. Hebard, *Nano Lett.* **2012**.
- [403] N. M. Gabor, J. C. W. Song, Q. Ma, N. L. Nair, T. Taychatanapat, K. Watanabe, T. Taniguchi, L. S. Levitov, P. Jarillo-Herrero, *Science* **2011**, *334*, 648.
- [404] D. Dragoman, M. Dragoman, *Appl. Phys. Lett.* **2007**, *91*, 203116.
- [405] Y. M. Zuev, W. Chang, P. Kim, *Phys. Rev. Lett.* **2009**, *102*, 096807.
- [406] P. Wei, W. Bao, Y. Pu, C. N. Lau, J. Shi, *Phys. Rev. Lett.* **2009**, *102*, 166808.
- [407] N. Xiao, X. Dong, L. Song, D. Liu, Y. Tay, S. Wu, L.-J. Li, Y. Zhao, T. Yu, H. Zhang, W. Huang, H. H. Hng, P. M. Ajayan, Q. Yan, *ACS Nano* **2011**, *5*, 2749.
- [408] T. J. Kang, S. Fang, M. E. Kozlov, C. S. Haines, N. Li, Y. H. Kim, Y. Chen, R. H. Baughman, *Adv. Funct. Mater.* **2012**, *22*, 477.
- [409] D. Choi, M.-Y. Choi, W. M. Choi, H.-J. Shin, H.-K. Park, J.-S. Seo, J. Park, S.-M. Yoon, S. J. Chae, Y. H. Lee, S.-W. Kim, J.-Y. Choi, S. Y. Lee, J. M. Kim, *Adv. Mater.* **2010**, *22*, 2187.
- [410] H.-J. Shin, W. M. Choi, D. Choi, G. H. Han, S.-M. Yoon, H.-K. Park, S.-W. Kim, Y. W. Jin, S. Y. Lee, J. M. Kim, J.-Y. Choi, Y. H. Lee, *J. Am. Chem. Soc.* **2010**, *132*, 15603.
- [411] P. Dhirman, F. Yavari, X. Mi, H. Gullapalli, Y. Shi, P. M. Ajayan, N. Koratkar, *Nano Lett.* **2011**, *11*, 3123.
- [412] J. Yin, Z. Zhang, X. Li, J. Zhou, W. Guo, *Nano Lett.* **2012**, *12*, 1736.
- [413] H. Xiang, K. Zhang, G. Ji, J. Y. Lee, C. Zou, X. Chen, J. Wu, *Carbon* **2011**, *49*, 1787.
- [414] J. Xiao, D. Mei, X. Li, W. Xu, D. Wang, G. L. Graff, W. D. Bennett, Z. Nie, L. V. Saraf, I. A. Aksay, J. Liu, J.-G. Zhang, *Nano Lett.* **2011**, *11*, 5071.
- [415] L. Wan, Z. Ren, H. Wang, G. Wang, X. Tong, S. Gao, J. Bai, *Diamond Relat. Mater.* **2011**, *20*, 756.
- [416] L. Ji, Z. Tan, T. Kuykendall, E. J. An, Y. Fu, V. Battaglia, Y. Zhang, *Energy Environ. Sci.* **2011**, *4*, 3611.
- [417] E. J. Yoo, J. Kim, E. Hosono, H.-S. Zhou, T. Kudo, I. Honma, *Nano Lett.* **2008**, *8*, 2277.
- [418] X. Zhao, C. M. Hayner, M. C. Kung, H. H. Kung, *Adv. Energy Mater.* **2011**, *1*, 1079.
- [419] J. J. Yoo, K. Balakrishnan, J. Huang, V. Meunier, B. G. Sumpter, A. Srivastava, M. Conway, A. L. M. Reddy, J. Yu, R. Vajtai, P. M. Ajayan, *Nano Lett.* **2011**, *11*, 1423.
- [420] Z. Fan, J. Yan, L. Zhi, Q. Zhang, T. Wei, J. Feng, M. Zhang, W. Qian, F. Wei, *Adv. Mater.* **2010**, *22*, 3723.
- [421] M. D. Stoller, S. Park, Y. Zhu, J. An, R. S. Ruoff, *Nano Lett.* **2008**, *8*, 3498.
- [422] L. L. Zhang, R. Zhou, X. S. Zhao, *J. Mater. Chem.* **2010**, *20*, 5983.
- [423] Y. Zhu, M. D. Stoller, W. Cai, A. Velamakanni, R. D. Piner, D. Chen, R. S. Ruoff, *ACS Nano* **2010**, *4*, 1227.
- [424] H. R. Byon, S. W. Lee, S. Chen, P. T. Hammond, Y. Shao-Horn, *Carbon* **2011**, *49*, 457.
- [425] Q. Wu, Y. Xu, Z. Yao, A. Liu, G. Shi, *ACS Nano* **2010**, *4*, 1963.
- [426] Y. Wang, Z. Shi, Y. Huang, Y. Ma, C. Wang, M. Chen, Y. Chen, *J. Phys. Chem. C* **2009**, *113*, 13103.
- [427] Y. Zhu, S. Murali, M. D. Stoller, K. J. Ganesh, W. Cai, P. J. Ferreira, A. Pirkle, R. M. Wallace, K. A. Cychoz, M. Thommes, D. Su, E. A. Stach, R. S. Ruoff, *Science* **2011**, *332*, 1537.
- [428] C. Liu, Z. Yu, D. Neff, A. Zhamu, B. Z. Jang, *Nano Lett.* **2010**, *10*, 4863.
- [429] T. Y. Kim, H. W. Lee, M. Stoller, D. R. Dreyer, C. W. Bielawski, R. S. Ruoff, K. S. Suh, *ACS Nano* **2010**, *5*, 436.
- [430] S. H. Lee, H. W. Kim, J. O. Hwang, W. J. Lee, J. Kwon, C. W. Bielawski, R. S. Ruoff, S. O. Kim, *Angew. Chem. Int. Ed.* **2010**, *49*, 10084.
- [431] X. Cao, Y. Shi, W. Shi, G. Lu, X. Huang, Q. Yan, Q. Zhang, H. Zhang, *Small* **2011**, *7*, 3163.
- [432] X. Yang, J. Zhu, L. Qiu, D. Li, *Adv. Mater.* **2011**, *23*, 2833.
- [433] M. F. El-Kady, V. Strong, S. Dubin, R. B. Kaner, *Science* **2012**, *335*, 1326.
- [434] J. R. Miller, R. A. Outlaw, B. C. Holloway, *Electrochim. Acta* **2011**, *56*, 10443.
- [435] J. R. Miller, R. A. Outlaw, B. C. Holloway, *Science* **2010**, *329*, 1637.
- [436] N. Shang, P. Papakonstantinou, P. Wang, S. R. P. Silva, *J. Phys. Chem. C* **2010**, *114*, 15837.
- [437] S. Sharma, A. Ganguly, P. Papakonstantinou, X. Miao, M. Li, J. L. Hutchison, M. Delichatsios, S. Ukleja, *J. Phys. Chem. C* **2010**, *114*, 19459.
- [438] R. Kou, Y. Shao, D. Mei, Z. Nie, D. Wang, C. Wang, V. V. Viswanathan, S. Park, I. A. Aksay, Y. Lin, Y. Wang, J. Liu, *J. Am. Chem. Soc.* **2011**, *133*, 2541.
- [439] Z. Yang, Z. Yao, G. Li, G. Fang, H. Nie, Z. Liu, X. Zhou, X. a. Chen, S. Huang, *ACS Nano* **2011**, *6*, 205.
- [440] H. R. Byon, J. Suntivich, Y. Shao-Horn, *Chem. Mater.* **2011**, *23*, 3421.
- [441] Y. Li, J. Wang, X. Li, D. Geng, M. N. Banis, R. Li, X. Sun, *Electrochim. Commun.* **2012**, *18*, 12.
- [442] C. Wang, D. Li, C. O. Too, G. G. Wallace, *Chem. Mater.* **2009**, *21*, 2604.
- [443] G. K. Dimitrakakis, E. Tylianakis, G. E. Froudakis, *Nano Lett.* **2008**, *8*, 3166.
- [444] V. Tozzini, V. Pellegrini, *J. Phys. Chem. C* **2011**, *115*, 25523.
- [445] I. Meric, M. Y. Han, A. F. Young, B. Ozilmez, P. Kim, K. L. Shepard, *Nat. Nanotechnol.* **2008**, *3*, 654.
- [446] Y.-M. Lin, P. Avouris, *Nano Lett.* **2008**, *8*, 2119.
- [447] G. Liu, W. Stillman, S. Rumyantsev, Q. Shao, M. Shur, A. A. Balandin, *Appl. Phys. Lett.* **2009**, *95*, 033103.
- [448] J. S. Moon, D. Curtis, D. Zehnder, S. Kim, D. K. Gaskill, G. G. Jernigan, R. L. Myers-Ward, C. R. Eddy, P. M. Campbell, K. M. Lee, P. Asbeck, *IEEE Electron Device Lett.* **2011**, *32*, 270.
- [449] P. Asbeck, L. Kangmu, M. Jeong-Sun, presented at *IEEE Wireless and Microwave Technology Conf.*, Clearwater Beach, FL, 18–19 April 2011.
- [450] T. Palacios, A. Hsu, H. Wang, *IEEE Commun. Mag.* **2010**, *48*, 122.
- [451] L. Liao, X. Duan, *Mat. Sci. Eng. R* **2010**, *70*, 354.
- [452] A. Akturk, N. Goldsman, *J. Appl. Phys.* **2008**, *103*, 053702.
- [453] L. Liao, J. Bai, R. Cheng, Y.-C. Lin, S. Jiang, Y. Qu, Y. Huang, X. Duan, *Nano Lett.* **2010**, *10*, 3952.
- [454] L. Liao, J. Bai, R. Cheng, H. Zhou, L. Liu, Y. Liu, Y. Huang, X. Duan, *Nano Lett.* **2012**, *12*, 2653.
- [455] S.-J. Han, Z. H. Chen, A. A. Bol, Y. N. Sun, *IEEE Electron Device Lett.* **2011**, *32*, 812.
- [456] H. Xu, Z. Zhang, H. Xu, Z. Wang, S. Wang, L.-M. Peng, *ACS Nano* **2011**, *5*, 5031.
- [457] A. Badmaev, Y. Che, Z. Li, C. Wang, C. Zhou, *ACS Nano* **2012**, *6*, 3371.

- [458] S.-J. Han, A. Valdes-Garcia, A. A. Bol, A. D. Franklin, D. Farmer, E. Kratschmer, K. A. Jenkins, W. Haensch, presented at *IEEE Int. Electron Devices Meeting*, Washington, DC, 5-7 December 2011.
- [459] Y.-M. Lin, K. A. Jenkins, A. Valdes-Garcia, J. P. Small, D. B. Farmer, P. Avouris, *Nano Lett.* **2009**, *9*, 422.
- [460] Y.-M. Lin, H.-Y. Chiu, K. A. Jenkins, D. B. Farmer, P. Avouris, A. Valdes-Garcia, *IEEE Electron Device Lett.* **2010**, *31*, 68.
- [461] D. B. Farmer, H.-Y. Chiu, Y.-M. Lin, K. A. Jenkins, F. Xia, P. Avouris, *Nano Lett.* **2009**, *9*, 4474.
- [462] H. Xu, Z. Zhang, Z. Wang, S. Wang, X. Liang, L.-M. Peng, *ACS Nano* **2011**, *5*, 2340.
- [463] Y. M. Lin, C. Dimitrakopoulos, K. A. Jenkins, D. B. Farmer, H. Y. Chiu, A. Grill, P. Avouris, *Science* **2010**, *327*, 662.
- [464] C. Dimitrakopoulos, Y.-M. Lin, A. Grill, D. B. Farmer, M. Freitag, Y. Sun, S.-J. Han, Z. Chen, K. A. Jenkins, Y. Zhu, Z. Liu, T. J. McArdle, J. A. Ott, R. Wisniewi, P. Avouris, *J. Vac. Sci. Technol. B* **2010**, *28*, 985.
- [465] Y.-M. Lin, K. A. Jenkins, J. Ott, C. Dimitrakopoulos, D. B. Farmer, Y. Wu, A. Grill, P. Avouris, presented at *IEEE Int. Microwave Symp.*, Baltimore, MD, 5–10 June 2011.
- [466] Y. Q. Wu, D. B. Farmer, A. Valdes-Garcia, W. J. Zhu, K. A. Jenkins, C. Dimitrakopoulos, P. Avouris, Y. M. Lin, presented at *IEEE Int. Electron. Devices Meeting*, Washington, DC, 5–7 December 2011.
- [467] N. Meng, J. F. Fernandez, E. Pichonat, O. Lancry, D. Vignaud, G. Dambrine, H. Happy, presented at *IEEE Int. Microwave Symp.*, Baltimore, MD, 5–10 June 2011.
- [468] H. Wang, A. Hsu, J. Wu, J. Kong, T. Palacios, *IEEE Electron Device Lett.* **2010**, *31*, 906.
- [469] O. M. Nayfeh, *IEEE Trans. Electron Devices* **2011**, *58*, 2847.
- [470] Y. Wu, Y.-M. Lin, A. A. Bol, K. A. Jenkins, F. Xia, D. B. Farmer, Y. Zhu, P. Avouris, *Nature* **2011**, *472*, 74.
- [471] S. Tanachutiwat, J. Lee, W. Wang, C. Sung, Proceedings of the 47th Design Automation Conference **2010**, 883.
- [472] J. Chauhan, J. Guo, *Nano Res.* **2011**, *4*, 571.
- [473] J. Bai, L. Liao, H. Zhou, R. Cheng, L. Liu, Y. Huang, X. Duan, *Nano Lett.* **2011**, *11*, 2555.
- [474] I. Meric, C. R. Dean, A. F. Young, N. Baklitskaya, N. J. Tremblay, C. Nuckolls, P. Kim, K. L. Shepard, *Nano Lett.* **2011**, *11*, 1093.
- [475] I. Meric, N. Baklitskaya, P. Kim, K. L. Shepard, presented at *IEEE Int. Electron Devices Meeting*, San Francisco, CA, 15–17 December 2008.
- [476] S.-J. Han, K. A. Jenkins, A. Valdes Garcia, A. D. Franklin, A. A. Bol, W. Haensch, *Nano Lett.* **2011**, *11*, 3690.
- [477] E. Guerriero, L. Polloni, L. G. Rizzi, M. Bianchi, G. Mondello, R. Sordan, *Small* **2012**, *8*, 356.
- [478] H. Wang, D. Nezich, J. Kong, T. Palacios, *IEEE Electron Device Lett.* **2009**, *30*, 547.
- [479] Y.-M. Lin, A. Valdes-Garcia, S.-J. Han, D. B. Farmer, I. Meric, Y. Sun, Y. Wu, C. Dimitrakopoulos, A. Grill, P. Avouris, K. A. Jenkins, *Science* **2011**, *332*, 1294.
- [480] O. Habibpour, S. Cherednichenko, J. Vukusic, K. Yhland, J. Stake, *IEEE Electron Device Lett.* **2012**, *33*, 71.
- [481] X. Yang, G. Liu, A. A. Balandin, K. Mohanram, *ACS Nano* **2010**, *4*, 5532.
- [482] J. Bai, Y. Huang, *Mat. Sci. Eng. R* **2010**, *70*, 341.
- [483] L. A. Ponomarenko, F. Schedin, M. I. Katsnelson, R. Yang, E. W. Hill, K. S. Novoselov, A. K. Geim, *Science* **2008**, *320*, 356.
- [484] F. Libisch, C. Stampfer, J. Burgdorfer, *Phys. Rev. B* **2009**, *79*, 115423.
- [485] M. Y. Han, B. Oezilimaz, Y. Zhang, P. Kim, *Phys. Rev. Lett.* **2007**, *98*, 206805.
- [486] Y.-W. Son, M. L. Cohen, S. G. Louie, *Nature* **2006**, *444*, 347.
- [487] L. Yang, C.-H. Park, Y.-W. Son, M. L. Cohen, S. G. Louie, *Phys. Rev. Lett.* **2007**, *99*, 186801.
- [488] X. Liu, J. B. Oostinga, A. F. Morpurgo, L. M. K. Vandersypen, *Phys. Rev. B* **2009**, *80*, 121407.
- [489] B. Oezilimaz, P. Jarillo-Herrero, D. Efetov, P. Kim, *Appl. Phys. Lett.* **2007**, *91*, 192107.
- [490] Z. Chen, Y.-M. Lin, M. J. Rooks, P. Avouris, *Physica E* **2007**, *40*, 228.
- [491] Y. Gotoh, K. Matsumoto, T. Maeda, *Jpn. J. Appl. Phys.* **2002**, *41*, 2578.
- [492] M. Kastner, *Rev. Mod. Phys.* **1992**, *64*, 849.
- [493] C. Stampfer, J. Guettler, F. Molitor, D. Graf, T. Ihn, K. Ensslin, *Appl. Phys. Lett.* **2008**, *92*, 012102.
- [494] C. Stampfer, E. Schurtenberger, F. Molitor, J. Guettler, T. Ihn, K. Ensslin, *Nano Lett.* **2008**, *8*, 2378.
- [495] K. A. Ritter, J. W. Lyding, *Nat. Mater.* **2009**, *8*, 235.
- [496] C. O. Girit, J. C. Meyer, R. Erni, M. D. Rossell, C. Kisielowski, L. Yang, C.-H. Park, M. F. Crommie, M. L. Cohen, S. G. Louie, A. Zettl, *Science* **2009**, *323*, 1705.
- [497] J. Y. Huang, F. Ding, B. I. Yakobson, P. Lu, L. Qi, J. Li, *Proc. Natl. Acad. Sci. USA* **2009**, *106*, 10103.
- [498] M. Engelund, J. A. Furst, A. P. Jauho, M. Brandbyge, *Phys. Rev. Lett.* **2010**, *104*, 036807.
- [499] M. C. Lemme, D. C. Bell, J. R. Williams, L. A. Stern, B. W. H. Baugher, P. Jarillo-Herrero, C. M. Marcus, *ACS Nano* **2009**, *3*, 2674.
- [500] D. V. Kosynkin, A. L. Higginbotham, A. Sinitskii, J. R. Lomeda, A. Dimiev, B. K. Price, J. M. Tour, *Nature* **2009**, *458*, 872.
- [501] C. G. Tao, L. Y. Jiao, O. V. Yazyev, Y.-C. Chen, J. J. Feng, X. W. Zhang, R. B. Capaz, J. M. Tour, A. Zettl, S. G. Louie, H. J. Dai, M. F. Crommie, *Nat. Phys.* **2011**, *7*, 616.
- [502] L. Y. Jiao, L. Zhang, X. R. Wang, G. Diankov, H. J. Dai, *Nature* **2009**, *458*, 877.
- [503] X. L. Li, X. R. Wang, L. Zhang, S. W. Lee, H. J. Dai, *Science* **2008**, *319*, 1229.
- [504] T. W. Ebbesen, H. Hiuera, *Adv. Mater.* **1995**, *7*, 582.
- [505] Z. Wei, D. Wang, S. Kim, S.-Y. Kim, Y. Hu, M. K. Yakes, A. R. Laracuente, Z. Dai, S. R. Marder, C. Berger, W. P. King, W. A. de Heer, P. E. Sheehan, E. Riedo, *Science* **2010**, *328*, 1373.
- [506] G. Dobrik, L. Tapasztó, P. Nemes-Incze, *Phys. Status Solidi B* **2010**, *247*, 896.
- [507] X. Liang, Z. Fu, S. Y. Chou, *Nano Lett.* **2007**, *7*, 3840.
- [508] J. Bai, X. Duan, Y. Huang, *Nano Lett.* **2009**, *9*, 2083.
- [509] G. Y. Xu, J. C. M. Torres, J. Bai, J. S. Tang, T. Yu, Y. Huang, X. Duan, Y. G. Zhang, K. L. Wang, *Appl. Phys. Lett.* **2011**, *98*, 243118.
- [510] S. Tongay, M. Lemaitre, J. Fridmann, A. F. Hebard, B. P. Gila, B. R. Appleton, *Appl. Phys. Lett.* **2012**, *100*, 073501.
- [511] D. Wei, Y. Liu, H. Zhang, L. Huang, B. Wu, J. Chen, G. Yu, *J. Am. Chem. Soc.* **2009**, *131*, 11147.
- [512] J. Bai, X. Zhong, S. Jiang, Y. Huang, X. Duan, *Nat. Nanotechnol.* **2010**, *5*, 190.
- [513] A. Sinitskii, J. M. Tour, *J. Am. Chem. Soc.* **2010**, *132*, 14730.
- [514] X. Liang, Y.-S. Jung, S. Wu, A. Ismach, D. L. Olynick, S. Cabrini, J. Bokor, *Nano Lett.* **2010**, *10*, 2454.
- [515] Y. Lu, B. Goldsmith, D. R. Strachan, J. Lim, Z. Luo, A. T. C. Johnson, *Small* **2010**, *6*, 2748.
- [516] M.-W. Lin, C. Ling, Y. Zhang, H. J. Yoon, M. M.-C. Cheng, L. A. Agapito, N. Kioussis, N. Widjaja, Z. Zhou, *Nanotechnology* **2011**, *22*, 265201.
- [517] X. R. Wang, Y. J. Ouyang, X. J. Li, H. J. Wang, J. Guo, H. J. Dai, *Phys. Rev. Lett.* **2008**, *100*, 206803.
- [518] D. Gunlycke, D. A. Areshkin, C. T. White, *Appl. Phys. Lett.* **2007**, *90*, 142104.
- [519] P. Gallagher, K. Todd, D. Goldhaber-Gordon, *Phys. Rev. B* **2010**, *81*, 115409.
- [520] F. Molitor, C. Stampfer, J. Guettler, A. Jacobsen, T. Ihn, K. Ensslin, *Semicond. Sci. Technol.* **2010**, *25*, 034002.

- [521] F. Sols, F. Guinea, A. H. C. Neto, *Phys. Rev. Lett.* **2007**, *99*, 166803.
- [522] M. Y. Han, J. C. Brant, P. Kim, *Phys. Rev. Lett.* **2010**, *104*, 056801.
- [523] L. Y. Jiao, X. R. Wang, G. Diankov, H. L. Wang, H. J. Dai, *Nat. Nanotechnol.* **2010**, *5*, 321.
- [524] M.-W. Lin, C. Ling, L. A. Agapito, N. Kioussis, Y. Zhang, M. M.-C. Cheng, W. L. Wang, E. Kaxiras, Z. Zhou, *Phys. Rev. B* **2011**, *84*, 125411.
- [525] W. Y. Kim, K. S. Kim, *Nat. Nanotechnol.* **2008**, *3*, 408.
- [526] F. Munoz-Rojas, J. Fernandez-Rossier, J. J. Palacios, *Phys. Rev. Lett.* **2009**, *102*, 136810.
- [527] N. M. R. Peres, A. H. C. Neto, F. Guinea, *Phys. Rev. B* **2006**, *73*, 241403.
- [528] N. Peres, A. Neto, F. Guinea, *Phys. Rev. B* **2006**, *73*, 195411.
- [529] Y. C. Huang, C. P. Chang, M. F. Lin, *Nanotechnology* **2007**, *18*, 495401.
- [530] J. Liu, A. R. Wright, C. Zhang, Z. Ma, *Appl. Phys. Lett.* **2008**, *93*, 041106.
- [531] C. Ritter, S. S. Makler, A. Latge, *Phys. Rev. B* **2008**, *77*, 195443.
- [532] T. S. Li, Y. C. Huang, S. C. Chang, C. P. Chang, M. F. Lin, *Philos. Mag.* **2009**, *89*, 697.
- [533] J. Bai, R. Cheng, F. Xiu, L. Liao, M. Wang, A. Shailos, K. L. Wang, Y. Huang, X. Duan, *Nat. Nanotechnol.* **2010**, *5*, 655.
- [534] J.-M. Poumirol, A. Cresti, S. Roche, W. Escoffier, M. Goiran, X. R. Wang, X. L. Li, H. J. Dai, B. Raquet, *Phys. Rev. B* **2010**, *82*, 041413.
- [535] J. B. Oostinga, B. Sacepe, M. F. Craciun, A. F. Morpurgo, *Phys. Rev. B* **2010**, *81*, 193408.
- [536] K. S. Novoselov, E. McCann, S. V. Morozov, V. I. Fal'ko, M. I. Katsnelson, U. Zeitler, D. Jiang, F. Schedin, A. K. Geim, *Nat. Phys.* **2006**, *2*, 177.
- [537] J. Hass, F. Varchon, J. E. Millan-Otoya, M. Sprinkle, N. Sharma, W. A. de Heer, C. Berger, P. N. First, L. Magaud, E. H. Conrad, *Phys. Rev. Lett.* **2008**, *100*, 125504.
- [538] E. V. Castro, K. S. Novoselov, S. V. Morozov, N. M. R. Peres, J. M. B. L. Dos Santos, J. Nilsson, F. Guinea, A. K. Geim, A. H. C. Neto, *Phys. Rev. Lett.* **2007**, *99*, 216802.
- [539] J. B. Oostinga, H. B. Heersche, X. Liu, A. F. Morpurgo, L. M. K. Vandersypen, *Nat. Mater.* **2008**, *7*, 151.
- [540] Y. Zhang, T.-T. Tang, C. Girif, Z. Hao, M. C. Martin, A. Zettl, M. F. Crommie, Y. R. Shen, F. Wang, *Nature* **2009**, *459*, 820.
- [541] F. Xia, D. B. Farmer, Y.-M. Lin, P. Avouris, *Nano Lett.* **2010**, *10*, 715.
- [542] W. Zhang, C.-T. Lin, K.-K. Liu, T. Tite, C.-Y. Su, C.-H. Chang, Y.-H. Lee, C.-W. Chu, K.-H. Wei, J.-L. Kuo, L.-J. Li, *ACS Nano* **2011**, *5*, 7517.
- [543] W. J. Yu, L. Liao, S. H. Chae, Y. H. Lee, X. Duan, *Nano Lett.* **2011**, *11*, 4759.
- [544] B. N. Szafranek, D. Schall, M. Otto, D. Neumaier, H. Kurz, *Nano Lett.* **2011**, *11*, 2640.
- [545] R. T. Weitz, M. T. Allen, B. E. Feldman, J. Martin, A. Yacoby, *Science* **2010**, *330*, 812.
- [546] J. Velasco, L. Jing, W. Bao, Y. Lee, P. Kratz, V. Aji, M. Bockrath, C. N. Lau, C. Varma, S. R. D. Smirnov, F. Zhang, J. Jung, A. H. MacDonald, *Nat. Nanotechnol.* **2012**, *7*, 156.
- [547] C. H. Lui, Z. Li, K. F. Mak, E. Cappelluti, T. F. Heinz, *Nat. Phys.* **2011**, *7*, 944.
- [548] S. H. Jhang, M. F. Craciun, S. Schmidmeier, S. Tokumitsu, S. Russo, M. Yamamoto, Y. Skourski, J. Wosnitza, S. Tarucha, J. Eroms, C. Strunk, *Phys. Rev. B* **2011**, *84*, 161408.
- [549] M. F. Craciun, S. Russo, M. Yamamoto, J. B. Oostinga, A. F. Morpurgo, S. Tarucha, *Nat. Nanotechnol.* **2009**, *4*, 383.
- [550] W. Bao, L. Jing, J. Velasco, Y. Lee, G. Liu, D. Tran, B. Standley, M. Aykol, S. B. Cronin, D. Smirnov, M. Koshino, E. McCann, M. Bockrath, C. N. Lau, *Nat. Phys.* **2011**, *7*, 948.
- [551] V. M. Pereira, A. H. Castro Neto, *Phys. Rev. Lett.* **2009**, *103*, 046801.
- [552] M. Huang, T. Pascal, H. Kim, W. Goddard III, J. R. Greer, *Nano Lett.* **2011**, *11*, 1241.
- [553] T. Low, F. Guinea, M. I. Katsnelson, *Phys. Rev. B* **2011**, *83*, 195436.
- [554] M. Huang, H. Yan, T. F. Heinz, J. Hone, *Nano Lett.* **2010**, *10*, 4074.
- [555] M. Huang, H. Yan, C. Chen, D. Song, T. F. Heinz, J. Hone, *Proc. Natl. Acad. Sci. USA* **2009**, *106*, 7304.
- [556] F. Ding, H. Ji, Y. Chen, A. Herklotz, K. Dörr, Y. Mei, A. Rastelli, O. G. Schmidt, *Nano Lett.* **2010**, *10*, 3453.
- [557] Y. Wang, R. Yang, Z. Shi, L. Zhang, D. Shi, E. Wang, G. Zhang, *ACS Nano* **2011**, *5*, 3645.
- [558] J. Zabel, R. R. Nair, A. Ott, T. Georgiou, A. K. Geim, K. S. Novoselov, C. Casiraghi, *Nano Lett.* **2011**, *12*, 617.
- [559] B. D. Briggs, B. Nagabhirava, G. Rao, R. Geer, H. Gao, Y. Xu, B. Yu, *Appl. Phys. Lett.* **2010**, *97*, 223102.
- [560] T. Li, Z. Zhang, *Nanoscale Res. Lett.* **2009**, *5*, 169.
- [561] S. Scharfenberg, N. Mansukhani, C. Chialvo, R. L. Weaver, N. Mason, *Appl. Phys. Lett.* **2012**, *100*, 021910.
- [562] J. Lahiri, Y. Lin, P. Bozkurt, I. I. Oleynik, M. Batzill, *Nat. Nanotechnol.* **2010**, *5*, 326.
- [563] D. Rainis, F. Taddei, M. Polini, G. León, F. Guinea, V. I. Fal'ko, *Phys. Rev. B* **2011**, *83*, 165403.
- [564] E. Prada, P. San-Jose, L. Brey, *Phys. Rev. Lett.* **2010**, *105*, 106802.
- [565] A. Fert, *Angew. Chem. Int. Ed.* **2008**, *47*, 5956.
- [566] E. W. Hill, A. K. Geim, K. Novoselov, F. Schedin, P. Blake, *IEEE Trans. Magn.* **2006**, *42*, 2694.
- [567] S. Cho, Y.-F. Chen, M. S. Fuhrer, *Appl. Phys. Lett.* **2007**, *91*, 123105.
- [568] O. V. Yazyev, M. I. Katsnelson, *Phys. Rev. Lett.* **2008**, *100*, 047209.
- [569] M. Wimmer, I. Adagideli, S. Berber, D. Tomanek, K. Richter, *Phys. Rev. Lett.* **2008**, *100*, 177207.
- [570] A. Saffarzadeh, R. Farghadan, *Appl. Phys. Lett.* **2011**, *98*, 023106.
- [571] O. Hod, V. Barone, J. E. Peralta, G. E. Scuseria, *Nano Lett.* **2007**, *7*, 2295.
- [572] Y.-T. Zhang, H. Jiang, Q.-f. Sun, X. C. Xie, *Phys. Rev. B* **2010**, *81*, 165404.
- [573] M. Zeng, Y. Feng, G. Liang, *Nano Lett.* **2011**, *11*, 1369.
- [574] A. Candini, S. Klyatskaya, M. Ruben, W. Wernsdorfer, M. Affronte, *Nano Lett.* **2011**, *11*, 2634.
- [575] W. Han, K. Pi, W. Bao, K. M. McCreary, Y. Li, W. H. Wang, C. N. Lau, R. K. Kawakami, *Appl. Phys. Lett.* **2009**, *94*, 222109.
- [576] W. Han, K. Pi, K. M. McCreary, Y. Li, J. J. I. Wong, A. G. Swartz, R. K. Kawakami, *Phys. Rev. Lett.* **2010**, *105*, 167202.
- [577] W. Han, W. H. Wang, K. Pi, K. M. McCreary, W. Bao, Y. Li, F. Miao, C. N. Lau, R. K. Kawakami, *Phys. Rev. Lett.* **2009**, *102*, 137205.
- [578] M. Shiraishi, M. Ohishi, R. Nouchi, N. Mitoma, T. Nozaki, T. Shinjo, Y. Suzuki, *Adv. Funct. Mater.* **2009**, *19*, 3711.
- [579] A. Rycerz, J. Tworzydlo, C. W. J. Beenakker, *Nat. Phys.* **2007**, *3*, 172.
- [580] H. Schomerus, *Phys. Rev. B* **2010**, *82*, 164309.
- [581] D. Gunlycke, C. T. White, *Phys. Rev. Lett.* **2011**, *106*, 136806.
- [582] P. San-Jose, E. Prada, E. McCann, H. Schomerus, *Phys. Rev. Lett.* **2009**, *102*, 247204.
- [583] D. Reddy, L. F. Register, E. Tutuc, S. K. Banerjee, *IEEE Trans. Electron Devices* **2010**, *57*, 755.
- [584] T. Low, F. Guinea, *Nano Lett.* **2010**, *10*, 3551.
- [585] T. Fujita, M. B. A. Jalil, S. G. Tan, *Appl. Phys. Lett.* **2010**, *97*, 043508.
- [586] F. Zhai, X. Zhao, K. Chang, H. Q. Xu, *Phys. Rev. B* **2010**, *82*.
- [587] A. Chaves, L. Covaci, K. Y. Rakhimov, G. A. Farias, F. M. Peeters, *Phys. Rev. B* **2010**, *82*, 205430.
- [588] B. Soodchomshom, P. Chantngarm, *J. Supercond. Novel Magn.* **2011**, *24*, 1885.
- [589] B. Soodchomshom, *Physica E* **2011**, *44*, 579.
- [590] Z. Feng, M. Yanling, Z. Ying-Tao, *J. Phys.: Condens. Matter* **2011**, *23*, 385302.

- [591] J. P. Zheng, K. L. Jiao, W. P. Sshen, W. A. Anderson, H. S. Kwok, *Appl. Phys. Lett.* **1992**, *61*, 459.
- [592] M. A. Khan, J. N. Kuznia, D. T. Olson, M. Blasingame, A. R. Bhattacharai, *Appl. Phys. Lett.* **1993**, *63*, 2455.
- [593] T. J. Echtermeyer, L. Britnell, P. K. Jasnos, A. Lombardo, R. V. Gorbachev, A. N. Grigorenko, A. K. Geim, A. C. Ferrari, K. S. Novoselov, *Nat. Commun.* **2011**, *2*, 458.
- [594] Y. Liu, R. Cheng, L. Liao, H. Zhou, J. Bai, G. Liu, L. Liu, Y. Huang, X. Duan, *Nat. Commun.* **2011**, *2*.
- [595] X. Xu, N. M. Gabor, J. S. Alden, A. M. van der Zande, P. L. McEuen, *Nano Lett.* **2010**, *10*, 562.
- [596] F. Xia, T. Mueller, Y.-M. Lin, A. Valdes-Garcia, P. Avouris, *Nat. Nanotechnol.* **2009**, *4*, 839.
- [597] L. Prechtel, L. Song, D. Schuh, P. Ajayan, W. Wegscheider, A. W. Holleitner, *Nat. Commun.* **2012**, *3*, 646.
- [598] T. Mueller, F. Xia, P. Avouris, *Nat. Photonics* **2010**, *4*, 297.
- [599] Q. Bao, H. Zhang, Y. Wang, Z. Ni, Y. Yan, Z. X. Shen, K. P. Loh, D. Y. Tang, *Adv. Funct. Mater.* **2009**, *19*, 3077.
- [600] Z. Sun, T. Hasan, F. Torrisi, D. Popa, G. Privitera, F. Wang, F. Bonaccorso, D. M. Basko, A. C. Ferrari, *ACS Nano* **2010**, *4*, 803.
- [601] M. Liu, X. Yin, E. Ulin-Avila, B. Geng, T. Zentgraf, L. Ju, F. Wang, X. Zhang, *Nature* **2011**, *474*, 64.
- [602] Q. Bao, H. Zhang, B. Wang, Z. Ni, C. H. Y. X. Lim, Y. Wang, D. Y. Tang, K. P. Loh, *Nat. Photonics* **2011**, *5*, 411.
- [603] K. R. Ratinac, W. Yang, S. P. Ringer, F. Braet, *Environ. Sci. Technol.* **2010**, *44*, 1167.
- [604] P. Hu, J. Zhang, L. Li, Z. Wang, W. O'Neill, P. Estrela, *Sensors* **2010**, *10*, 5133.
- [605] P. Laaksonen, M. Kainlauri, T. Laaksonen, A. Shchepetov, H. Jiang, J. Ahopelto, M. B. Linder, *Angew. Chem.* **2010**, *122*, 5066.
- [606] T. Premkumar, K. E. Geckeler, *Prog. Polym. Sci.* **2012**, *37*, 515.
- [607] Y. Wang, Z. Li, J. Wang, J. Li, Y. Lin, *Trends Biotechnol.* **2011**, *29*, 205.
- [608] F. J. Hernandez, V. C. Ozalp, *Biosensors* **2012**, *2*, 1.
- [609] L. Feng, Y. Chen, J. Ren, X. Qu, *Biomaterials* **2011**, *32*, 2930.
- [610] S. Guo, Y. Du, X. Yang, S. Dong, E. Wang, *Anal. Chem.* **2011**, *83*, 8035.
- [611] H. Hong, K. Yang, Y. Zhang, J. W. Engle, L. Feng, Y. Yang, T. R. Nayak, S. Goel, J. Bean, C. P. Theuer, T. E. Barnhart, Z. Liu, W. Cai, *ACS Nano* **2012**, *6*, 2361.
- [612] C. A. Merchant, K. Healy, M. Wanunu, V. Ray, N. Peterman, J. Bartel, M. D. Fischbein, K. Venta, Z. Luo, A. T. C. Johnson, M. Drndic, *Nano Lett.* **2010**, *10*, 2915.
- [613] S. Garaj, W. Hubbard, A. Reina, J. Kong, D. Branton, J. A. Golovchenko, *Nature* **2010**, *467*, 190.
- [614] B. M. Venkatesan, D. Estrada, S. Banerjee, X. Jin, V. E. Dorgan, M.-H. Bae, N. R. Aluru, E. Pop, R. Bashir, *ACS Nano* **2011**, *6*, 441.
- [615] Y. Shao, J. Wang, H. Wu, J. Liu, I. A. Aksay, Y. Lin, *Electroanalysis* **2010**, *22*, 1027.
- [616] M. Purmera, A. Ambrosi, A. Bonanni, E. L. K. Chng, H. L. Poh, *TrAC, Trends Anal. Chem.* **2010**, *29*, 954.
- [617] H. Chang, L. Tang, Y. Wang, J. Jiang, J. Li, *Anal. Chem.* **2010**, *82*, 2341.
- [618] R. Arsat, M. Breedon, M. Shafiei, P. G. Spizziri, S. Gilje, R. B. Kaner, K. Kalantar-zadeh, W. Włodarski, *Chem. Phys. Lett.* **2009**, *467*, 344.
- [619] F. Schedin, A. K. Geim, S. V. Morozov, E. W. Hill, P. Blake, M. I. Katsnelson, K. S. Novoselov, *Nat. Mater.* **2007**, *6*, 652.
- [620] T. O. Wehling, K. S. Novoselov, S. V. Morozov, E. E. Vdovin, M. I. Katsnelson, A. K. Geim, A. I. Lichtenstein, *Nano Lett.* **2008**, *8*, 173.
- [621] Y. Dan, Y. Lu, N. J. Kybert, Z. Luo, A. T. C. Johnson, *Nano Lett.* **2009**, *9*, 1472.
- [622] J. D. Fowler, M. J. Allen, V. C. Tung, Y. Yang, R. B. Kaner, B. H. Weiller, *ACS Nano* **2009**, *3*, 301.
- [623] J. T. Robinson, F. K. Perkins, E. S. Snow, Z. Wei, P. E. Sheehan, *Nano Lett.* **2008**, *8*, 3137.
- [624] V. Dua, S. P. Surwade, S. Ammu, S. R. Agnihotra, S. Jain, K. E. Roberts, S. Park, R. S. Ruoff, S. K. Manohar, *Angew. Chem. Int. Ed.* **2010**, *49*, 2154.
- [625] Y. Lu, B. R. Goldsmith, N. J. Kybert, A. T. C. Johnson, *Appl. Phys. Lett.* **2010**, *97*, 083107.
- [626] W. Li, X. Geng, Y. Guo, J. Rong, Y. Gong, L. Wu, X. Zhang, P. Li, J. Xu, G. Cheng, M. Sun, L. Liu, *ACS Nano* **2011**, *5*, 6955.
- [627] H. G. Sudibya, Q. He, H. Zhang, P. Chen, *ACS Nano* **2011**, *5*, 1990.
- [628] P. K. Ang, W. Chen, A. T. S. Wee, K. P. Loh, *J. Am. Chem. Soc.* **2008**, *130*, 14392.
- [629] F. Chen, J. Xia, D. K. Ferry, N. Tao, *Nano Lett.* **2009**, *9*, 2571.
- [630] F. Chen, Q. Qing, J. Xia, J. Li, N. Tao, *J. Am. Chem. Soc.* **2009**, *131*, 9908.
- [631] Y. Ohno, K. Maehashi, Y. Yamashiro, K. Matsumoto, *Nano Lett.* **2009**, *9*, 3318.
- [632] Z. Cheng, Q. Li, Z. Li, Q. Zhou, Y. Fang, *Nano Lett.* **2010**, *10*, 1864.
- [633] Q. He, H. G. Sudibya, Z. Yin, S. Wu, H. Li, F. Boey, W. Huang, P. Chen, H. Zhang, *ACS Nano* **2010**, *4*, 3201.
- [634] X. Dong, Y. Shi, W. Huang, P. Chen, L.-J. Li, *Adv. Mater.* **2010**, *22*, 1649.
- [635] Y. Ohno, K. Maehashi, K. Matsumoto, *J. Am. Chem. Soc.* **2010**, *132*, 18012.
- [636] T. Cohen-Karni, Q. Qing, Q. Li, Y. Fang, C. M. Lieber, *Nano Lett.* **2010**, *10*, 1098.
- [637] B. Zhang, T. Cui, *Appl. Phys. Lett.* **2011**, *98*, 073116.
- [638] R. A. Barton, J. Parpia, H. G. Craighead, *J. Vac. Sci. Technol. B* **2011**, *29*, 050801.
- [639] S.-E. Zhu, R. Shabani, J. Rho, Y. Kim, B. H. Hong, J.-H. Ahn, H. J. Cho, *Nano Lett.* **2011**, *11*, 977.
- [640] X. Xie, L. Qu, C. Zhou, Y. Li, J. Zhu, H. Bai, G. Shi, L. Dai, *ACS Nano* **2010**, *4*, 6050.
- [641] H. Tian, T.-L. Ren, D. Xie, Y.-F. Wang, C.-J. Zhou, T.-T. Feng, D. Fu, Y. Yang, P.-G. Peng, L.-G. Wang, L.-T. Liu, *ACS Nano* **2011**, *5*, 4878.
- [642] C.-L. Wong, M. Annamalai, Z.-Q. Wang, M. Palaniapan, *J. Micro-mech. Microeng.* **2010**, *20*, 115029.
- [643] T. Georgiou, L. Britnell, P. Blake, R. V. Gorbachev, A. Gholinia, A. K. Geim, C. Casiraghi, K. S. Novoselov, *Appl. Phys. Lett.* **2011**, *99*, 093193.
- [644] J. S. Bunch, A. M. van der Zande, S. S. Verbridge, I. W. Frank, D. M. Tanenbaum, J. M. Parpia, H. G. Craighead, P. L. McEuen, *Science* **2007**, *315*, 490.
- [645] D. Garcia-Sanchez, A. M. Van der Zande, A. S. Paulo, B. Lassagne, P. L. McEuen, A. Bachtold, *Nano Lett.* **2008**, *8*, 1399.
- [646] Y. Xu, C. Chen, V. V. Deshpande, F. A. DiRenzo, A. Gondarenko, D. B. Heinz, S. Liu, P. Kim, J. Hone, *Appl. Phys. Lett.* **2010**, *97*, 243111.
- [647] A. M. van der Zande, R. A. Barton, J. S. Alden, C. S. Ruiz-Vargas, W. S. Whitney, P. H. Q. Pham, J. Park, J. M. Parpia, H. G. Craighead, P. L. McEuen, *Nano Lett.* **2010**, *10*, 4869.
- [648] R. A. Barton, B. Ilic, A. M. van der Zande, W. S. Whitney, P. L. McEuen, J. M. Parpia, H. G. Craighead, *Nano Lett.* **2011**, *11*, 1232.
- [649] J. Atalaya, J. M. Kinaret, A. Isacsson, *Europhys. Lett.* **2010**, *91*, 48001.
- [650] C. Chen, S. Rosenblatt, K. I. Bolotin, W. Kalb, P. Kim, I. Kymissis, H. L. Stormer, T. F. Heinz, J. Hone, *Nat. Nanotechnol.* **2009**, *4*, 861.
- [651] A. Eichler, J. Moser, J. Chaste, M. Zdrojek, I. Wilson-Rae, A. Bachtold, *Nat. Nanotechnol.* **2011**, *6*, 339.
- [652] S. M. Kim, E. B. Song, S. Lee, S. Seo, D. H. Seo, Y. Hwang, R. Candler, K. L. Wang, *Appl. Phys. Lett.* **2011**, *99*, 023013.
- [653] K. M. Milaninia, M. A. Baldo, A. Reina, J. Kong, *Appl. Phys. Lett.* **2009**, *95*, 183105.
- [654] Q. Tannock, *Nat. Mater.* **2012**, *11*, 2.

- [655] B. Radisavljevic, M. B. Whitwick, A. Kis, *ACS Nano* **2011**, *5*, 9934.
- [656] P. Y. Huang, S. Kurasch, A. Srivastava, V. Skakalova, J. Kotakoski, A. V. Krasheninnikov, R. Hovden, Q. Mao, J. C. Meyer, J. Smet, D. A. Muller, U. Kaiser, *Nano Lett.* **2012**, *12*, 1081.
- [657] B. Lalmi, H. Oughaddou, H. Enriquez, A. Kara, S. Vizzini, B. Ealet, B. Aufray, *Appl. Phys. Lett.* **2010**, *97*, 223109.
- [658] K. Novoselov, D. Jiang, F. Schedin, T. Booth, V. Khotkevich, S. Morozov, A. Geim, *Proc. Natl. Acad. Sci. USA* **2005**, *102*, 10451.
- [659] J. N. Coleman, M. Lotya, A. O'Neill, S. D. Bergin, P. J. King, U. Khan, K. Young, A. Gaucher, S. De, R. J. Smith, I. V. Shvets, S. K. Arora, G. Stanton, H.-Y. Kim, K. Lee, G. T. Kim, G. S. Duesberg, T. Hallam, J. J. Boland, J. J. Wang, J. F. Donegan, J. C. Grunlan, G. Moriarty, A. Shmeliov, R. J. Nicholls, J. M. Perkins, E. M. Grieveson, K. Theuwissen, D. W. McComb, P. D. Nellist, V. Nicolosi, *Science* **2011**, *331*, 568.
- [660] B. Radisavljevic, A. Radenovic, J. Brivio, V. Giacometti, A. Kis, *Nat. Nanotechnol.* **2011**, *6*, 147.
- [661] R. H. Baughman, H. Eckhardt, M. Kertesz, *J. Chem. Phys.* **1987**, *87*, 6687.
- [662] D. Malko, C. Neiss, F. Viñes, A. Görling, *Phys. Rev. Lett.* **2012**, *108*, 086804.
- [663] X.-L. Sheng, Q.-B. Yan, F. Ye, Q.-R. Zheng, G. Su, *Phys. Rev. Lett.* **2011**, *106*, 155703.
- [664] M. Gibertini, A. Singha, V. Pellegrini, M. Polini, G. Vignale, A. Pinczuk, L. N. Pfeiffer, K. W. West, *Phys. Rev. B* **2009**, *79*, 241406.
- [665] K. K. Gomes, W. Mar, W. Ko, F. Guinea, H. C. Manoharan, *Nature* **2012**, *483*, 306.
- [666] L. Tarruell, D. Greif, T. Uehlinger, G. Jotzu, T. Esslinger, *Nature* **2012**, *483*, 302.
- [667] L. Nádvorník, M. Orlita, N. A. Goncharuk, L. Smrčka, V. Novák, V. Jurka, K. Hruška, Z. Výborný, Z. R. Wasilewski, M. Potemski, K. Výborný, *New J. Phys.* **2012**, *14*, 053002.
- [668] T. Palacios, *Nat. Nanotechnol.* **2011**, *6*, 464.
- [669] T. D. Ladd, F. Jelezko, R. Laflamme, Y. Nakamura, C. Monroe, J. L. O'Brien, *Nature* **2010**, *464*, 45.
- [670] N. Engheta, *Science* **2007**, *317*, 1698.
- [671] P. Tassin, T. Koschny, M. Kafesaki, C. M. Soukoulis, *Nat. Photonics* **2012**, *6*, 259.